

AFM - CSLM MICRORHEOLOGY OF AGGREGATED EMULSIONS

Diana Filip - Boar

The work described in this thesis has been carried out in the group Physics of Complex Fluids at University of Twente. The work is part of the research programme of the 'Stichting voor Fundamenteel Onderzoek der Materie (FOM)', which is financially supported by the 'Nederlandse Organisatie voor Wetenschappelijk Onderzoek (NWO)'.

Printed by Wöhrmann Print Service, Zutphen
Copyright © 2006 Diana Filip-Boar
Cover artwork © 2006 G. Blaj

ISBN 90-365-2359-1

AFM-CSLM MICRORHEOLOGY OF AGGREGATED EMULSIONS

DISSERTATION

to obtain
the doctor's degree at the University of Twente,
on the authority of the rector magnificus,
prof. dr. W.H.M. Zijm,
on account of the decision of the graduation committee,
to be publicly defended
on Wednesday 24 May 2006 at 15.00

by

Diana Filip-Boar

born on 02 July 1972
in Timisoara, Romania

This dissertation is approved by:

promoters: prof. dr. J. Mellema and prof. dr. W.G.M. Agterof

assistant promotor: dr. M.H.G. Duits

CONTENTS

CHAPTER 1. Introduction	9
1.1 AIM OF THE PROJECT	9
1.2. PHYSICAL ASPECTS OF WATER-IN-OIL EMULSIONS	10
1.2.1 Surface forces and how to measure them	10
1.2.2 Stability and sedimentation	12
1.2.3 Water-in-oil aggregated emulsions and emulsion-gels: literature review	13
1.3. OUTLINE OF THE THESIS	16
CHAPTER 2. The Model Fluid and Measuring Instruments	19
2.1 THE MODEL FLUID	19
2.1.1 Formulation of the emulsion network	19
2.1.2. Materials and preparation	21
2.3. EXPERIMENTAL TECHNIQUES	23
2.3.1 Atomic Force Microscopy	23
2.3.2. Confocal Scanning Laser Microscopy	26
2.3.3 AFM-CSLM combined	28
CHAPTER 3. Influence of Bulk Elasticity and Interfacial Tension on the Deformation of Gelled W/O Emulsion Droplets	31
3.1. INTRODUCTION	32
3.2. THEORETICAL BACKGROUND	33
3.3 EXPERIMENTAL SECTION	35
3.3.1. Materials and sample preparation	35
3.3.2. Methods	37
3.4. RESULTS AND DISCUSSION	38
3.4.1. Deformation of water droplets	38

3.4.2. Deformation of internally gelled droplets.....	44
3.4.3. Stability diagram.....	52
3.5. CONCLUSIONS	53
CHAPTER 4. Microrheology of Aggregated Emulsion Droplet Networks	57
4.1. INTRODUCTION	58
4.2. EXPERIMENTAL	60
4.2.1 Emulsion preparation.....	60
4.2.2 Microscopy Techniques.....	62
4.2.3 Data processing.....	64
4.3. RESULTS AND DISCUSSION.....	66
4.3.1. Layer structure before indentation.....	66
4.3.2 Structural changes during indentation	69
4.3.3 Force curves during indentation	71
4.3.4. Influence of deformation timescale	74
4.3.5. Rheological modeling.....	76
4.4. DISCUSSION.....	80
4.4.1. Mechanical behavior of our aggregated emulsion network.....	80
4.4.2. AFM-CSLM as a microrheological method	81
CHAPTER 5. Plastic-to-Elastic Transition in Aggregated Emulsion Networks.....	91
5.1. INTRODUCTION	92
5.2. EXPERIMENTAL	94
5.2.1 Sample preparation	94
5.2.2 Microscopy Techniques.....	94
5.3. RESULTS AND DISCUSSION.....	95
5.3.1. Evolution of the droplet network structure.....	96
5.3.2 Indentation force curves.....	100
5.4. DISCUSSION.....	104
5.4.1. AFM-CSLM as a microrheological method	105

5.4.2. Possible mechanisms for ageing	107
5.5. CONCLUSIONS	109
SUMMARY	111
SAMENVATTING	115

CHAPTER 1. Introduction

1.1 AIM OF THE PROJECT

An emulsion is a two-phase oil/water system where one of the phases is dispersed as (micron sized) droplets in the other. Emulsions can be either of the oil-in-water (O/W) type, known as a direct emulsion, or the water-in-oil (W/O) type, known as inverse emulsion. In the former case, oil is the dispersed phase while in the latter the dispersed phase is water. To obtain an emulsion, one needs to prevent the two liquids from separating into two immiscible phases, which is the thermodynamically favored state. This is achieved by adding a small amount of emulsifier (or “surfactant”) to the mixture during formulation. The effects hereof are twofold: it leads to a decrease in the interfacial tension between the oil and the water (which facilitates emulsion formation) and it also allows the droplets to get a coating (which provides stability against coalescence and subsequent phase separation).

Emulsions form the basis of a wide variety of natural and manufactured materials, including foods, pharmaceuticals, biological fluids, agrochemicals, petrochemicals, cosmetics etc. [1]. The desired stability of the emulsion-based materials varies widely depending on their intended application. Some emulsions need to remain stable for a short period (between two processing steps), whereas others must remain stable for relatively long periods (weeks, months, years). Here, stability can be defined as a resistance against droplet coalescence (loss of droplet integrity), against aggregation (local excess of droplets), or against settling or creaming due to gravity (loss of macroscopic homogeneity). Also different rheological properties can be desired for practical emulsions. Here rheology is defined as the deformation and flow of matter under external forces. For certain emulsions (or for certain stages in their preparation), a low viscosity is preferred, whereas in other cases highly viscous, or viscoelastic properties may be desirable. Therefore manufacturers of emulsion-based products need a good understanding of both emulsion stability and rheology.

In spite of many scientific achievements made in emulsion research in the past decades, getting this understanding is still a complex task. A main reason for this is that different factors are of importance, and that these factors work together in ways that are not always known. For example, to protect droplets against coalescence one could add surfactant, and/or one could jellify the droplet phase. However, surfactants can also cause the droplets to aggregate. Jellifying the droplets can make them less deformable, and hence modify the strength of adhesive contacts between the droplets. Also interactions between the surfactant and the gelling agent might play a role.

Considering the rheological properties of aggregated emulsions, not only the interactions between droplet pairs, but also the structure of the emulsion (network) needs to be considered. Viscous and elastic properties of emulsions, as encountered or

measured at macroscopic length scales, find their origin in stress-loading of (at least) the droplet-droplet bonds that enabled the formation of the network. Since this generally involves many bonds simultaneously, the way the stress and deformations are distributed, will depend on the arrangements of the droplets with respect to each other. Breaking the bonds results in changes in the network structure, which in turn will change the rheological properties.

Several studies were done on a mesoscopic scale to characterize the microscopic structural changes of aggregated emulsions or suspensions during applied external mechanical forces that simulate shear or elongational flow. Most of them concern the breakup of aggregates in shear flow followed by means of microscopy combined with a shearing device [see for example references 2a-c]. However, a deeper scientific understanding required new combinations of modern techniques that bring new information about the connection between pair-wise particle interaction, network structure and mechanical strength on a meso/microscopic level and the corresponding material's macroscopic rheological properties like yield stress, elasticity, relaxation, etc.

This thesis aims to make a contribution to this field, by addressing for a particular model W/O emulsion, the issues of droplet stability, deformability, network structure and mechanical / rheological properties on microscopic/mesoscopic length scales. For this we have done experimental studies using Atomic Force Microscopy and Confocal Scanning Laser Microscopy. These experiments allowed us to measure the force and deformation responses of single droplets as well as of aggregated droplet networks in a very detailed way. This made it possible to get a hitherto not achieved closer look on the forces and deformation mechanisms which are underlying the macroscopic behavior of aggregated emulsions.

1.2. PHYSICAL ASPECTS OF WATER-IN-OIL EMULSIONS

In this section the most prominent aspects which played a role during our study on aggregated emulsions will be reviewed.

1.2.1 Surface forces and how to measure them

The knowledge of the forces acting between colloidal particles is of primary importance in understanding the behavior of dispersed systems. The total interaction potential for two (deformed) droplets U is assumed to be the sum of several contributions:

$$U=U^S + U^{VW} + U^E + U^{St} + \Delta U \quad (1.1)$$

Here U^S is the contribution due to change of surface energy during droplet deformation (if applicable), U^{VW} is due to van der Waals interaction, U^E is the electrostatic term, U^{St} is related to the steric (repulsive) interaction of the surfactant or polymer layer adsorbed at the droplet surface and ΔU stands for other possible interactions (depletion, structural, etc). The corresponding formula and theoretical assumptions are well described in the literature [3].

For incompressible (but deformable) water droplets in oil continuum, the most basic repulsive forces are determined by: a) the excluded volume; b) the work done against the interfacial tension when two droplets deform as they are forced together (related to U^S) and c) the surfactant layer providing a short range steric repulsion (disjoining pressure) that prevents droplet coalescence (related to U^{St}). The consequences of these repulsion forces are sketched in figure 1.1 by the rise for the droplet pair interaction potential U near and below the separation $r = 2a$ (a -droplet radius). The basic attractive forces are determined by the (short range) van der Waals interaction U^{VW} (always attractive between colloidal particles from the same material suspended in a given continuous phase), and possibly depletion forces induced by excess volume of non-adsorbing polymer, micelles or other small particles (related to ΔU). Attractive emulsions show a potential well ($U < 0$) of significant magnitude compared to the thermal energy $k_B T$ (figure 1.1). In this case the droplets can flocculate into aggregates or even into large networks.

In relation to forces in water-in-oil emulsion, we should discuss also the possibility of electrostatic forces acting in such systems (U^E in terms of interaction potential). It is well known that the number density of ions in non-aqueous media is considerably lower than in water. The low concentration of ions means an increase of thickness of double layers such that the potential becomes very flat with distance from the particle, in this way eliminating the repulsion force [4]. This is consistent with the fact that we could not detect the presence of a double layer, the droplets being able to approach each other at very short distances and to aggregate into a rigid network.

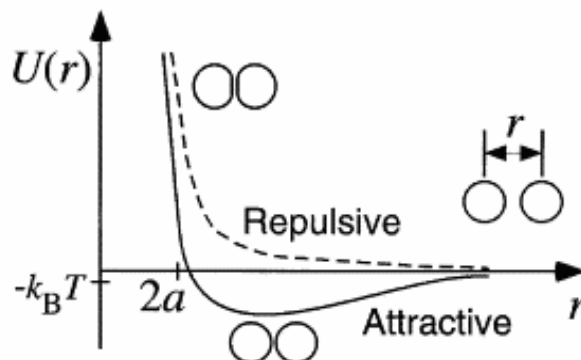


Figure 1.1. Attractive and repulsive pair-potentials

During the last decades, important advances have been made in estimating the magnitude of the colloidal forces due to the development of various techniques. The possibility to directly measure colloidal forces represented a qualitative change from the indirect way of estimation using aggregation kinetics, bulk properties or phase behavior. For solid macroscopic surfaces this can be achieved using the Surface Force Apparatus (SFA) or the Measurement and Analysis of Surface Interaction Forces (MASIF) method. Forces between a (rigid or viscoelastic) particle and a macroscopic surface (or another particle) can be measured by means of the Atomic Force Microscope (AFM) or the Total Internal Reflection Microscope (TIRM). Measurement of forces between two liquid interfaces can be done using the Thin Film Balance (TFB) technique for macroscopic single films or by employing the Liquid Surface Force Apparatus (LSFA) between a droplet and a macroscopic liquid surface.

Another technique used to measure force-distance profiles between droplets of colloidal size is using ferrofluid emulsions in magnetic fields. Recently, the AFM proved to be a powerful tool to study interactions also between a colloidal probe and emulsion droplets or bubbles, or for droplet-droplet interaction [5a-c].

1.2.2 Stability and sedimentation

As already mentioned in section 1, different types of instability can be defined for emulsions. The most dramatic one is the unification of two droplets in close proximity into a new and larger droplet, a phenomenon called coalescence. Usually this is an ongoing process which eventually leads to dramatic changes in the droplet size distribution. For coalescence to occur, the oil film in between the water droplets has to rupture [6]. The coalescence of the water droplets can be avoided by insuring a stiff interface, for example using surfactants that form a strong steric layer [7], proteins that immobilize the interface [8] or additives that form crystals at the interface (ex. fat crystals or wax) [9], by adding salt to the water phase [10,11] or by gelling the inner phase of the droplets, for example by adding a (bio)polymer.

In the last case, also a partial coalescence is possible, where due to the permanent elastic network formed within the droplets, the original droplets will only be able to deform locally to a certain extent (see figure 1.2).

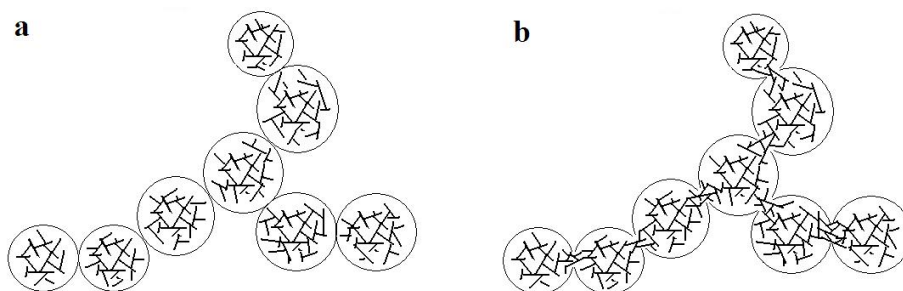


Figure 1.2. Partial coalescence of gelled droplets: a) before and b) after coalescence

Aggregation between droplets without affecting their size and shape distributions is another form of instability. Different mechanisms may be responsible for droplet aggregation. The reversible attraction between colloidal particles induced by non-adsorbing polymers was first described by Asakura and Osawa [12] and Vrij [13] and is called depletion flocculation. When the depletion zones around the colloids (induced by steric exclusion) overlap (see figure 1.3), there is an unbalance of the osmotic force created, resulting in an attractive interaction dependent on the diameter and volume fraction of the polymer. Such effect can be induced, beside polymers, also by excess surfactant micelles or smaller colloidal particles or droplets present in the continuous phase. [14]. On diluting the flocculant (below its critical concentration), the attraction between the colloids disappears and a stable dispersion / emulsion is again obtained.

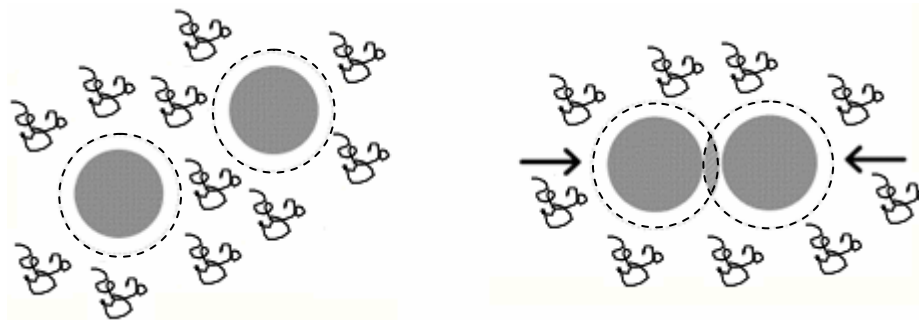


Figure 1.3. Depletion flocculation

A third type of instability is that against gravity. In most W/O emulsions, the droplet phase has a significantly higher mass density. As a consequence, even single droplets will eventually accumulate at the bottom of the container. For aggregated or coalesced droplets, the effects will be much more dramatic, considering that for uniform spheres the steady sedimentation velocity is proportional to the square of the radius. Conventional strategies to counteract sedimentation involve the use of stabilizers (usually polymers) to increase the continuous phase viscosity and hence to retard the process. Such strategies however also carry the risk of flocculating the droplets either reversibly (via non-adsorbing polymer) or irreversibly (via adsorbing polymer that induces bridging between the droplets) [15]. While (more rapid) settling of the dispersed phase is thus a consequence of aggregation or coalescence, the resulting high concentration of droplets near the bottom in turn serves to enhance the aggregation and coalescence rates, by “providing close proximity”.

Sedimentation of single droplets can also be used as a method to separate a polydisperse emulsion into fractions with different sizes (through the different sedimentation speeds), or to concentrate droplets near an interface (and make a droplet layer). Both methods have been used in this thesis.

1.2.3 Water-in-oil aggregated emulsions and emulsion-gels: literature review

In this section the most closely related recent literature about aggregating emulsions will be reviewed. We have studied W/O emulsions with a gelatin containing aqueous phase, and an oil phase containing dodecane (solvent), Span80 (surfactant) and PDMS (flocculant). The gelatin network formed inside the droplet assured a better interfacial resistance against coalescence and also gave the opportunity to vary the droplet deformability and study whether it had or not a role in the interaction strength. Dodecane was chosen as oil for its purity and for being a good solvent for reasonable amount of the surfactant. Span 80 is a well studied surfactant, suitable for the formulation of water-in-oil emulsions. PDMS was used to flocculate the droplets. From these components, we made concentrated networks in which the droplets were held together by adhesive forces.

We will start by pointing out that the first condition for a particulate gel formation is the overcoming of the so-called “gelation threshold”. Aggregated droplet structures will only be able to resist stress if, through bonding and/or confinement, the droplets have lost some degree of freedom, and can only be displaced by the interference of an external force. At low concentrations, droplet(cluster)s move freely through the medium and the emulsion remains liquid like. Increasing the

concentration of the dispersed phase, the clusters start to overlap, and eventually at a certain concentration the system becomes solid-like. The location of this transition between fluidlike and solidlike behavior is called the gelation threshold. Its magnitude has been found (for a range of systems) to depend on the strength of the attractive interactions: the stronger the interaction, the lower the critical concentration for gelation. Berli et al found that the critical volume fraction to achieve gelation decreases exponentially with the magnitude of the interaction [16]. Also the aggregation kinetics and even the presence/absence of noncentral forces can play a role in the formation of the gel. Bibette et al found [17] that in particular emulsion compositions, a connected, solid network can be produced even at extremely low droplet volume fraction (as low as $10^{-3}\%$). This structure formation turned out to be governed by the so-called “diffusion-limited cluster aggregation” (DLCA) process.

One way to aggregate colloidal droplets or particles into gels in a controllable manner is to induce depletion interaction by adding a non-adsorbing polymer to the continuous phase. For emulsion-gels, Bibette and coworkers were the first to relate quantitatively their phase transitions to depletion induced forces [18]. Below the gelation threshold the emulsions behaved like homogeneous, fluid-like dispersions, while above this threshold gelation was observed. The clusters formed in the network (by attractive depletion forces) were nearly equal sized and spaced and were identified to be fractal-like. In relation to this, the network was found to have a well-defined characteristic length scale which depended on the initial droplet volume fraction. When the interaction was made strongly adhesive, the droplets deformed and adhered to each other, retaining still their integrity (no coalescence).

An important aspect related to the life-time of colloidal gels is their transient behavior. Particulate or emulsion gels formed via weak attractions like polymer depletion, show pronounced time dependent (i.e. transient) properties, in contrast to the permanent particle gels formed by irreversibly aggregating systems. At high droplet volume fractions the clusters are more compact and the network fractures in time into independent, more compact flocs, thereby eliminating the rigidity of the emulsion gel [19]. The weak bonding (bonds can be broken and reformed) allows the rearrangement of the gel structure, eventually leading to the collapse of the gel by local compaction. Evidence of fractures in depletion flocculated silica suspensions was also shown by Verhaegh et al by means of confocal microscopy [20]. They connect the end of the gel lifetime to the increase of number of fractures which weakened the gel strength to such extent that it collapsed.

The rigidity of the network may be induced by non-central forces or packing constraints. Depletion forces are not necessarily the only forces that hold an aggregated network together. A remarkable feature of emulsion gels is that, despite the fact that the network is composed entirely of liquid droplets and the gel formed is weak, the tenuous network maintains some inherent rigidity. This rigidity has a profound implication on the nature of the adhesion: it suggests that there must be no slip between two adjacent droplets (otherwise the droplets could rotate), otherwise the resultant rearrangements would lead to a significantly less tenuous structure. The origin of the non-central forces (preventing slip) between the emulsion droplets is not yet elucidated. One suggested possibility was that in some cases the surfactant forms a solid layer at the interface [21]. In more densely packed particulate or droplet networks, packing constraints of the gel preclude rearrangement, even though the surfactant layer at the interface remains fluid.

Emulsions can experience strong attractive interactions without coalescing. As a result, neighbor droplets are deformed and exhibit contact angles. This phenomenon, called adhesion, has been observed in both direct and inverted emulsions and can lead to the formation of emulsion gels. [22] The flocculation of deformable emulsion droplets was extensively studied by Danov [23], Denkov [24], Petsev [25] and Ivanov [26]. They showed that the most important factors for droplet stability against coalescence in an aggregated state are the droplet deformability and the surface fluidity. Calculations showed that for weak attraction the deformation is small leading to a small contact angle (smaller than one degree), while strong attraction leads to a large deformation and contact angles of up to fifty degrees. In the first case the droplets can be considered to interact as non-deformed spheres. The magnitude of the attractive energy between two deformed drops is usually much larger than that between two non-deformed spheres of the same size in the same conditions.

Fewer studies are dedicated to aggregated W/O emulsions (at medium to low volume fractions) compared to O/W emulsions. Leal-Calderon et.al. reported the formation of W/O emulsion gels of submicron sized droplets with excess of Span 80 present in the (dodecane) oil phase [27]. They found a phase transition between liquid and solid-like emulsions, governed by the Span concentration, the droplet diameter, as well as the temperature. The phase diagram of 5% volume fraction emulsion had 3 distinct regions: one of free droplets, an intermediate one of aggregates coexisting with free droplets and one of emulsion gel. The gel structure was determined with optical microscopy and also studied through its sedimentation behavior.

The molecular properties of the solvent (can) play an important role in the formation of emulsion gels. Leal-Calderon et.al. [28] studied the emulsion phase behavior in various nonaqueous continuous phases. They found two distinct, independent aggregation mechanisms: one controlled by the refractive index mismatch (related to Van der Waals forces), the other controlled by the chain length of the solvent. This was concluded from experiments in which the gelation threshold was measured at constant (water) volume fraction but different chain lengths for the solvent. For long chains, a hard core depletion is found to be the driving mechanism. For small chains, the mechanism it is not well understood.

The main technique to characterize the (macroscopic) mechanical properties of colloidal matter, in particular in our case emulsion-gels, is (up to this date) rheology. Relatively few rheological studies have been performed on W/O emulsion aggregates and gels. Pal [29] studied the effect of the dispersed-phase concentration and surfactant concentration on the steady, oscillatory and creep/recovery behavior of flocculated emulsions, in mineral oil and with Span 80 as surfactant. He observed that excess of surfactant induced strong flocculation, and explained results by the formation of droplet network (emulsion-gel) via depletion flocculation due to surfactant micelles. Rheological measurements indicated a strong shear thinning and a viscoelastic behavior for the flocculated emulsions.

1.3. OUTLINE OF THE THESIS

The work in this thesis describes the structural and mechanical properties of weakly aggregated emulsion networks below close-packing volume fraction at a meso- and microscopic level, achieved by using a simultaneous combination of two experimental techniques: Atomic Force Microscopy and Confocal Scanning Laser Microscopy. Our approach was to prepare a "model" system (described in chapter 2) where the droplet deformability is controlled by gelation of droplet bulk and the attractive interaction strength is tuned by varying the concentration of a non-adsorbing polymer added to the continuous phase. An Atomic Force Microscope (AFM) was used to impose and measure (static or dynamic) loading forces as function of the probe-sample distance and the data were translated into the mechanical properties of the studied sample, while the network structure and its deformation in 3D was followed using the Confocal Scanning Laser Microscope (CSLM). By using this combination of techniques, we aim to get a deeper understanding of the mechanism(s) responsible for the elasticity, deformation and yielding of the aggregates composing the network, as well as the optimal experimental conditions for the new method of microrheological characterization.

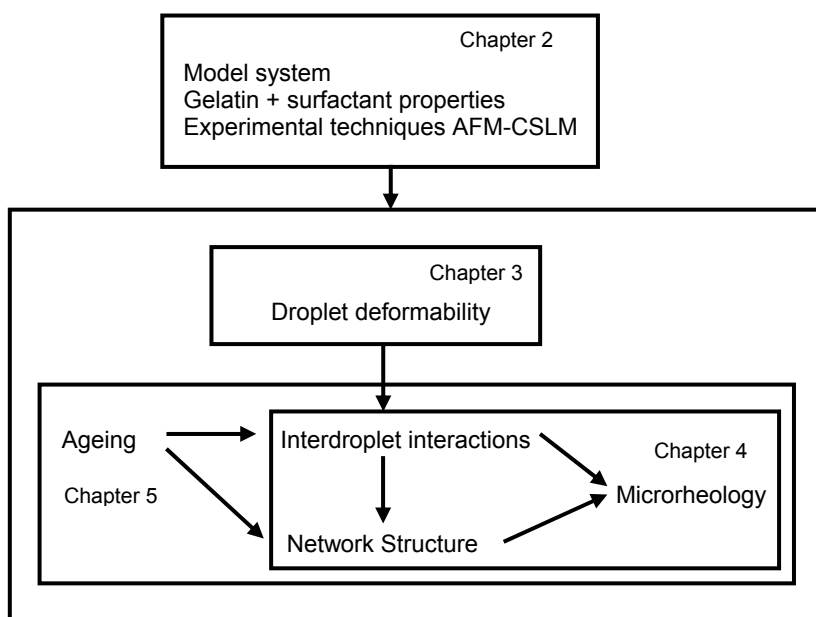


Figure 1.4. General overview of the structure of thesis

This thesis has the following structure (see figure 1.4): chapter 2 describes the requirements, preparation and instability issues of the studied samples and describes also the experimental techniques. In Chapter 3 we discuss the interfacial stability of gelled emulsion droplets and their deformability as a function of interfacial tension and bulk elasticity, studied by means of colloidal probe AFM and optical microscopy. We compare the results with results for a model system having purely viscous water droplets. Chapter 4 is dedicated to the study of weakly aggregated emulsion networks. A new method of characterization using the combined AFM-CSLM techniques is described. The local yielding of the network under the indentation of an AFM

colloidal probe and the elastic response of the neighboring force-chains in the network is interpreted in terms of a macroscopic mechanical model. Chapter 5 deals with the comparison of the behavior of the same sample that had typically plastic behavior when studied in a fresh state and an unusual hysteretic elastic behavior after the sample was aged for few weeks. We show again the capability of the combined AFM-CSLM techniques to distinguish between apparently identically structured networks that have different behavior and we relate the strong increase of the network stiffness with the change of the bonding strength in time (ageing effect).

REFERENCES

- (1) Dekker, M. "Encyclopedia of *emulsion* technology", vol.2, Becher, P. (Eds), New York 1985.
- (2a) Tolpekin, V.A.; Duits, M.H.G.; van den Ende, D.; Mellema, J. *Langmuir* **2003**, 19, 4127.
- (2b) Tolpekin, V.A.; Duits, M.H.G.; van den Ende, D.; Mellema, J. *Langmuir* **2004**, 20, 2614.
- (2c) Tolpekin, V.A.; Duits, M.H.G.; van den Ende, D.; Mellema, J. *Langmuir* **2004**, 20, 8460
- (3) Danov, K.D.; Petsev, D.N.; Denkov, N.D.; Borwankar, R. *J. Phys. Chem.* **1993**, 99, 7179.
- (4) Mishchuk, N.A.; Sanfeld, A.; Steinchen, A. *Adv. Coll. Interf. Sci.* **2004**, 112, 129
- (5a) Butt, H.-J. *J. Colloid Interface Sci.* **1994**, 166, 109.
- (5b) Gillies, G.; Prestidge, C.A. *Adv. Coll. Interf. Sci.* **2004**, 108–109, 197.
- (5c) Dagastine, R.R.; White, L.R. *J. Colloid Interface Sci.* **2002**, 247, 310.
- (6) Dekker, M. "Encyclopedia of *emulsion* technology", vol.4, Becher, P. (Eds), New York 1996, 43.
- (7) Gunning, A. P., Mackie, A. R., Wilde, P. J.; Morris, V. J. *Langmuir* **2004**, 20, 116.
- (8) Knoth, A.; Scherze, I.; Muschiolik, G.; *Food Hydrocolloids* **2005**, 19, 635.
- (9) Hodge, S.M.; Rousseau, D.; *Food Research International* **2003**, 36, 695.
- (10) Aronson, M.P.; Petko, M.F. *J. Coll. Interf. Sci.* **1993**, 159, 134.
- (11) Kent, P.; Saunders, B.R. *J. Coll. Interf. Sci.* **2001**, 242, 437.
- (12) Asakura, S.; Oosawa, F. *J. Chem. Phys.* **1954**, 22, 1255.
- (13) de Hek, H.; Vrij, A. *J. Coll. Interf. Sci.* **1979**, 70, 592.
- (14) Tuinier, R.; Rieger, J.; de Kruif, C.G. *Adv. Coll. Interf. Sci.* **2003**, 103, 1.
- (15) Blijdenstein, T.B.J.; van Winden, A.J.M.; van Vliet, T.; van der Linden, E.; van Aken, G.A.; *Coll. Surf. A* **2004**, 245, 41.

- (16) Berli, C.L.A.; Quemada, D.; Parker, A. *Coll. Surf. A* **2003**, 215, 201.
- (17) Bibette, J.; Mason, T.G.; Gang, H.; Weitz, D.A. *Phys Rev Lett* **1992**, 69, 981.
- (18) Bibette, J.; Roux, D., Nallet, F. *Phys Rev Lett* **1990**, 65, 2470
- (19) Bibette, J.; Mason, T.G.; Gang, H.; Weitz, D.A.; Poulin, P. *Langmuir* **1993**, 9, 3352.
- (20) Verhaegh, N.A.M. ;Asnaghi, D.; Lekkerkerker, H.N.W.; *Physica A* **1999**, 264, 64
- (21) Leal-Calderon, F.; Poulin, P; *Curr. Op. Coll. Interf. Sci.* **1999**, 4, 223.
- (22) Poulin, P.; Bibette, J.; *Phys. Rev. Lett.* **1997**, 79, 3290.
- (23) Danov, K.D.; Petsev, D.N.; Denkov, N.D.; Borwankar, R. *J. Phys. Chem.* **1993**, 99, 7179.
- (24) Denkov, N.D.; Petsev, D.N.; Danov, K.D. *J. Coll. Interf. Sci.* **1995**, 176, 189.
- (25) Petsev, D.N.; Denkov, N.D.; Kralchevsky, P.A. *J. Coll. Interf. Sci.* **1995**, 176, 201.
- (26) Ivanov, I.B.; Danov, K.D.; Kralchevsky, P.A. *Coll. Surf. A* **1999**, 152, 161.
- (27) Bibette, J.; Leal-Calderon, F.; Poulin, P; *Rep. Prog. Phys.* **1999**, 62, 969.
- (28) Leal-Calderon, F.; Mondain-Monval, O.; Pays, K.; Royer, N.; Bibette, J. *Langmuir* **1997**, 13, 7008.
- (29) Pal, R. *Chem. Eng. Sci.* **1997**, 52, 1177.

CHAPTER 2. The Model Fluid and Measuring Instruments

One motivation for this study is the use of aggregated emulsion fluids in consumer products such as food and cosmetics. In general such products are gel-like; which can be generated in various ways. A method is to use viscosifiers in the continuous phase. Another way is to build a network of the emulsion particles present. An example has been described in a recent patent (WO 0191570). In this Unilever report reference was made to open literature. In this study we modified the emulsion system somewhat to fulfill all requirements for the study. This model fluid will be discussed below.

Furthermore, another goal of this chapter is to provide (as a complement to what will be presented also in chapters 3-5) some extra information regarding the physico-chemical characteristics of the main ingredients (surfactant and gelatin) that determined the droplets properties and a more detailed explanation of our experimental setup, which will be only briefly described in the other thesis chapters.

2.1 THE MODEL FLUID

2.1.1 Formulation of the emulsion network

Several components were used to formulate the studied water-in-oil (W/O) emulsion. The water phase contained: glycerol and gelatine and RITC (fluorescent dye). The oil phase contained an emulsifier and a flocculant. Adding the latter resulted in fluids in which the emulsion droplets were aggregated but without coalescence. These components and their role will be subsequently discussed.

While the thesis research was (partly) motivated by potential applications for the food industry, it turned out during the course of the project that we had to modify the emulsion system somewhat, to make it suitable for the microrheological AFM-CSLM studies as described in this thesis. In this context, one could describe the used emulsion as a “model system”. What were needed in the end were more-or-less homogeneous layers of roughly monodisperse droplets, which could be made to stick together with a controllable adhesive strength, and which could be visualized. Below we will elaborate on these aspects.

To control the aggregation of an emulsion, one has to start with a stable system. It has to be stable against coalescence, but also to aggregation. Whether an emulsion is stable can also be a matter of time. Our strategy was to make a stock emulsion, which could be kept for long times to allow many experiments with the

same system. To make the (stock) emulsion stable we had available a surfactant, as well as a gelling agent for the droplet (water) phase. For the oil/surfactant combination, dodecane/Span80 was chosen. Gelatin was chosen as the gelling agent (both components will be discussed in more detail in section 2.1.2).

Both Span 80 and gelatine have a direct influence on emulsion stability: SPAN 80 is an emulsifier which dissolved preferentially in the oil phase and adsorbes strongly at the W/O interface, stabilizing an W/O emulsion against coalescence and facilitating the generation of small water droplets. Coalescence is also counteracted by the dissolution of gelatine in the discontinuous water phase. In this way the (apparent) viscosity of that phase is increased strongly, with the consequence that the drainage of a fluid film in between emulsion droplets is hampered if a coalescence event sets in.

There are also (potential) indirect effects: gelatin may influence the adsorption of Span at the O/W interface. In addition, the ability of droplets to deform can also influence their interaction strength (as already discussed in chapter 1). Chapter 3 describes our study into the stability and deformability of water/dodecane droplets as a function of the Span80 (/oil) and gelatin (/water) contents. While this study was focused on large (100 μm) droplets, the results were translated to formulations for smaller (1 μm) droplets.

Emulsions of micron-sized droplets were prepared with an Ultrathurrax. To make gelatin-containing droplets, the emulsion had to be prepared from preheated phases, and mixed also at elevated temperature, to keep the aqueous phase liquid-like until the final droplets had been formed. The resulting droplet size distributions were rather polydisperse. To make the system more monodisperse, the emulsions were fractionated using differences in the sedimentation speeds for droplets of unequal size.

A simultaneous requirement was that the droplets should have favorable optical properties for visualizing them with a microscope, even at optical depths corresponding to many droplet diameters. Given the available (confocal scanning laser) microscope (see section 2.3.1.2) the choice was made to stain the droplets with trace amounts (concentration 0.05wt%) of fluorescent molecules. Here RITC (Rhodamine Isothyocyanate) was chosen, in view of the available laser wavelength (568 nm), its low/modest photobleaching and its preference for solving in water rather than oil. Deep optical penetration into emulsions of 1 micron droplets is only possible if the refractive indices of the droplets and of the continuous phase are nearly equal: if not, then the light scattering by the droplets will give rise to a noticeable turbidity (i.e. blurred objects) even for layers of just a few tens of microns thick. (Near) refractive index matching was achieved by adding glycerol (55wt% ratio to water) to the aqueous phase, after it had been verified that the aqueous phase still formed gels in its presence.

From these stable emulsions of (on average) 1 μm droplets, weakly aggregated systems were made by adding to the oil phase a “floculant”, at a targeted concentration. Silicone oils (PDMS) were selected as flocculants, after phase behavior experiments had shown that aggregated emulsions could be obtained above a (low) threshold concentration c^* , and that lowering the PDMS concentration below c^* was sufficient to restore the dispersed state. The low value of c^* was favorable, in that it allowed to vary the aggregation strength for the same (batch emulsion) droplets, without changing the refractive index of the continuous phase too much: in this way, the aggregation strength and the optical properties were practically “decoupled”.

In making thin droplet layers, simple use could be made of gravity settling, due to the mass density difference between the aqueous and oil phases. Even individual droplets of micron size experience a sufficiently high gravity force (and a sufficiently low viscous drag) to make them settle at speeds that allow them to reach the substrate overnight. Also the droplet sedimentation length is small enough to ensure that practically all droplets will end up at the bottom. This served to make a more-or-less sharp interface between a droplet layer and a clear liquid. In addition it allowed to roughly predict the thickness of the layer, from the criterion of mass conservation. The only unknown here was the droplet packing fraction in the layer that resulted from the sedimentation.

Rather than allowing the emulsions to aggregate in bulk, and the aggregates to settle and form a layer, we followed a strategy in which the attractive interdroplet forces were kept as weak as possible, until the layer had been formed. This resulted in dense and regular layers. Subsequently (extra) flocculant was carefully added to the system, to allow the droplet-droplet bonds to become stronger.

2.1.2. Materials and preparation

The provenience of materials and the specific preparation details are given further in each chapter, depending on the systems used for our studies. With the following two paragraphs we aim to describe shortly the main physical-chemical properties of the surfactant and gelatin.

2.1.2.1. Sorbitane monooleate (Span 80)

Many properties of Span80 are already known, and the fact that knowledge was already available spoke in favor of selecting this surfactant. Although from what follows it might seem that this choice brought some complications for our system, since we were aware of certain problems we could find our way to circumvent these.

Span 80 is a mixture of different sorbitane esters [1]. The main component of Span 80 is sorbitane monooleate, it has a linear structure of length ~ 2.5 nm and one unsaturated bond. It is a non-ionic surfactant with the hydrophilic-lipophilic balance $HLB = 4.3$. In principle, Span 80 is oil soluble, so it should dissolve in “dry” dodecane into a clear solution, but the sorbitol component is strongly hydrophilic and precipitates spontaneously from the organic medium [1]. To remove this component, we prepared a 20wt% solution of Span 80 in dodecane, left it for one month to precipitate and afterwards centrifuged it for 2 hours at a speed of 20.000 rot/min. The clear solution was separated carefully from the precipitate and the new concentration was determined by weighing. The loss was about 0.5wt%. The clear solution was diluted further to 1 wt% solution (or other concentrations, when needed). Abou-Nemeh et al. studied the microstructures formed by Span 80 in dodecane [2]. Light scattering experiments give a typical size of 5 nm, indicating that micelles are formed.

Opwale and Burges studied the influence of Spans interfacial properties on water-in-oil emulsion stability [3]. Their experimental results showed that Span 80 is still changing its interfacial elasticity even after 2 hours, first 10 minutes very fast and afterwards slowly, so molecular reorganization still takes place.

In the above cited references [1-3] about 0.45-0.8% Span 80 was used to stabilize a 50% water-in-dodecane emulsion, and 5% Span 80 gave aggregated emulsions at this volume fraction. The critical micelle concentration (CMC) of Span 80 in dodecane was determined by us (see chapter 3) as being around 0.17mM ($\sim 10^{-3}$ wt%). Above this concentration, micelles are formed that can play a role in the aggregation of the emulsion droplets. We have tried to utilize these micelles for preparing flocculated sediments, but they turned out to be so weak that we had to find another flocculating agent that induced stronger depletion forces.

In table 2.1 we present some of the physical-chemical characteristics (the surface pressure π at CMC, the area per molecule A at CMC, the Gibbs free energy of micellization ΔG_{mic} and the Gibbs free energy of adsorption ΔG_{ad}) of Span 80 at the water-dodecane interface, determined by Peltonen et al [4].

Table 2.1: Characteristics of Span 80 at water-dodecane interface for the CMC

π (mN/m)	A (10^{-20} m ²)	ΔG_{mic} (kJ/mol)	ΔG_{ad} (kJ/mol)
30.5	37	-26.6	-37.9

2.1.2.2. Gelatin

Gelatin is a biopolymer derived from collagen and is extracted from (pig, fish, etc) ossein by either acid or base hydrolysis. Structurally, gelatin molecules contain repeating sequences of glycine-X-Y triplets, where X and Y are frequently proline and hydroxyproline amino acids. These sequences are responsible for the formation of triple helical structures that build up further into gels (providing the temperature is below ~ 40 °C), where the helical regions form in the gelatin protein chains immobilizing water. The water molecules are placed in interstitial positions and stabilize the triple helices by establishing hydrogen bonds between adjacent chains. Also the polar groups such OH, NH₂, CO and the charged NH⁺ or COO⁻ groups interact with water molecules in solution (coil conformation) by making hydrogen bonds or via dipolar interactions. [5]

The gelatin molecule comprises positive (arginine, lysine), negative (glutamate, aspartate), hydrophilic (hydroxyprolyne, serine) and hydrophobic (glycine, proline, alanine) amino acid subunits. Consequently, gelatin molecules are amphoteric, carrying simultaneously both negatively and positively charged groups with a net charge depending on the pH of the solution. The isoelectric point (IEP) is the pH value at which the molecules are neutral (in our case, the IEP was around 5).

Experimental results of Olijve et al [6] suggest that gelatin hydrophobic sites have a good affinity to hydrophobic n-dodecane. However, despite its amphoteric character and the presence of hydrophilic and hydrophobic chains, gelatin is generally accepted as being a poor emulsifier.

Gelatin molecules are well soluble in water where they dissociate if the temperature is above ~ 40 °C. Joly-Duhamel et al [7] showed that mixing glycerol into the gelatin solution has as effect a slight shifting of the gelatin gel melting

temperatures. This effect did not affect our experiments. On reducing temperature, physical gels are formed thermoreversibly. Images of gelatin gel networks were obtained by Djabourov et al by means of TEM [8].

The most important attribute of gelatin is its gel strength and the standard parameter used by the manufacturers to characterize it is the Bloom Strength. Another way to do it is by means of rheological measurements. The main parameters that determine the strength of a gelatin gel are the gelatin concentration and the time they are left to gel. The higher the concentration of gelatin molecules, the larger the number density of triple helices that can form and such, the stronger the gel will be. In a similar manner, for a given gel, the longer the ageing time, the bigger the chance of internal molecular rearrangements in such manner that more triple helices are formed, so ageing determines the stiffening of the gels.

Ageing has a strong influence on the elastic (G') and loss (G'') modulus of gelatin. Rheological measurements on our macroscopic 10% gelatin gels show that within 10 days, G' increased from 3.75 kPa to 34.5 kPa and for a 30% gel G' increased from 24 kPa to 112 kPa. The limit of the saturation for the G' , G'' is not known thus, but we can assume that after 3 months of ageing (the time between the preparation and first experiments) further changes are extremely small and can be considered negligible.

Finally, macroscopic gelatin gels are biodegradable. The macroscopic gels that we followed for describing their ageing could not be studied on a longer term (than 10 days) due to contamination of the macroscopic gelatin gel with bacteria that determined the breaking of the network and loss of its elasticity [9]. This was not the case for our emulsions, where the microscopic gelatin network formed inside the droplets was protected by the continuous oil phase against bacteria present in the air.

2.3. EXPERIMENTAL TECHNIQUES

2.3.1 Atomic Force Microscopy

The Atomic Force Microscope (AFM) is an instrument that operates by measuring attractive or repulsive forces between a tip and a sample [10]. The rigid connection of the tip to a cantilever (a leaf spring) allows to determine the force from the measured cantilever deflection and the known spring constant. The resolution of this vertical deflection is generally in the nanometer range, which allows to measure forces down to the picoNewton range. To bring the tip close enough to the surface so that the forces can be measured, the other end of the cantilever is driven by piezo electronics.

To achieve the high (positional or force) resolution, most AFMs today use the optical lever, a device that achieves a resolution comparable to that of an interferometer [11,12]. The optical lever operates by reflecting a laser beam off the cantilever. Angular deflection of the cantilever causes a twofold larger angular deflection of the laser beam. The reflected laser beam strikes a position-sensitive photodetector consisting of two side-by-side photodiodes. The difference between the two photodiode signals indicates the position of the laser spot on the detector and thus

the angular deflection of the cantilever (see figure 2.1a). Because the cantilever-to-detector distance generally measures $O(1000)$ times the length of the cantilever, the optical lever greatly magnifies motions of the tip.

The functional principle of an Atomic Force Microscope (AFM) is monitoring the mechanical interaction of a very sharp tip with the studied surface. Perhaps the best known application is the one in which the tip is horizontally scanned over a hard (profiled) surface, and the deflection signal is used to measure the surface topography. Besides this application for high resolution imaging, AFM has also another very important application: the so-called force-distance mode. In this mode, the cantilever base is driven vertically, while the cantilever deflection is continuously monitored. The AFM modes are extensively described in the review paper by Capella et al [13].

In the present thesis, AFM is used in force-distance mode to study the interaction forces in systems of colloidal particles. Also colloidal interactions between the tip and a surface have been measured. The latter experiment is sketched in figure 2.1b. When the tip approaches the surface, the cantilever will at a certain point bend under the repulsive or attractive forces exerted by the substrate surface. Eventually the repulsive force will dominate. The presence of the repulsive regime allows to define a “contact point” from the force-distance curve. Different (operational) definitions for this point are possible, also depending on the system [13].

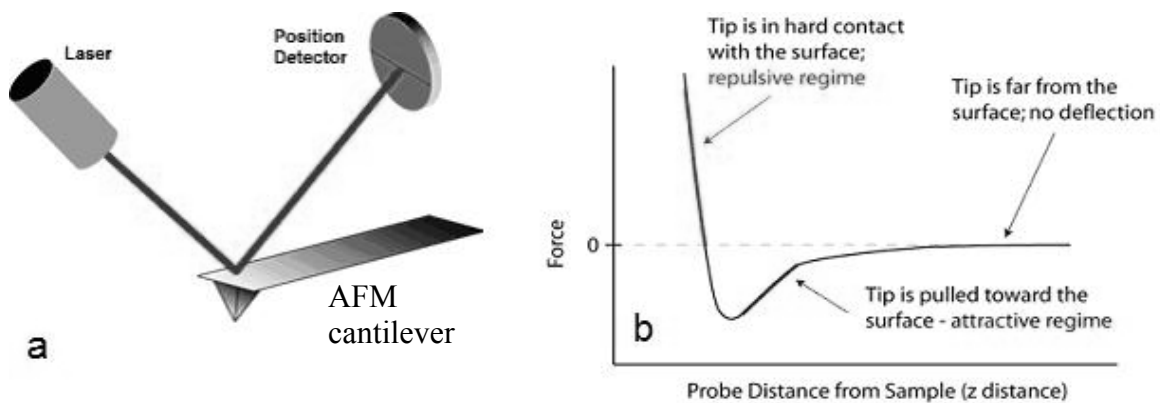


Figure 2.1. a) Cantilever deflection ; b) Force-distance curve [15]

For soft samples (i.e. that deform under the AFM load), the location of the contact point is also needed to define the indentation (i.e. how deep the tip penetrates into the material). Since the indentation describes exclusively the deformation of the material, this is also the quantity that appears in physical models that relate the AFM measurements to the mechanical properties of the material. A well-known example hereof is the Hertz law, which applies to elastic solids, and from which the Young's modulus can be calculated. This model has been used to measure or estimate the elastic properties of many soft samples like polymer gels [14], even in cases where the samples were not purely elastic.

In soft condensed materials, in which the mechanical behavior is dominated by structures at lengthscales in the (sub) micron range, conventional AFM tips (with a curvature radius of 20-50 nm at the apex) are not always the most suitable. For this reason, also cantilevers with modified tips have been used, the modification

consisting in many cases of (1-10 μm) large colloidal spheres attached to the tip or directly to the cantilever beam. Ducker et al. [16] were the first to report on experiments in which a colloidal probe was attached to the AFM cantilever. Ever since, this “Colloidal Probe AFM” has been extensively used to measure colloidal forces between rigid surfaces in solution [17]. More recently, also forces between a colloidal probe and a liquid interface have been measured [18a-c]. The interpretation of these measurements is more complicated, due to the more extended degrees of freedom for a liquid interface to deform: also wetting phenomena, viscous dissipation and film rupture can come into play. To attach a hard colloidal probe to the cantilever, gluing techniques are generally used. For soft particles and droplets such an attachment has to be achieved using the wetting properties of the droplets [19].

Force distance-curves are always recorded at finite speeds. In the simple case of a purely elastic sample, the measured curve will correspond to a (quasi-)static force equilibrium, regardless of the speed of the up-down ramp. For viscoelastic materials, or for systems immersed in liquid, both viscous and elastic forces may come into play. The magnitude of the viscous forces will be proportional to the viscosity and the deformation speed (for a given flow pattern). One way to assess their importance is therefore, to measure the force distance curve at various speeds. A well-known example of viscous contributions to force-distance curves is the so-called “baseline split”, measured at large distances from the sample: this is due to the hydrodynamic drag of the cantilever.

Two kinds of AFM measuring heads were used for the experiments to be described in the forthcoming chapters. For the droplet deformation experiments (chapter 3), a previously developed (for single molecule imaging) compact AFM-head based on the stand-alone principle [20], was used to measure forces between a spherical indenter and individual O(100 μm) large aqueous emulsion droplets in dodecane / Span 80 oil phase. This AFM was used in combination with a conventional inverted microscope to position the AFM probe with respect to the emulsion droplet.

For the droplet network deformation experiments (chapters 4 and 5), a much bigger ramping amplitude range (20 μm) was needed, while also compatibility with a Confocal Scanning Laser Microscope was needed, to allow visualization of both the cantilever and the deformations in the droplet network during compression, relaxation and decompression. For this purpose, a new AFM head was designed and built. In this new setup, a piezostage with XYZ position feedback is fixed to the CSLM table and an AFM deflection module is mounted on top of it (figure 2.2).

For compression experiments, we used cantilevers with attached borosilicate glass spheres supplied by Novascan Technologies, Ames, USA. We started with a rather large range of spring constants: $k = 0.01\text{-}0.1$ N/m and particle diameter: $d=1\text{-}10$ μm . The values of the cantilevers’ spring constants, calculated using the thermal excitation spectrum, agreed within 10% with the ones given by the supplier. Further particular details about the chosen spring constant, ramping amplitude or ramping speed will be given in each experimental section of chapters 3, 4 and 5.

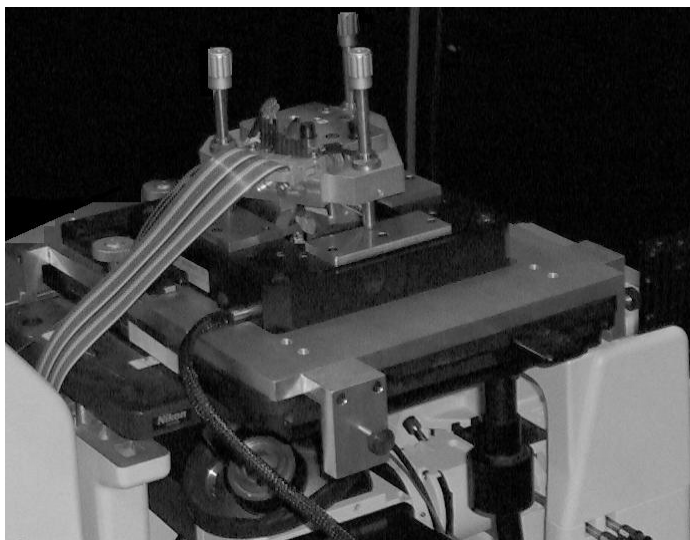


Figure 2.2. Photo of the home-made AFM head

2.3.2. Confocal Scanning Laser Microscopy

Confocal Scanning Laser Microscopy (CSLM) (see figure 2.3 for an illustration of the principle) is a valuable tool for obtaining high resolution images and 3-dimensional (3D) reconstruction of a variety of specimens. In CSLM, a laser beam is focused through a high-resolution objective onto a 2D plane (optical section) within the specimen, and scanned across this plane by means of a mirror, acousto-optical deflector or a spinning disk with pinholes. Generally, both the illuminating light and the light returning from the specimen are focused onto a pinhole. This pinhole acts like a spatial filter, blocking out-of-focus light from reaching the detector, thus restricting the depth of the image. Hence, much of the out-of-focus light is prevented from contributing to the image. In many cases, confocal microscopy is combined with fluorescence. By labeling the component(s) of interest with a fluorescent dye that has an excitation spectrum near the wavelength of the laser, one can obtain very selective images. This selectivity is further enhanced by bandpass filters which separate the reflected laser light from the emitted fluorescent light.

Our CLSM equipment (Ultraview, from Perkin Elmer, UK) consisted of a Yokogawa CSU10 confocal module connected to the side port of a Nikon Eclipse TE200 inverted microscope. With the mentioned confocal module, the laser beam is swept across the image plane by means of a fast scanning double disk, one with pinholes and the other with microlenses. This allows simultaneous illumination of many spots with high brightness, and hence short image acquisition times (a typical exposure time per image was 100 ms). For the objective we used a 100x, N.A. 1.30 oil immersion objective, mounted into a high speed, computer-controlled PI piezoscanner, which allowed for reproducible vertical displacements of the objective, with submicron resolution. The fluorescent RITC dye inside the droplets is excited with a Kr laser ($\lambda=568$ nm). The confocal images (672 x 512 pixels, each pixel corresponding to (130×130) nm² were recorded with a Hamamatsu CCD camera and stored into the computer as 12-bit tiff files. Generally, image quality was good enough

(and image capture rate high enough) to display live images on the computer screen. Both Z-series (i.e., stacks of images taken at consecutive Z-positions inside the samples) and time-series (i.e., images recorded at a fixed Z-location, but at consecutive moments in time) were recorded. The stability of the microscope in XYZ was ensured by means of a passive vibration damping table (using air pressure), and turned out to be good enough to allow accurate comparisons of the droplet network structure before, during and after indentation with the AFM probe. This allowed to analyze the 3D image data via intensity difference maps.

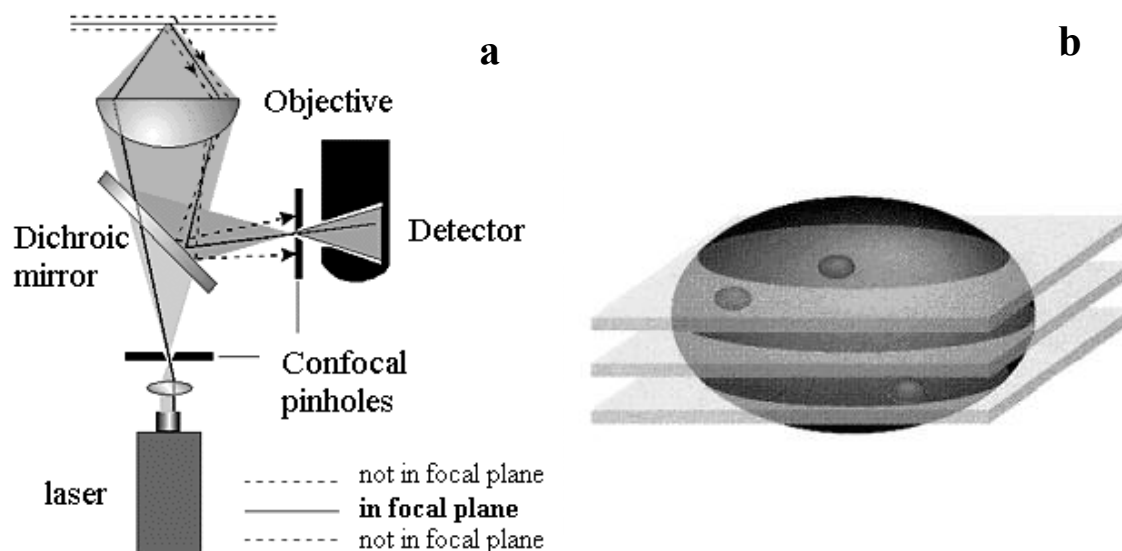


Figure 2.3. a) The principle of an inverted confocal laser scanning microscope [21a];
b) Optical sectioning of a sphere by confocal planes [21b]

The XY resolution of our CSLM images was comparable to the wavelength of the Kr laser, good enough as to be able to resolve clearly individual (non-aggregated) particles having diameters above approximately 500 nm. The resolution in height (on Z axis) was slightly less, but serving well our purposes. Z-position scanning was done with steps of 0.5 μm up to a height of 30-40 μm . Despite the powerful resolution possibilities of the instrument, for the aggregated emulsions it was difficult to distinguish each individual droplet (although the large majority of the droplets had a diameter between 1-3 μm) in the aggregate and for this reason we followed rather the local distortion of the network than the movement of each particle. Moreover, the optical depth could not be improved to further than $h \sim 25 \mu\text{m}$ (above the glass slide), due to the (multiple) scattering of the laser light by many droplets. We adapted our experimental conditions to these two limitations by choosing an appropriate height for the sediment so the top could be visualized, and by matching as good as possible the refractive index of the water and the oil phase.

2.3.3 AFM-CSLM combined

The combination of the two microscopic techniques, i.e. AFM and CSLM, is becoming a more and more a popular tool in biology, physics and biophysics when it comes to imaging small samples like individual cells or tissues [22]. However, hardly any research has been done up to now, in using AFM as a tool to determine mechanical (i.e. microrheological) characteristics of samples in combination with the benefits of the CSLM in following the 3D deformation of the sample during and after indentation.

One set of studies to be mentioned here is that of Vinogradova et al [23-26]. They studied the deformation of filled polyelectrolyte microcapsules indented with a colloidal probe. The confocal microscope was used to center the position of the colloidal sphere above the apex of the capsule by using graticule lines for alignment. Their capsules had a diameter of $4.5\mu\text{m}$, while the colloidal probe had a diameter of $40\mu\text{m}$. They compared the stiffness of hollow vs. filled capsules [23], the influence of the molecular weight and ageing effects [24], of the capsule radius and shell thickness [25] and the concentration of the inner polyelectrolyte solution [26].

In this thesis, the CSLM was used for studying the 3D network morphology in real time. As a rule, also the AFM probe sphere could be visualized with the CSLM, making use of the fluorescence contrast with its surroundings. CSLM imaging was done “simultaneously” with the AFM measurements, using separate computer controls for the two microscopes. Our goal was to use the CSLM for observing the extent of the network deformation under the pressure applied by the colloidal probe of the AFM, as well as the eventual “breakups” at the weaker points of the network. Figure 2.4 presents a simplified sketch of the AFM-CSLM combination used for our study. Further details about the experimental setup are given in each chapter, according to the specific AFM instrumentation that was used.

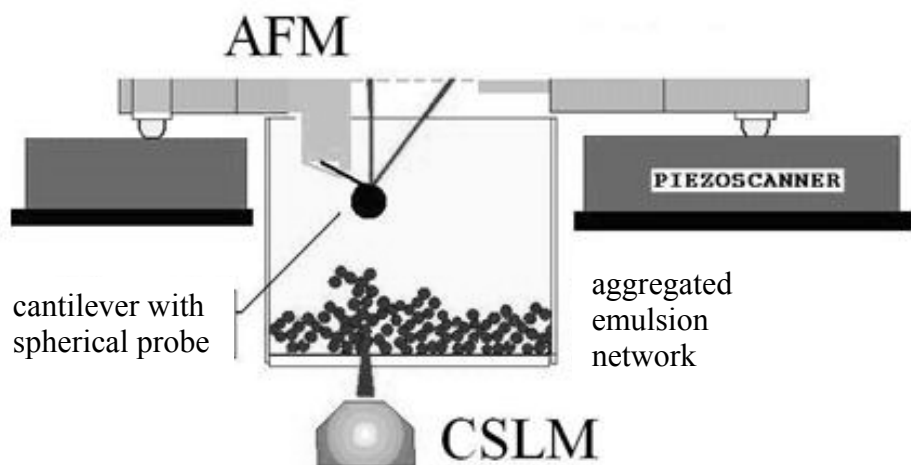


Figure 2.4. AFM-CSLM combination used for our compression experiments into aggregated emulsion sediments

REFERENCES

- (1) Abou-Nemeh, I.; van Peteghem, A.P. *Chem. Ing. Tech.* **1990**, 62, 420.
- (2) Abou-Nemeh, I.; Bart, H.J. *Langmuir* **1998**, 14, 4451.
- (3) Opwale, F.O.; Burgess, D.J. *J. Colloid Interface Sci.* **1998**, 197, 142.
- (4) Peltonen, L.; Hirvonen, J.; Yliruusi, J. *J. Colloid Interface Sci.* **1998**, 240, 272.
- (5) Djabourov, M.; Leblond, J.; Papon, P. *J. Phys. France* **1988**, 49, 319.
- (6) Olijve, J.; Mori, F.; Toda, Y. *J. Colloid Interface Sci.* **2001**, 243, 476.
- (7) Joly-Duhamel, C.; Hellio, D.; Djabourov, M. *Langmuir* **2002**, 18, 7208.
- (8) Djabourov, M.; Bonnet, N.; Kaplan, H.; Favard, N.; Favard, P.; Lechaire, J.P.; Maillard, M.; *J. Phys. II France* **1993**, 3, 611.
- (9) Nellisen, R.; *Master thesis* **2001**.
- (10) Binning, G.I.; Quate, C.F.; Gerber, C. *Phys. Rev. Lett.* **1986**, 56, 930.
- (11) Meyer, G.; Amer, N.G. *Appl. Phys. Lett.* **1988**, 53, 1045.
- (12) Alexander, S.; Hellemans, L.; Marti, O.; Schneir, J.; Elings, W.; Hansma, P.K.; Longmire, M.; Gurley, J. *J. Appl. Phys.* **1989**, 65, 164.
- (13) Capella, B.; Dietler, G. *Surf. Sci. Rep.* **1999**, 34, 1.
- (14) Uricanu, V.I.; Duits, M.H.G.; Nelissen, R.M.F.; Bennink, M.L.; Mellema, J., *Langmuir* **2003**, 19, 8182.
- (15) from <http://www.nanoscience.com/education/AFM.html>
- (16) Ducker, W.A.; Senden, T.J.; Pashley, R.M. *Nature* **1991**, 353, 239.
- (17) Andersson, K.M.; Bergstrom, L.; *J. Coll. Interf. Sci.* **2002**, 246, 309.
- (18a) Mulvaney, P.; Perera, J.M.; Biggs, S.; Grieser, F.; Stevens, G.W. *J. Colloid Interface Sci.* **1996**, 183, 614.
- (18b) Snyder, B.A.; Aston, D.E.; Berg, J.C. *Langmuir* **1997**, 13, 590.
- (18c) Hartley, P.G.; Grieser, F.; Mulvaney, P.; Stevens, G.W. *Langmuir* **1999**, 15, 7282.
- (19) Dagastine, R.R.; Stevens, G.W.; Chan, D.Y.C.; Grieser, F. *J. Coll. Interf. Sci.* **2004**, 273, 339.
- (20) Werf, K.O., van der; Putman, C.A.J.; Grooth, B.G., de; Segerink, F.B.; Schipper, E.H.; Hulst, N.F., van; Greve, J. *Rev. Sci. Instrum.* **1993**, 64, 2892.
- (21a) from <http://paperproject.org/slcmtechnology.html>
- (21b) from <http://www.mih.unibas.ch/Booklet/Booklet96/Chapter1/Chapter1.html>
- (22) You, H.X.; Lowe, C.R.; *Curr. Op. Biotechnology* **1996**, 7, 78.
- (23) Lulevich, V.; Radtchenko, I.; Sukhorukov, G.B.; Vinogradova, O.I. *Macromolecules* **2003**, 36, 2832.
- (24) Lulevich, V.V.; Nordschild, S.; Vinogradova, O.I. *Macromolecules* **2004**, 37, 7736.
- (25) Vinogradova, O.I.; Andrienko, D.; Lulevich, V.V.; Nordschild, S.; Sukhorukov, G.B. *Macromolecules* **2004**, 37, 1113.
- (26) Lebedeva, O.V.; Kim, B.S.; Vinogradova, O.I. *Langmuir* **2004**, 20, 10685.

CHAPTER 3. Influence of Bulk Elasticity and Interfacial Tension on the Deformation of Gelled W/O Emulsion Droplets *

ABSTRACT

We used AFM to study the deformation and wetting behavior of large (50-250 μm) emulsion droplets upon mechanical loading with a colloidal glass probe. Our droplets were obtained from water-in-oil emulsions. By adding gelatin to the water prior to emulsification, also droplets with a bulk elasticity were prepared. Systematic variations of surfactant and gelatin concentrations were made, to investigate their effect on the deformation and wetting behavior of the droplets, and to identify the contributions of interfacial tension, bulk elasticity and expelled water. The AFM experiments were performed in force-distance mode and showed on approach a repulsive regime which in many cases was terminated by a jump-in of the probe. In the case of pure water (*i.e.* gelatin-free) droplets, the repulsive part of the curve showed a good linearity, thus allowing the extraction of an effective droplet spring constant. This quantity was found to decrease on raising the surfactant concentration from below the critical micelle concentration (CMC) to well above the CMC, and its numerical values were found to correspond remarkably well to literature values for the interfacial tension. Our findings indicate that, on gelatin increase inside the droplets, the bulk elasticity gradually becomes dominant and droplets' stiffness does not depend anymore on surfactant concentration. Also the stability of the droplet interface against wetting, as measured by the force at which the jump-in instability occurs, was enhanced by gelatin. For gelatin concentrations $\geq 15\%$, the droplets were found to behave like purely elastic bodies. Both gelatin and surfactant contribute positively to the stability against interface breakup.

* *Published as: D. Filip, V. I. Uricanu, M. H. G. Duits, W. G. M. Agterof, and J. Mellema, in Langmuir; 2005; 21(1), p. 115 - 126*

3.1. INTRODUCTION

Emulsions form the basis of a wide variety of natural and manufactured materials, including food products, pharmaceuticals, biological fluids, agrochemicals, petro-chemicals, cosmetics, and so forth [1]. Some products such as margarine or mayonnaise may contain a high volume fraction (up to 90%) of dispersed droplets of one immiscible phase into another one. Comparing these volume fractions to typical maximum packing fractions for *rigid spheres*, it is implied that in concentrated *emulsions*, large droplet deformations must occur. The mechanical properties in such systems are set by an interplay between colloidal forces and forces due to the droplet deformability. When droplets deform as a consequence of colloidal forces, then these forces change as well, due to the modified surface distance and area involved. The consequences of this mutual dependence can be different. As long as colloidal *repulsions* dominate, the deformability will enhance the prevention of interdroplet contacts improving stability against aggregation and coalescence. However when the colloidal *attractions* dominate, the deformability will allow a larger contact area, thus increasing the adhesion strength. In practice this means that the stability of an emulsion can be drastically changed by manipulating the elasticity of the *droplet inner-phase*. However, only a few studies have so far been aimed to a closer look into the interplay between colloidal and elastic forces.

One powerful technique for studying colloidal interactions and the deformation in soft materials is atomic force microscopy (AFM). After Ducker et al. [2] reported the use of a colloidal particle attached to the cantilever to probe surface forces, Butt [3] was the first to study the deformation of bubbles and droplets under compression by a colloidal probe. Since then, several studies were reported for bubbles [4-11] and oil droplets in aqueous surroundings [12-18].

Also theoretical studies on the deformation of pinned (to a substrate) droplets or bubbles, under mechanical loading with an AFM spherical indenter, were reported. Attard and Miklavcic [19, 20] derived that the ‘spring constant’ as defined from the slope of an AFM force-distance curve, is almost equal to the interfacial tension. The forces between a rigid probe particle and a liquid interface were extensively analyzed by Chan et al [21] and Dagastine [22]. The equilibrium shape of bubbles/droplets was determined by Bhatt et al [23] using the augmented Young-Laplace equation. Bardos [24] gave an extensive analysis of how the contact angle between a pinned drop and the substrate depends on the *probe-drop* force in AFM measurements. Nespolo *et al* [18] took into account the detailed expression of the disjoining pressure and calculated the complete force-distance curves using as input Derjaguin-Landau-Verwey-Overbeek (DLVO) type potentials.

To our knowledge, no experimental studies have yet been reported on *aqueous droplets in non-polar media*, despite many industrial applications of such systems. In this chapter, we report on AFM experiments on aqueous droplets in dodecane, with Span 80 being present as the surfactant. In the first part of chapter 3, we describe the behavior of typically viscous water droplets as a model system. The second part of the chapter deal with aqueous but gelled elastic droplets. In this system, two types of stability can be defined. The first one is related to the *bond strength* between droplets which maintain their integrity. It is set by the colloidal attractions (e.g., van der Waals or polymer induced) and modulated by the droplet deformability. The second one is

the stability of the droplet interface against *coalescence*. Commonly, this type of stability is achieved via a protective layer, created by emulsifiers, proteins, copolymers, and so forth, through adsorption at the water-oil interface. Considering the long-term stability or the stability under compression, such an interfacial barrier is not always strong enough to prevent coalescence of the droplets. Another method that could improve the stability is the addition of a gelling agent to the droplet phase. Gelatin stimulates the formation of an elastic network inside the droplets, which could lead to an increased resistance against interface breakup and coalescence.

Making use of the AFM capabilities, we analyze in the present paper the influence of both the bulk elasticity and interfacial strength against breakup of water-in-oil (W/O), elastic, gelled emulsion droplets. Up till now, only the paper of Gilles and Prestidge [25] focused on both these parameters, their samples being viscoelastic poly(dimethylsiloxane) (PDMS) droplets/particles in sodium dodecyl sulfate (SDS) aqueous solutions. A key ingredient in our study is the comparison between pure water droplets and gelled droplets having various degrees of gelation strength. By varying the surfactant content around the CMC, we also varied the interfacial tension. A colloidal glass probe was used to compress into individual emulsion droplets. The diameter ratio between the droplet and the probe was chosen to be at least 10, so that the droplet interface can be regarded as a flat surface and the capillary pressure of the droplet does not play a significant role.

3.2. THEORETICAL BACKGROUND

To describe the geometric configurations adopted locally by the interface (of two otherwise immiscible liquids) as an AFM probe advances towards it, both the colloidal interaction between probe and droplet (i.e. the disjoining pressure, Π) and the surface tension γ of the W/O interface are needed. Different mechanical regimes have been mentioned in literature [19] and are briefly reviewed here. When the probe is so far away from the interface that no interaction between the two exists, the interface is undeformed. Approaching closer to the droplet, mutual probe-droplet interactions come into play and produce a local change in the droplet's curvature. If the equilibrium shape of the interface is concave, the curvature (J) is positive, while for convex curvatures J assumes negative values. The latter is anticipated for the regime addressed in the present study. The equilibrium shape of the interface is determined by the relative magnitudes of the disjoining pressure (Π , between the probe and the droplet) and the Laplace pressure ($P =$ the difference in pressure between inside and outside the droplet). For our system of aqueous droplets in oil, the Laplace pressure can be written as: $P = 2 \gamma J$.

As long as the pressure exerted by the probe is smaller than the sum ($\Pi + P$), a thin liquid layer is maintained between the glass indenter and the (deforming) droplet (see Figure 3.1a,b). For small enough pressures (or forces $F \ll 2\pi \gamma R_p$, with R_p the radius of the indenting probe), "wrapping" will occur. This refers to a compression regime where the interface profile near the probe changes its curvature, to accommodate the probe (without rupture of the interface). For this to happen, the maximum in the disjoining pressure has to satisfy the condition:

$$\Pi_{\max} > 2\gamma \left(\frac{1}{R_p} + \frac{1}{R_0} \right) \quad (3.1),$$

with R_0 the drop's initial local radius of curvature along the vertical axis. If eq. (3.1) is violated, the interaction becomes unstable and probe wetting occurs.

In the following, we will consider the regime where eq. (3.1) is satisfied. Describing the modified interface profile with a parabola, and assigning a 'wrapping radius' R_w to characterize the local curvature, R_w will change from $-R_0$ at small loads to R_p at larger loads. Assuming that the range of the repulsion which facilitates the wrapping can be characterized by a decay length κ^{-1} much smaller than R_p (i.e., $\kappa R_p \gg 1$), Attard and Miklavcic [19] derived that, on increasing the loading force (F), a (constant) minimum distance D_{\min} between the probe and the (deformed) droplet interface is reached.

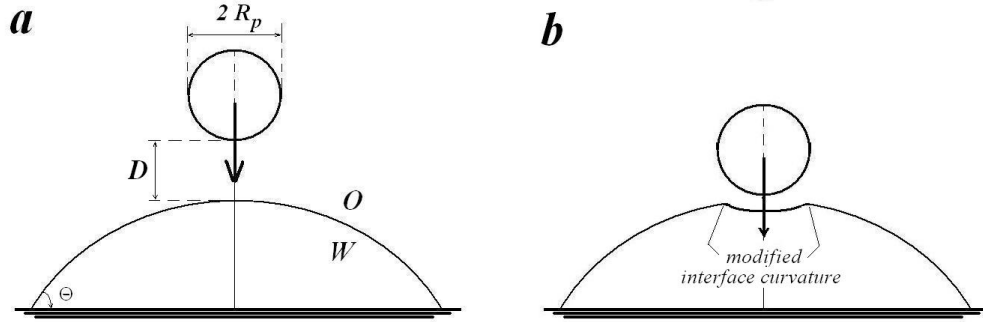


Figure 3.1. Snap-shots of the geometry encountered during probe – drop AFM experiments, with the indenting (upper) glass bead far above the O/W interface (a) and in the wrapping regime (b). (The deformation is not shown to scale.)

Using an approximation of the condition (3.1), these authors associated the minimum probe-droplet distance to a maximum disjoining pressure:

$$\Pi_{\max}(D_{\min}) \cong 2\gamma/R_p \quad (3.2)$$

and derived that any further compression will result in a linear relation between the loading force (F) and the indentation (δ) into the drop:

$$F = K_d \delta \quad (3.3)$$

where δ is measured along the droplet's central (vertical) axis and K_d is the effective spring constant of the droplet, given by:

$$K_d^{-1} = \frac{-1}{4\pi\gamma} \left\{ \ln \left[\frac{R_p}{2\kappa R_0^2} \frac{(1 + \cos\theta)^2}{\sin^2\theta} \right] + \frac{4 - 5\cos\theta + 2\cos^2\theta - \cos^3\theta}{2 - \cos\theta - \cos^3\theta} \right\} \quad (3.4)$$

with θ the contact angle of the (pinned) droplet at the substrate.

The literature-term: "constant compliance regime" refers to the interface (and droplet) compression under the condition (3.3).

For various oil/water systems, it was found that: $K_d \cong \alpha\gamma$, with $\alpha \approx 1$ (maximum deviation: 20%). The dependence of K_d on R_p , R_0 , κ and θ turned out to be weak around the working points of the studies cited in reference [19]. For systems with a repulsion other than electrostatic (e.g., contact in air) the boundary radius of the wrapping regime is different but the (almost) quantitative correspondence between the spring constant and the interfacial tension should be retained according to ref. [19].

Application to an aqueous drop in oil

Looking at eq. (3.4) the question is, which repulsion type and with which corresponding decay length κ^{-1} is responsible for entering the wrapping regime. This κ^{-1} has to be used for predicting K_d from eq. (3.4). We have attempted to estimate it for our system of a glass probe interacting with an aqueous drop in dodecane.

One possibility is that electrostatic interactions (i.e., likewise charged surfaces) provide a sufficiently strong repulsion. Calculating the Debye length however requires knowledge of the electrolyte concentration(s) in the dodecane. In view of the low dielectric constant of dodecane (i.e., 2.0), this can only involve small numbers of ions, which are difficult to measure. Instead of making a theoretical calculation, we have attempted to estimate a typical decay length κ^{-1} from our AFM force-distance curves. For pure water droplets, the ascendant part of the *cantilever deflection (D) versus piezo displacement (Z)* curve (from now on termed D-Z curve) showed deviations from “*constant compliance*” for piezo displacements between 30 and 200 nm, corresponding to ≈ 170 nm tip displacement, but this 170 nm could also include some droplet deformation. For the hard (glass) substrate, the D-Z curve showed a typical non-linear part of 30-50 nm. These numbers suggest a typical κ^{-1} ranging in between 10 and 100 nm. Combining this with typical values of $R_p = 2.5 \cdot 10^{-6}$ m ; $R_0 \approx 25 - 125 \cdot 10^{-6}$ m; $\theta \approx 120 - 150^\circ$, we obtain:

$$K_d^{-1} \approx (0.55-1.09) \gamma^{-1} \text{ or } K_d \approx (0.92-1.82) \gamma.$$

In any case there will be a steric repulsion due to the (Span 80) surfactant adsorbed at the interface. Assuming that this repulsion determines the wrapping regime, a decay length κ^{-1} of 1-3 nm should be used, corresponding to:

$$K_d^{-1} \approx (0.82-1.27) \gamma^{-1} \text{ or } K_d \approx (0.79-1.22) \gamma.$$

3.3 EXPERIMENTAL SECTION

3.3.1. Materials and sample preparation

Analytical grade (99+% purity) dodecane was obtained from Aldrich. The Span 80 surfactant (sorbitane monooleate), purchased from Fluka, had an HLB value of 4.3. Gelatin powder (from alkali-treated source, isoelectric point at pH = 5 and Bloom strength of 180 g) was kindly provided by Delft Gelatin BV, The Netherlands.

Water in oil emulsions were prepared at 60°C by slowly pouring a “water phase” into an “oil phase” while mixing with a magnetic stirrer at a speed of 1000 rpm for 5 minutes. The water phase consisted of either pure Milli-Q water, or of a gelatin solution herein. Gelatin solutions were prepared as follows: a known amount of gelatin powder was left to soak in water for 30 minutes and was then kept for 1 h in an oven at 60 °C to dissolve the gelatin granules, after which the hot liquid solution was homogenized by stirring. The “oil phase” consisted of dodecane and Span 80 surfactant. Several oil phases were prepared, at different surfactant concentrations. To avoid gelation upon mixing, the oil phase was preheated to the same temperature as the gelatin solution. “Fresh emulsions” thus prepared were directly transferred to the AFM cell, as described below. Table 3.1 summarizes the formulations of the studied emulsion samples (1 wt% Span 80 = 23.3mM).

Table 3.1. Composition and index of the studied emulsion samples

Surfactant concentration in dodecane (mM)	samples index, aqueous phase					
	Pure water	Gelatin gels (wt% of the polymer in water)				
		5% gel	10% gel	15% gel	20% gel	30% gel
0.023	<i>A1</i>	<i>B1</i>	<i>C1</i>	<i>D1</i>		
0.12	<i>A2</i>	<i>B2</i>	<i>C2</i>	<i>D2</i>	<i>E2</i>	<i>F2</i>
0.17	<i>A3*</i>					
0.23	<i>A4*</i>	<i>B4</i>	<i>C4</i>	<i>D4</i>	<i>E4</i>	<i>F4</i>
1.16	<i>A5*</i>	<i>B5</i>	<i>C5</i>	<i>D5</i>		
2.33	<i>A6*</i>					

* Formulations for which spontaneous emulsification was seen (see details in the text).

The range of surfactant concentrations used in preparing the samples was adjusted according to observations done in preliminary experiments. For smaller (than 0.023 mM) surfactant concentration, the water phase has a high affinity for the AFM indenter and the recordings are disturbed by snap-into-contact jumps so large that the reflected laser beam does not fall on the detector anymore. On the other extreme, for larger amounts of Span 80 in the oil phase, spontaneous emulsification (SE) is stimulated even for the gelatin-containing droplets.

A few more comments are worthwhile to add regarding this last issue. In another study performed by us [26], it was seen that, above certain threshold values of the Span 80 concentration, immersion of water or water/gelatin droplets under dodecane with Span 80 stimulates the formation of small (around 600 nm diameter) satellite droplets at the surface of the aqueous reservoirs. For the surfactant concentrations used in the present study, SE was observed only for a few samples (see Table 3.1). The extent of the SE process is far less than what was reported for high surfactant concentrations. Here only a small number of SE tiny droplets are formed and most of them tend to roll-over the curved surface of the mother-reservoirs, leaving a “clean” (free from satellites) interface between the oil and the aqueous phase. Measuring on clean interfaces excludes any possible extra-influence (on the AFM data) coming from SE.

Glass slides were used as substrates to attach the emulsion droplets. Before mounting in the AFM liquid cell, the substrates were cleaned with Piranha solution for 15 minutes, extensively washed afterwards with water and ethanol and dried under nitrogen. For each given formulation, few hundred microliters of the emulsion were inserted (with a syringe) in the corresponding oil phase (1 ml, thermostated at room-temperature) already placed in the AFM cell. All samples were left to equilibrate overnight as to allow the emulsion droplets to settle on the glass. Meanwhile, also the gelation process inside the gelatin-containing droplets progressed. In all cases experiments were performed after 24 h from preparation, meaning that there are no differences in the aging history among our samples.

3.3.2. Methods

A home-built AFM equipment, based on the stand-alone principle [27], was used to measure forces between a spherical indenter and individual water-based emulsion droplets in dodecane / Span 80. During experiments, the sample is kept immobile while the *xyz* piezoscanner makes controlled cantilever movements. For compression experiments, we used cantilevers having a spring constant: $K_c = 0.1$ N/m, with attached borosilicate glass spheres (5.1 μm diameter) The roughness of these beads has been checked by the manufacturer, by ourselves with Scanning Electron Microscopy (SEM) and by other users with AFM and indicated the absence of sharp substructures. The values of the spring constants were checked (using the thermal excitation spectrum) and found to agree with the ones given by the supplier (Novascan Technologies, Ames, IA USA). Before each experiment, the cantilever was rinsed thoroughly with ethanol and left to dry at room temperature. To allow thermal and adsorption equilibration, the cantilever was then immersed and left for 30 min. in the oil phase, far above the substrate / droplets.

The results reported in the present chapter are based on data acquisition during approach-retraction cycles with a constant velocity (in the z-direction): 4.6 $\mu\text{m/s}$, of the cantilever base. To explore the significance of hydrodynamic forces and/or droplet visco-elasticity, a few experiments with higher (up to 12.4 $\mu\text{m/s}$) velocities were performed. For gelatin-containing droplets, curves measured at the different speeds superimposed nicely. For one selected pure-water droplet, it was observed that increasing the speed from 4.6 to 9.2 $\mu\text{m/s}$ or higher led to a smaller initial slope of the D-Z curve. However, for 3 nN or higher (i.e., the most relevant part of the curves for the present study, see sec. 3.4.1.), the slopes became identical. Each AFM scan provided 256 D-Z curves at different spots on an area of 1 μm^2 of the droplet. Prior to and after each set of experiments on the droplets of a given sample, the deflection sensitivity of the cantilever was determined by recording few D-Z curves on the bare glass substrate, in the same AFM cell.

Our AFM setup includes a built-in, inverted optical microscope with 10x magnification. This allows us to select the droplet and precisely position the cantilever above the droplet center. Moreover, it reassures that the measurements are done on droplets non-affected by spontaneous emulsification.

In our AFM experiments, for each given composition, droplets with different diameters were sampled. To facilitate centering and to minimize capillary pressure effects, only large droplets (with diameters between 50 and 250 μm) were chosen. All

droplets were observed with the microscope to maintain a circular cross section. Most of them appeared to be well attached to the substrate, as evidenced by the absence of droplet movement under compression with the AFM.

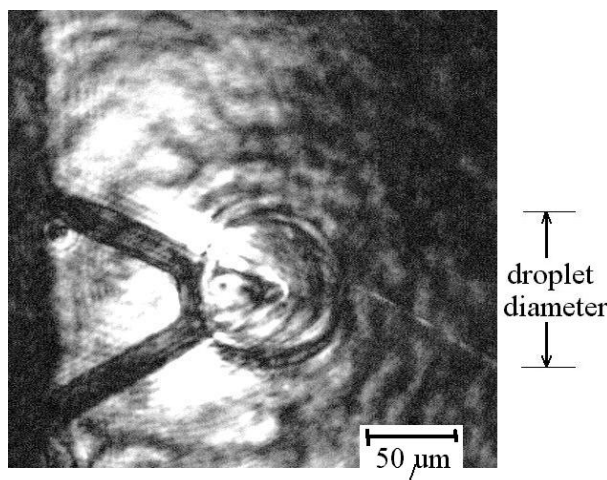


Figure 3.2. Optical (transmission) image of a triangular cantilever centered on the top of a water droplet

The few droplets that were *not* attached to the glass bottom showed a clear lateral movement under compression. Presumably, adhesion of these droplets was still prevented by a thin film of oil (plus surfactant). Figure 3.2 shows the image of a droplet and the cantilever (dark triangle-shaped), recorded with the CCD camera attached to the optical microscope. Due to its size, smaller than the cantilever width ($\approx 20\mu\text{m}$), the colloidal probe is not visible in Figure 3.2.

3.4. RESULTS AND DISCUSSION

3.4.1. Deformation of water droplets

3.4.1.1 General behavior

Systems A1-A6 (water droplets in dodecane with Span 80) showed similarities in their mechanical behavior upon loading with a glass probe. Some representative D-Z curves, at different Span 80 concentrations, are presented in Figure 3.3.

At low Span 80 concentrations ($\leq 0.12\text{ mM}$), a strong attractive force caused the probe to jump into contact with the water droplet on almost all approaches (jump-in frequency 90-100%). In a few cases ($< 10\%$) the interface showed a resistance before the jump-in (like in Figure 3.3a). The associated maximum force could reach values up to 3-5 nN.

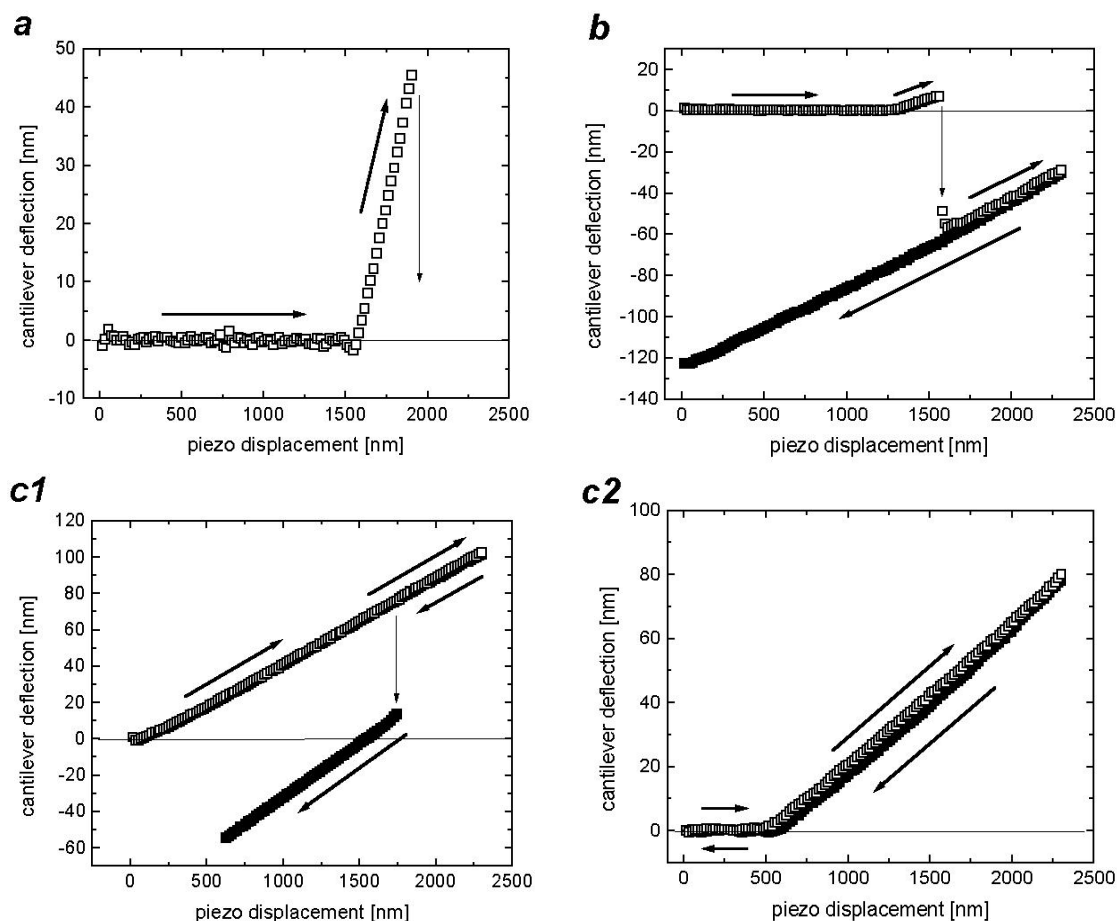


Figure 3.3 Typical D - Z curves for water droplets in dodecane, as a function of surfactant concentration: 0.12 mM (a), 0.23 mM (b) and 2.33 mM (c1, c2). Approach curves, open symbols; retract curves, closed symbols. At the lowest Span 80 concentration, the retraction curve could not be registered as the probe was unable to snap out of contact. At the highest surfactant concentration, snap-in and snap-out events were only rarely observed. In panel c1 snap-in occurs upon retracting.

On retraction, the force holding back the tip was so large that a piezo travel of 2 microns was insufficient to get out of contact. Snap-out had to be forced manually here. At a Span 80 concentration slightly above 0.12 mM, it was possible to obtain some curves without snap-in (jump-in frequency about 30%). At much higher Span 80 concentrations (≥ 1.16 mM), the reverse was the case: only a few jump-ins (frequency 10-20%) were observed, indicating a high resistance to break-up. Figure 3.3.c2. gives an example where no jump-in is present even for compression with an equivalent force close to 9 nN. Curves such as this were observed many times and turned out to be highly reproducible, symmetric (i.e., without hysteresis between the approach and retraction cycles) and predominantly linear. For compression forces around 11 nN, the probe-droplet system appeared to be in a critical condition for jump-into-contact. Sometimes such a snap-into-contact happened during the *retraction* cycle; this is illustrated in Figure 3.3.c1.

3.4.1.2. Approach curves before snap-in

In this regime, the physical interpretation of the D-Z curves should be the least complicated, since no wetting has occurred yet. In this case, the probe interacts with the droplet through the dodecane/Span medium. We had a closer look on two main aspects. The first one concerns the stability of the intermediate oil layer, as measured by the maximum force F_{max} (the force associated with point C in Figure 3.5) experienced by the probe just before snap-into-contact with the water reservoir underneath. Inspecting many D-Z curves measured on water droplets revealed that F_{max} depends on the Span 80 concentration, but also shows an appreciable spread (see Figure 3.4).

On average, the maximum force preceding the *snap-in* grows with surfactant concentration. This is in accordance with expectation: raising the surfactant concentration leads to an increased adsorption at the interface, with the consequence that (a) the disjoining pressure becomes more repulsive at distances comparable to the size of the molecule (steric repulsion) and (b) the Laplace pressure becomes lower due to the reduced surface tension, leading to a more flexible surface. Both these effects are co-operative in preventing wetting (see eq. 3.1).

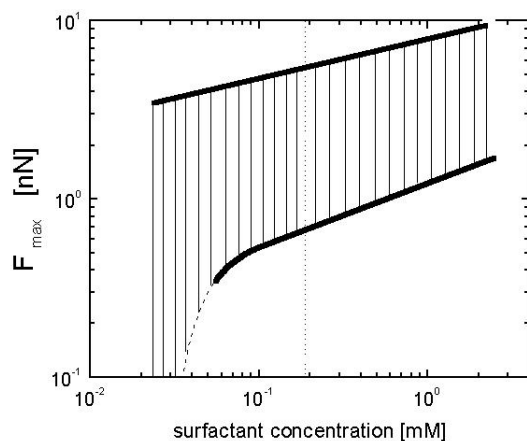


Figure 3.4. The maximum compression force measured just before the transition to probe-droplet contact (i.e., snap-in) varies with surfactant concentration. The range of F_{max} values is shown by the dashed area. The vertical dotted line indicates the CMC.

The spread in F_{max} suggests that the transition from wrapping to wetting is a statistical event: apparently the jump from the former to the latter regime is governed not only by the force, but also by a certain probability. We think that this probability depends on both the thickness of the oil film near wetting critical conditions and on the time during which these conditions apply. The occasional occurrence of snap-ins *on retraction* (as illustrated in Figure 3.3c1) corroborates the time aspect: it is hard to imagine that a gradual lowering of the compression force should induce wetting. A much more likely explanation is that an unstable interface has a certain life-time due to unstable thermal fluctuations and needs some time to reach its stable (wetting) state.

The second aspect inspected was the slope of the *D-Z curves* before wetting. To extract quantities with a physical meaning (like the droplet spring constant K_d) from these data, a few conceptual considerations are needed first. While some (weak) long-ranged repulsions appear to be present in our system (see for example Figure 3.5), we think that it is eventually the short-ranged *surfactant* contribution to Π

which provides enough repulsion to enter the wrapping regime. Since our surfactant is non-ionic, its effects on the disjoining pressure should be localized to the 1-3 nm before contact between the probe and the droplet. In other words, the competition between the Laplace and disjoining pressures (wetting or wrapping) becomes only critical on a length scale comparable to the dimension of the Span 80 molecules. The implication of a negligible contribution of long-ranged (e.g., electrostatic) repulsions, is that the total deformation can be attributed almost completely to the droplet itself. Essentially it is the deformation of the droplet surface that is probed by our AFM experiments.

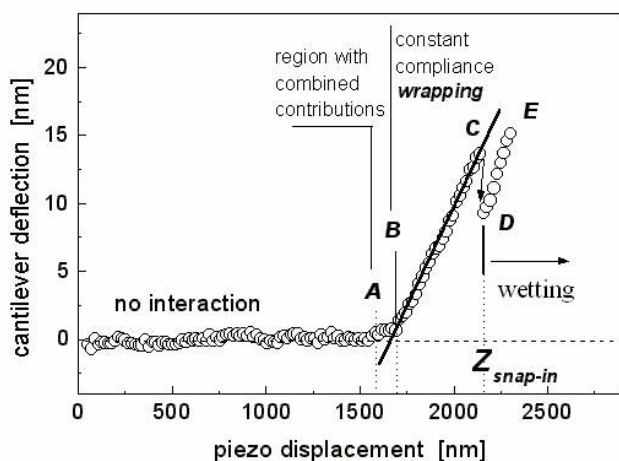


Figure 3.5. AFM D-Z curve obtained on compressing (into) a water droplet (diameter, 120 μm) immersed in dodecane with 1.16 mM Span 80.

The implication for analyzing the D-Z curves is that the slope just before the snap-in point provides the best measure for the droplet spring constant. At smaller compressions, also other contributions may have to be reckoned with (to be elaborated further on). In what follows, we shall discuss the *equivalent spring model* for droplets [4-6,11,14-15,18,21-22] and the corresponding procedure for data processing. Scrutinizing all data sets, for each single D-Z curve it was possible to make a distinction between four main regions (see Figure 3.5). In the first region (up to point A), the colloidal probe is far from the droplet and no interaction is sensed (i.e., zero cantilever deflection). As the glass particle is brought closer to the droplet, the cantilever deflects from its equilibrium position due to the probe-droplet interaction(s). In this second region (region A-B), the cantilever deflection is determined by the interplay between three forces: one generated by the probe-droplet interaction (through the oil/surfactant medium), one due to droplet deformation, and one pertaining to the bending of the cantilever. They can be seen as three serial springs, each of them transmitting the same force. Generally, the colloidal interaction corresponds to a (highly) non-linear spring.

At larger displacements, a third, *constant compliance region* (region B-C) is observed, i.e., the cantilever deflection increases linearly with the piezo displacement. In the literature, this behavior has been captured by considering the droplet as a linear spring, serially connected to the cantilever spring. For systems in which also colloidal forces are present, the corresponding “colloidal spring” can be left out from the modeling if, in the part of the D-Z curve that is analyzed, any further compliance of

this particular spring can be neglected. We believe that for our system this is the case. Under these assumptions, the droplet spring constant K_d can be calculated from:

$$K_d = K_c \frac{S}{1-S} \quad (3.5)$$

where K_c is the cantilever spring constant and S is the slope of the D - Z curve. One question was, which part of the D - Z curve to select for measuring this slope. In line with the foregoing discussion, we have started our fitting at the point just before snap-in, working back from there to smaller deflections. Linear fits were made, starting from $Z_{snap-in}$ and going down in Z until the local derivative of the D - Z curve diverged by a factor of 2 from average, followed by a linear regression on the first 30% of the points to determine the slope at maximum compression.

The linearity of the fitted part was also checked by fitting the experimental data with a power-law dependence: here we found exponent values between 1.0 and 1.1. The obtained slopes from the linear fits were plotted as histograms (not shown), averaged and translated into K_d values using eq. (3.5).

The dependence of these K_d values on the Span 80 concentration is shown in Figure 3.6a. On increasing the surfactant concentration, K_d initially shows a decrease and then saturates to a minimum value. Given the similarity of this behavior to that of the interfacial tension (γ), and in view of the presented theory, it is interesting to compare our K_d data with γ values taken from literature.

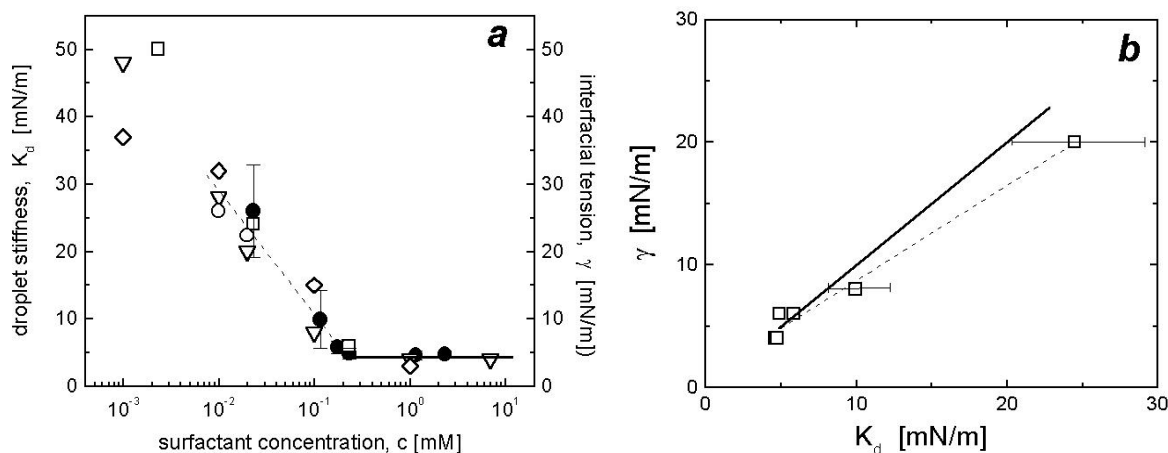


Figure 3.6. (a) Calculated values for the droplet stiffness (K_d , full symbols with error bars) versus the Span 80 concentration in bulk dodecane. Interfacial tensions (γ , open symbols) from the literature: [28] – down triangles, [29] – diamonds, [30] – squares and [31] – circles. (b) Correspondence between our K_d values (symbols) and γ values interpolated from ref. [28] to the same concentrations of Span 80. The drawn lines indicate: $K_d = \gamma$ (full) and $K_d = 1.3 \gamma$ (dashed).

According to Oliveira [32] and Li [33], the interfacial tension at the water–dodecane interface is around 40–50 mN/m. For the same liquids, Peltonen et al. [31] measured $\gamma=22.4$ mN/m in the presence of 0.019 mM Span 80 (their reported CMC). In the same paper, they showed that, for similar oils (like pentane, hexane, decane,

etc.), the interfacial tensions and the corresponding CMCs have similar values. Remarkably enough, the CMC values found by Peltonen differ from those obtained by other investigators. For example, Evans [28] found for Span 80 in n-decane a CMC of 0.3 mM, and a corresponding surface tension of $\gamma_{CMC} = 4$ mN/m. For Span 80 in hexadecane, Lobo [34] found $\gamma = 3.5$ mN/m for 23.3 mM surfactant. Campanelli [35] measured $\gamma = 5$ mN/m for 1.2 mM Span 80 in hexadecane (i.e., above their reported CMC of 0.8 mM). Valenzuela [29] found a $\gamma \sim 4$ mN/m for 1 mM surfactant and Opwale [30] found $\gamma = 6$ mN/m for 0.2 mM Span 80.

For our oil/surfactant mixtures, we believe that the CMC must be close to 0.17 mM (0.0075 % wt), where the droplets' spring constant (roughly equivalent to the interfacial tension) reaches a saturation value. It is interesting to note that the threshold value associated with the appearance of spontaneous emulsification for pure water in dodecane/ Span 80 falls in the same region, namely $C_w^{SE} = 0.14$ mM (≈ 0.006 % wt Span 80) [26]. This suggests that the SE mechanism must be connected with the drastic decrease of the interfacial tension (down to 4-5 mN/m) and the existence of surfactant micelles in the bulk dodecane.

One of our principal findings for the water droplets, shown by Figures 3.6a-b, is the good linear correlation between K_d and γ (from the literature). An unambiguous decision on the exact value of the prefactor cannot be made; both values (1.0 and 1.3) are suitable and correspond to a short-ranged (1-3 nm) repulsion in the context of the Attard model (see section 3.2). From this we conclude that for pure water droplets, the mechanical resistance against deformation is determined by the interfacial tension, if the steric barrier is sufficiently strong. Even if the steric barrier is weak (at low surfactant content) and jump-in events make it difficult to enter the *constant compliance regime*, the *equivalent spring* method can still be used to obtain a rough value for the interfacial tension.

3.4.1.3 Comparison of different probes

All data and calculations reported in the present chapter up to this point were related to experiments using one particular indenter (probe 1). To see whether our AFM measurements showed any dependence on the selected indenter, we also performed experiments (on selected formulations) using a different probe (probe 2). This latter probe had the same manufacturer specifications as probe 1 (although it came with a different batch) and was given the same cleaning treatment (see section 3.3.2).

Both panels a and b of Figure 3.7 show that apparent differences in surface properties for the two beads are not reflected in the *qualitative* dependence of the force-jumps on surfactant concentration. However, the magnitudes of the force-jumps for (a) the transition from wrapping to wetting and (b) the rupture of the droplet-probe contact in the retraction cycle clearly *do* show a dependence on the probe used. The fact that both the (average) $F_{snap-in}$ and $F_{snap-out}$ forces are significantly larger for probe 2 corroborates that both phenomena are related to wetting. Differences in local surface roughness or surfactant adsorption, or even different degree of hydrophilicity of the glass particles used as probes could all cause the difference between probe 1

and probe 2. However, it was beyond the purpose of this paper to study the cause of the difference in wetting in more depth.

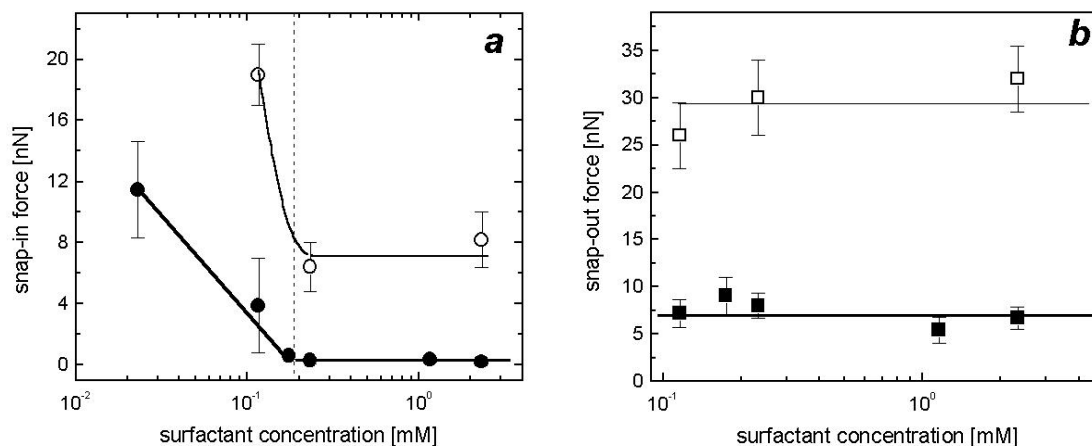


Figure 3.7. Force-jump magnitudes for the snap into contact (a) and snap out of contact (b) for pure water droplets: probe 1, full symbols; probe 2, open symbols. Forces higher than 22 nN were not determined from the software-registered AFM curves (due to a cut-off condition in the computer program). Instead, they were read as in voltages from an oscilloscope, and converted into (nano)Newtons. Hence the error bars are larger (see upper values in panel b).

Having established this remarkable difference between the two probes, we would like to stress here that other quantities (including the principal ones for the present study) were found *not* to depend on the used probe:

- (a) the general trends in the D - Z curves (as discussed in sec. 3.4.1.1)
- (b) the K_d values extracted from the constant compliance regime, which varied only 10% or less between the two probes;
- (c) the maximum force F_{max} at the end of the wrapping regime, which showed for both probes a variation as in Figure 3.4.

3.4.2. Deformation of internally gelled droplets

In the experiments considered so far, the droplets' inner-phase was always pure water. Below we report on the mechanical behavior of water droplets containing also gelatin in the inner phase (probe 1 was used as indenter in all these experiments). By cooling a gelatin solution at temperature below 30°-35°C, the molecules form crosslinks and with time they build up a network (gel). The strength of the gel depends on both the gelatin concentration and the thermal history (i.e., setting temperature and aging). For a comprehensive review on these issues, the reader can consult the review of Wolf [37].

3.4.2.1 General features for $G_{10\%}$ - gelled droplets

AFM D-Z curves on droplets with 10% gelatin prepared in 0.023 mM Span 80 / dodecane reveal a number of features which were also seen for the pure water droplets. Again, the approach curves ended with a snap-in (Figure 3.8a) and, on retraction, the capillary bridge between the droplet and the probe could not be ruptured by the software-controlled movement of the cantilever (release of the probe from contact had to be forced manually). Also for gelatin-containing droplets, a higher surfactant concentration in the oil helps to build a barrier against wetting. Most of the curves recorded above the CMC look like the ones in Figure 3.8b,c: snap-in (i.e., wetting) occurs at a large force (Figure 3.8b), or does not occur anymore (Figure 3.8c). By analyzing many D-Z curves for each Span 80 concentration, the probability for snap-in could be also estimated here. The results shown in Figure 3.10c indicate that the frequency of the snap-in behavior falls on the trend observed for pure water.

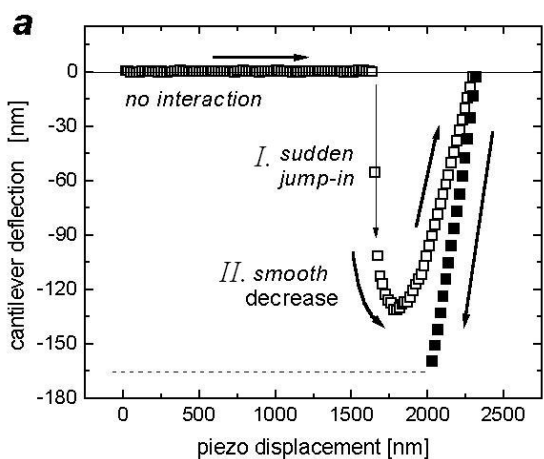
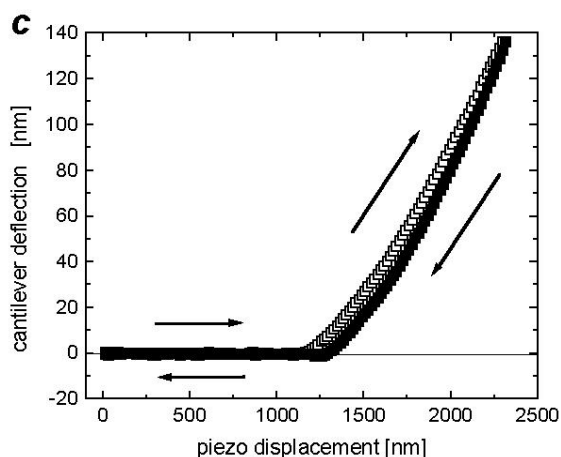
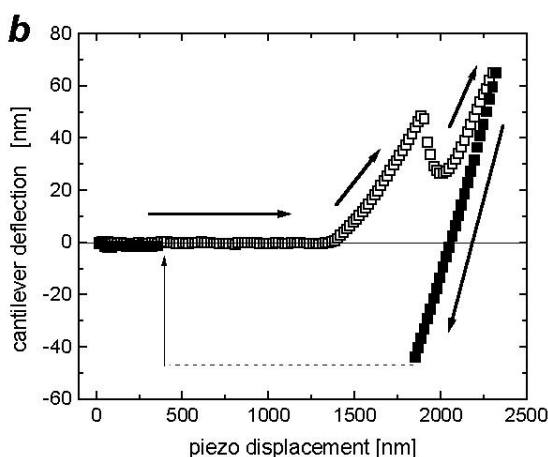


Figure 3.8. Typical D-Z curves recorded during approach (open symbols) and retraction (closed symbols) on $G_{10\%}$ - gelled droplets and two Span 80 concentrations: 0.023 mM (a) and 0.23 mM (b,c). Portions of the retraction curves (below the horizontal dotted lines) are not shown in the graphs.



Extending our analysis to the snap-in and snap-out force-jumps, more interesting information emerges. In the presence of gelatin, the jump-in behavior consists in fact of two stages (best seen from Figure 3.8a): an instantaneous jump (true snap-in) (part I), followed by a more smooth approach of a local force minimum (part II). Since for pure water droplets the part II was never observed, its origin must be related to the presence of gelatin inside the droplets. The duration of the II-nd

process was calculated to be 15–25 ms, after converting piezo displacements to real time using the approach speed. This number agrees in order of magnitude with the characteristic relaxation time of 4–8 ms observed in a previous AFM study on 10% gelatin samples [38]. We think that in both studies a viscoelastic response of the gelatin network was measured, but the volume of gelatin network and the strain involved may have been somewhat different.

Dividing the total force-jump from the snap-in critical point till the force minimum into the two parts as previously defined,

$$F_{\text{snap-in / total}} = F_{\text{snap-in / I}} + F_{\text{snap-in / II}}.$$

the question arises, which of the force-jumps should be compared to the force-jumps for the pure water droplets. Depending on the mechanistic details of the wetting, either the part I or the total force could qualify for this: if one assumes that free (e.g., expelled) water at the gelatin/oil interface is responsible for snap-in, then the part I force should be most suitable. In the case that the probe gets wetted by a gelatin network, then the total force is most suitable. Based on Figure 3.9a, it is not possible to make a distinction. Regarding the *snap-out* behavior, Figure 3.9b illustrates that there are appreciable differences between the force-jumps measured for water and for gelled droplets, using the same probe.

3.4.2.2 Influence of gelatin and surfactant concentrations on wetting and dewetting

Figures 3.9 and 3.10 present a mapping of the snap-in and snap-out behavior dependence on the gelatin and surfactant concentrations. Below we propose a qualitative picture which can explain the main trends. A very detailed explanation is not feasible in our opinion, considering the disbalance between the complexity (both the initial and the final state have to be considered, there may be a time dependence, and probabilistic elements can play a role) and the available information. Both the probability and the magnitude of the force-jumps should be considered. The snap-in and snap-out instabilities will be considered separately, as the mechanisms are partially different.

For snap-in, two different possible mechanisms have to be distinguished: 1) colloidal attraction and 2) wetting. The first case applies for a minimum in the disjoining pressure curve (i.e., an attractive force, not preceded by a repulsion). This case should become apparent in the AFM curve as a snap-in starting at the $F=0$ axis. Although a few such curves were encountered at very low Span 80 concentrations (see for example Figure 3.8a), most of our other experiments (for both water and gelled droplets) showed the $F \neq 0$ case. This fact suggests that wetting occurred, i.e., the repulsive disjoining pressure was not large enough to guarantee the stability of the oil film.

The probabilistic nature of the jump-in phenomenon is also consistent with wetting. Following eq. 3.1, a probabilistic wetting should occur when the maximum disjoining pressure and the Laplace pressure are of comparable magnitude. In this regime, both changes in the maximum disjoining pressure and in the surface tension can affect the wetting probability. In this picture, increasing the Span80 concentration

should disfavor wetting along both ways, at least up to the CMC. The results of Figure 3.10c are in line with this.

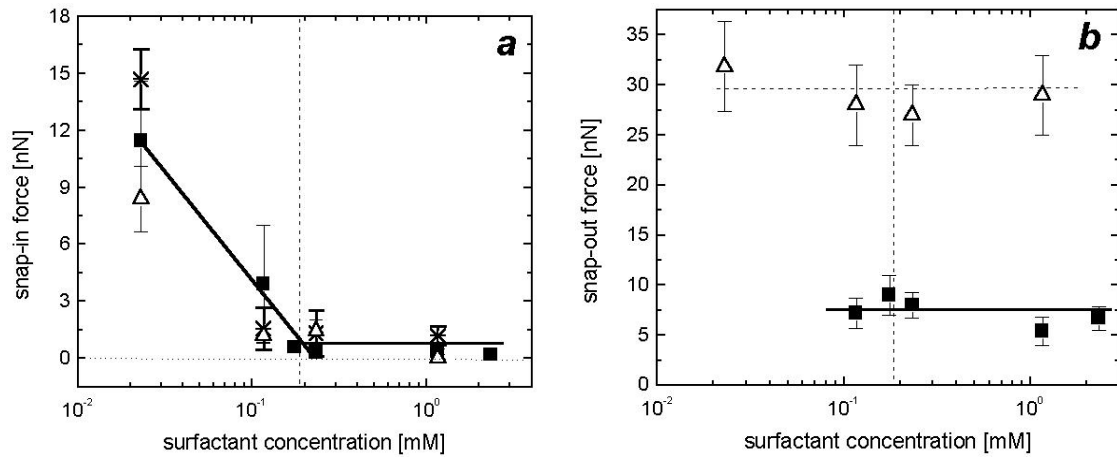


Figure 3.9. Snap-in (a) and snap-out (b) force-jumps measured on water (full symbols) or G_{10%} droplets (open symbols). The dotted vertical line indicates the CMC. In panel (a), different symbols distinguish $F_{snap-in/1}^{10\% gel}$ (open) and $F_{snap-in/total}^{10\% gel}$ (stars).

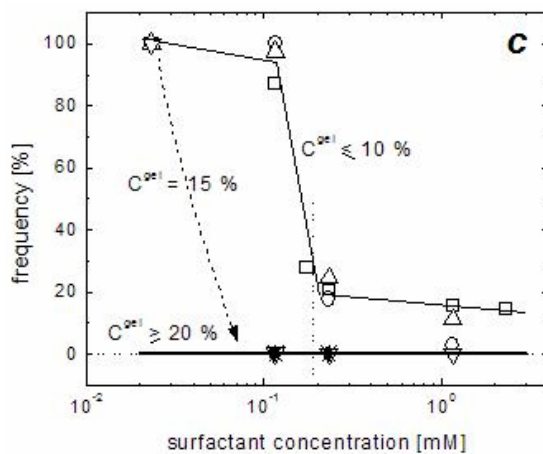
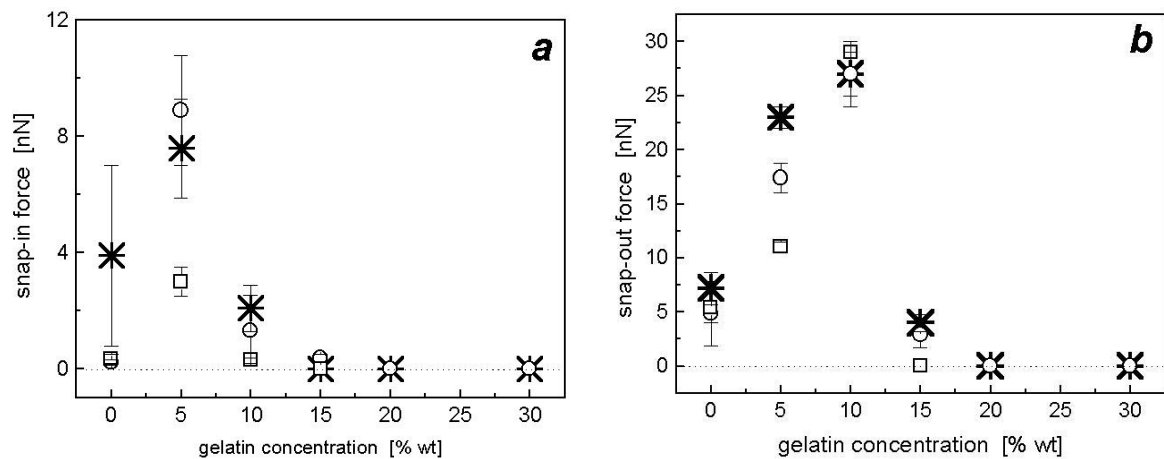


Figure 3.10. Snap-in (a) and snap-out (b) force jumps measured on gelled droplets for 0.12 mM (stars), 0.23 mM (circles) and 1.16 mM (squares) Span 80. (c) Frequency of encountering a wetting instability, based on at least 250 D-Z curves per composition. Lines are drawn to guide the eye. Legends: water (squares), 5% gelatin (up triangles), 10% gelatin (circles), 15% gelatin (down triangles), 20% gelatin (stars)

The magnitude of the snap-in force-jump is set by the force difference between the repulsive state before wetting, and the wetted state. Considering that the interfacial tension probably appears as a multiplier both in the “critical wetting force” (see eq. 3.1) and in the (quasi-equilibrium) “wetting force”, one might expect a close-to-linear relation between the force-jump and the interfacial tension. This would explain the decreasing snap-in force up to the CMC in Figure 3.9a. Also the initial increase of the snap-in force with gelatin concentration in Figure 3.10a could be explained by this, considering that gelatin may partially displace Span 80 from the interface, thus raising the interfacial tension. In the presence of sufficient amounts of gelatin to obtain (visco)elastic droplets, the “wetting equilibrium” becomes modulated by the reduced compliance (or increased elastic resistance) of the droplets, having as a result a smaller contact area and a reduced wetting force. Increasing the gelatin content, the latter effect will eventually become dominant, and this explains the decrease in Figure 3.10a.

Snap-out occurs only if preceded by a snap-in (in the cases discussed here). For our system it is related to a dewetting of the probe, via the breakage of the neck formed during probe retraction. Since the final state is a balance of forces, the critical snap-out force is equal to the jump amplitude. In principle, two failure mechanisms could play a role: an instability in the neck itself or an adhesive failure at the surface of the probe. In the first case, both the increased surface tension and the increased (visco)elasticity due to the gelatin could cause the initial increase of the snap-out force in Figure 3.10b. In the second case, an increased adhesion due to gelatin should be responsible. On the basis of our experiments, we cannot discriminate between the two situations. Also the difference in magnitude observed between water and 10% gelatin droplets in Figure 3.9b does not provide information about the nature of the jump-out mechanism. Irrespective of this, for both cases the explanation for the subsequent reduction of the snap-out force in Figure 3.10b is the same. The reduced contact area achieved in the compression stage, together with the reduced ability of the “neck” to recruit material from the “droplet”, causes a decrease of the snap-out force. Eventually at still higher gelatin content the wetting becomes completely absent (as no snap-in occurs). This explains the maximum in Figure 3.10b.

3.4.2.3 Elastic response of gelled droplets

In the foregoing sections, it was demonstrated that beyond certain (combinations of) Span 80 and gelatin concentrations, our droplets can resist deformation without wetting the probe. The corresponding D - Z curves allow us to address one of the principal questions of this study: *which elastic response is obtained upon mechanical loading of a gelled droplet?* Aqueous droplets with gelatin in the bulk and enough Span 80 at the interface with the dodecane (so that the disjoining pressure is steep and droplets are in the wrapping regime) can resist deformation via both the interfacial tension and the bulk elasticity. The question is how these mechanisms work together. Let us first consider the two extreme cases. For pure water droplets, the *equivalent spring* model was seen to apply, with a good correspondence between the spring constant and the interfacial tension. For droplets with high gelatin concentration, one may expect an elastic response which is almost entirely due to the bulk modulus of the gel.

In the latter case, the Hertz model [39] could apply. In this model, linear elastic behavior is assumed, together with a smooth tip-sample contact during loading. The geometry of the indenter then determines the functional F - δ dependence, with δ being the indentation. For a spherical probe with radius R_p , the F - δ loading curve is described by:

$$F = K_c D = \frac{4}{3} \frac{E^*}{R_p^{1/2}} \delta^{3/2} \quad (3.6)$$

Fitting eq. (3.6) to experimental F - δ curves, the relative elastic modulus (E^*) of the compressed material can be obtained. This approach requires the calculation of δ values from the D - Z curves. For a purely elastic material (i.e., without any interactions prior to the direct contact between the indenter and the material) δ can be accurately defined as:

$$\delta = (Z - Z_0) - D \quad (3.7)$$

with Z_0 the piezo displacement just before the first nonzero deflection in the approach curves and D the cantilever deflection. In our case, things are slightly more complicated due to the presence of colloidal interactions. Strictly speaking one would need a model to take them into account, and correct for their contribution to the overall deformation. In view the large maximum forces applied in our compression experiments, we have ignored the colloidal contribution, and defined δ as in eq. (3.7).

A few representative F - δ curves for a given surfactant (0.23 mM) and different gelatin concentrations are shown in Figure 3.11. Adding more gelatin to the aqueous phase clearly increases the response level of the curves. Moreover, while the F - δ dependence for water looks linear, for gelled droplets the F - δ curve becomes noticeably curved.

To assess the extent to which the *linear spring* or the *Hertz* model could describe the data, we have attempted to fit our F - δ curves with a general power-law function:

$$F = A \delta^B \quad (3.8)$$

where an exponent $B = 1$ corresponds to the linear spring model, while for $B = 1.5$ the Hertz model is recovered.

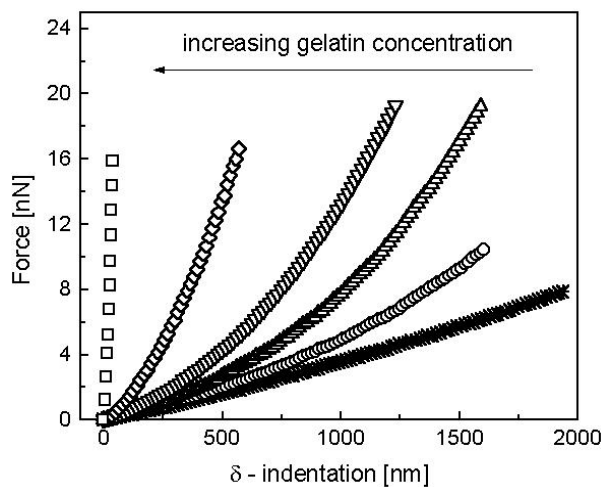


Figure 3.11. Force-indentation curves for droplets with various amounts of gelatin: 0% (stars), 5% (circles), 10% (up triangles), 15% (down triangles), 20% (diamonds) and 30% (squares). All samples were prepared with 0.23 mM Span 80. Note that for $G_{30\%}$ samples the F - δ curve cannot be distinguished from that of a hard substrate (using a cantilever with $K_c = 0.1$ N/m). Note also the increased resistance (maxima) compared to the water.

Analyzing all our experimental F - δ data with the fitting function (3.8), the obtained exponent B was found to depend on the range of F values chosen for the fitting (especially for the 5% gelatin case). To analyze this dependence in more detail, we have followed a “variable-trigger”-approach, in which each F - δ curve was subjected to a number of fits between $F = 0$ and $F_{trigger}$, taking the latter as a variable. The results are shown in Figure 3.12.

For pure water droplets, B reaches the value 1.0 at small indentations and remains constant thereafter: this corroborates the *equivalent linear spring* behavior (section 3.4.1). The B values below 1.0 might represent the influence of the colloidal force (region A-B in Figure 3.5).

A trend observed for gelatin contents below 15% (see Figures 3.12a,b) is that there is not a single power law that fits the curves (the fit depends on the trigger point). For the $G_{5\%}$ and $G_{10\%}$ gelled droplets, B increases with $F_{trigger}$, starting around 0.9 and approaching a “saturation value” of 1.5. For the $G_{15\%}$ droplets, the latter value is reached already at small compressions. We explain this variation as being the result of the interplay between the interfacial tension and the bulk elasticity contributions. Under 15% gelatin, at small deformations the interfacial tension contributes to the droplet deformation and that determine the variation of the B exponent between the extreme values: 1.0 and 1.5 (Figure 3.12a,b). As deformation increases, bulk elasticity gains more and more influence, and from a certain point will start to dominate over the influence of the interfacial tension. At that point, B reaches the value 1.5 and stays constant for any deeper indentation. For 15% gelatin and above, the bulk elasticity is already so high that it dominates already for small indentations over the interfacial tension, the droplets behaving like pure elastic bodies for any indentation.

The $G_{5\%}$ droplets turned out to be a special case: in contrast to droplets at higher gelatin concentrations, there appeared to be appreciable scatter between different B - $F_{trigger}$ curves (three examples are presented in Figure 3.12a). Even so, the general trend is conserved: for a larger $F_{trigger}$, a higher power-law exponent is found. Also the mathematical dependence of individual curves suggests a complex behavior. For a low gelatin content like 5%, the probability of an inhomogeneous interface is higher. Gelled regions as well as “water pockets” might be present inside the droplet, near the interface. Having a weak network, water could also be easily expelled during the compression. Thus, pressing on such a surface can give various responses, depending whether there is only water contribution or also a contribution from the network inside. This could explain both the variation in the curve shape (as described by variation of the exponent B in Figure 3.12a) and the relatively good wettability of the probe (similar to the water case). On the other hand, for high gelatin concentrations, a denser, more homogeneous network reduces the number and size of possible water pockets and binds the water more strongly to the stiffer network (also via the hydrogen-bonding of the water molecules to the gelatin).

For droplets with gelatin concentrations above 5%, fitting the F - δ curves with a superposition of a linear and a Hertzian force law (corresponding to a parallel arrangement of springs), revealed that the Hertzian contribution was dominant. The relative Young moduli E^* obtained using the Hertz model for high indentations ($F_{trigger} = F_{max}$) for all $G_{10\%}$, $G_{15\%}$ and $G_{20\%}$ formulations are shown in Figure 3.13, along with a single result for a $G_{5\%}$ droplet (the upper curve in Figure 3.12a).

In this figure, also a comparison is made between the aforementioned E^*_{AFM} values and E^*_{macro} , with the later calculated from the G' , the elastic storage moduli

obtained from classical (i.e., macro) rheological measurements on bulk gels [38]. While the order of magnitude for the E^*_{AFM} and $E^*_{\text{macro rheology}}$ values is the same, there are obviously quantitative differences. Explaining these is beyond the scope of this thesis (considering also that it has not been settled in current literature that a quantitative correspondence should hold). However, the dependence of E^*_{AFM} on the amount of gelatin appears to be linear, and not with a power-law index of 1.8 as determined for macroscopic gelatin gels [40].

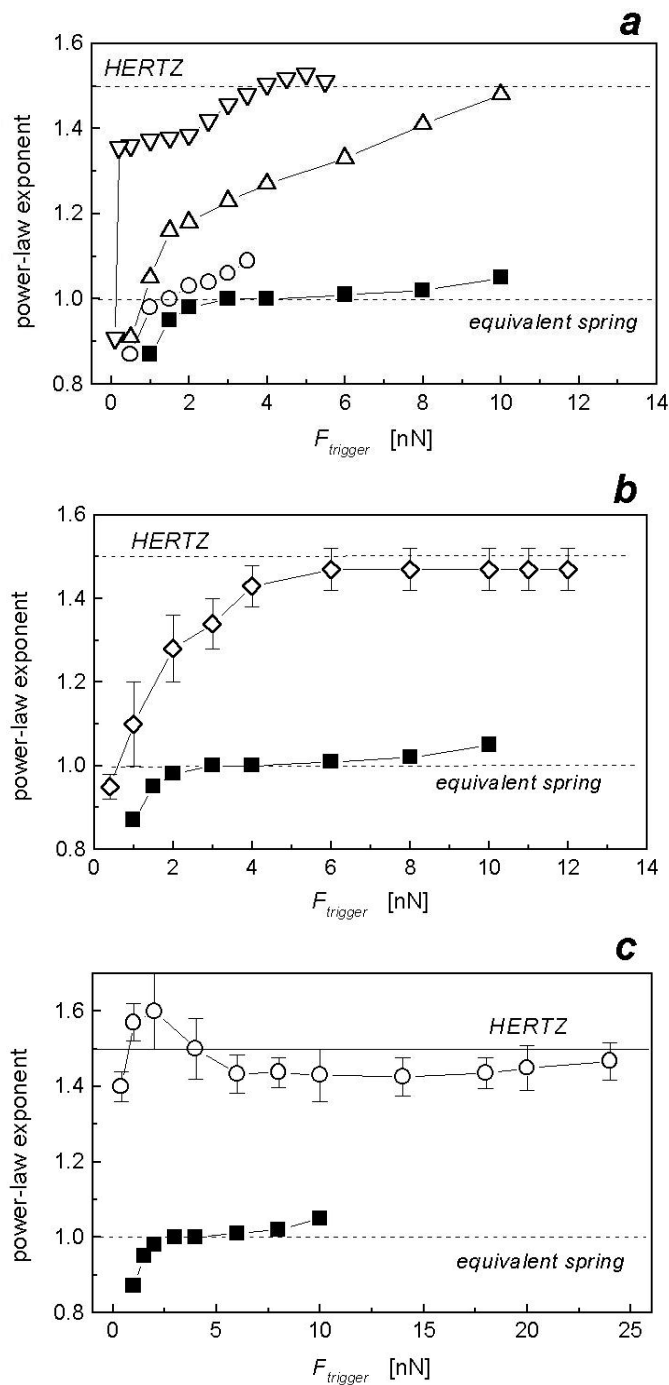


Figure 3.12. Calculated power-law exponents B based on fits using eq. (3.8) and the variable-trigger approach (described in the text). Open symbols in each plot correspond to gelled droplets with 5% (a), 10% (b) and 15% (c) gelatin. Closed symbols represent pure water droplets, as a reference case. All samples were prepared with 0.23 mM Span 80. For $G_{5\%}$ -gelled drops, a few individual B vs. F_{trigger} dependences are shown. For $G_{10\%}$ - and $G_{15\%}$ -droplets, averages over multiple B vs. F_{trigger} curves are presented.

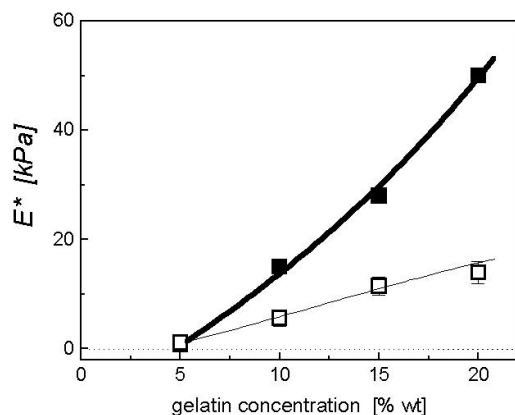


Figure 3.13. Relative Young moduli (E^*) determined using macrorheology (full symbols) [38] and AFM (open symbols) for several gelatin concentrations. The E^*_{AFM} values are calculated from compression curves for gelled droplets prepared with 0.23 mM Span 80.

3.4.3. Stability diagram

The findings of the present AFM study (together with some additional observations) allowed us to make a semi-quantitative mapping of droplet (in)stability areas as a function of gelatin and Span 80 concentration. The result is shown in Figure 3.14. Two kinds of interface instabilities were found in our experiments with single large droplets. The first instability concerns the wetting of a hydrophilic surface, measured with AFM. In assigning the (complete, partial or non-) wetting areas in Figure 3.14, we have based ourselves on the wetting probabilities shown in Figure 3.10c. In the presence of gelatin, the probability for wetting was found to decrease. Up to a certain gelatin concentration, also the presence of surfactant was found to contribute to the prevention of wetting. The second instability concerns “spontaneous emulsification”, that is, the formation of satellite emulsion droplets at the O/W interface of a mother droplet. We observed this with optical microscopy, above a certain surfactant concentration. Since the satellite droplet volume has to be made available from inner phase of the mother droplet, one can expect that SE is also modulated by the presence of gelatin.

The question now arises, how to connect the results of this study, to stability issues (e.g., preventing coalescence) for real emulsions made from the same constituents. First of all, one should then consider whether a glass bead-droplet interaction is sufficiently similar to a droplet-droplet interaction. The hydrophilic nature of both glass and aqueous surfaces (in contrast with dodecane) speaks in favor of this assumption. Also the observed wetting behavior of the water droplets would support this view: the increased resistance against probe-wetting near the CMC (0.17 mM) correlates well with the general observation that in real emulsions, stability against coalescence is also obtained near this point.

Another factor to consider is that in real emulsions, the droplet size is typically in between 1 and 10 microns. In principle, the droplet size will have an influence on the Laplace pressure, which plays a role in the wrapping-or-wetting issue (see eq. 3.1). Considering the occurrence of a reduced radius in the expression for the Laplace pressure, and the use of a 5 micron sized probe, the Laplace pressure for a pair of 10 micron droplets might be of comparable magnitude to those in our experiments (provided that nothing else but the size is changing, for much smaller droplets, the higher Laplace pressure should allow wetting at higher disjoining pressures, thus making them less stable).

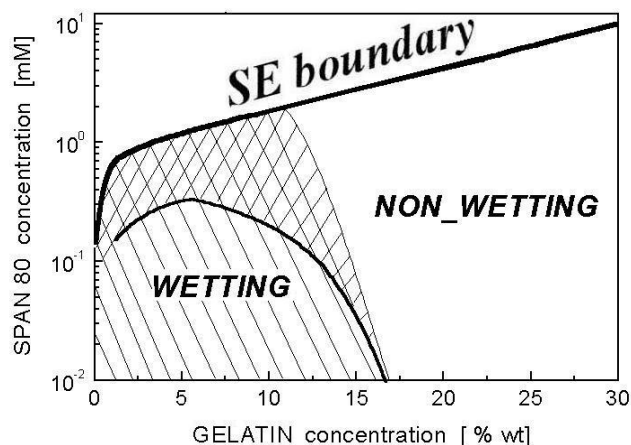


Figure 3.14. Stability diagram of emulsion droplets, mapped as a function of gelatin and surfactant concentrations. At high [Span 80], the droplets are affected by spontaneous emulsification. For low [gelatin] and/or [Span 80] the droplets show 100% wetting events (right-stripped zone) or partial (i.e., smaller frequency) wetting (rombs-zone). The diagram is semiquantitative, in that stability lines were generated from a limited number of observation points, and could not always be sharply drawn.

Also the magnitudes of the forces have to be considered. Colloidal forces between the droplets in real emulsions are usually much smaller (e.g., 10-200 pN for depletion forces) than the typical compression forces (1-20 nN) applied in our AFM experiments. We remark here that such high forces could however be encountered in highly concentrated emulsions under strong shear flows. Since in our AFM experiments, we found also a correlation between the wetting probability and the force applied, Figure 3.14 should in principle be given a third dimension, representing the force. Investigating this dimension would deserve further study.

3.5. CONCLUSIONS

We have studied the deformability of inverse (water-in-oil) emulsion droplets as a function of surfactant concentration using colloid-probe AFM in force-distance mode. The *equivalent spring* method was applied, after which the droplet spring-constants were compared to literature values for the W/O interfacial tension. A good linear correlation was found, with a prefactor of 1.0–1.3, which suggests, in the context of the Attard model, that the *probe-droplet* repulsion which prevents wetting is short-ranged (1-3 nm). Thus it is possible to measure the surface tension of W/O droplets (semi-) quantitatively with AFM.

The mechanical resistance of water droplets against deformation is determined by the interfacial tension, but only if the surfactant layer at the droplet interface provides sufficient colloidal stability. At surfactant concentrations below the CMC this steric barrier is weak, and wetting of the probe occurs, manifested via jump-in events. While a frequent occurrence of the latter made it difficult to measure droplet

spring-constants at low surfactant concentrations, the method could still be used to obtain a rough value for the interfacial tension. The CMC of Span 80 in dodecane was found to be ≈ 0.17 mM.

We also studied the influence of bulk elasticity on the droplet deformation. Increasing the gelatin concentration makes the system more stable against wetting, as evidenced by a less frequent occurrence of snap-in events. Also the dependence on surfactant concentration diminishes for higher gelatin concentrations. The elastic response is strongly enhanced on adding gelatin, and also the shape of the force-distance curve becomes nonlinear. To assess the extent to which the *equivalent spring* or the *Hertz* model could describe the data, we have fitted our F - δ curves with a general power-law function.

Below 15% gelatin, for small enough indentations, the interface and bulk contributions to the elasticity are of a comparable magnitude. However, for deeper indentations the bulk elasticity becomes dominant, causing a Hertzian response. For droplets with higher (>15%) gelatin concentrations, a dominant Hertzian contribution was found for all indentations, and did not depend on the surfactant concentration. The E^*_{AFM} values obtained using the Hertz model were of the same order of magnitude as the values obtained from macroscopic rheology experiments, but with a different concentration dependence.

Wetting of the probe turned out to be a complicating factor in the present study, especially at low surfactant and gelatin contents. Its probabilistic nature necessitated us to perform many experiments under these conditions. Its dependences on the particular probe used, droplet selected, or scan are still not fully elucidated but do not affect the main conclusions of the present chapter. The influence of gelatin on (probe) wetting and dewetting was clearly manifested as a (visco-) elastic contribution to the snap-in and snap-out forces. The fact that even at high gelatin concentration, wetting occasionally occurred, suggests the presence of exudated (i.e., expelled by the gelatin network) water at the interface.

REFERENCES

- (1) Dekker, M. "Encyclopedia of emulsion technology", vol.2, Becher, P. (Eds), New York 1985.
- (2) Ducker, W.A.; Senden, T.J.; Pashley, R.M. *Nature* **1991**, 353, 239.
- (3) Butt, H.-J. *J. Colloid Interface Sci.* **1994**, 166, 109.
- (4) Ducker, W.A.; Xu, Z.; Israelachvili, J.N. *Langmuir* **1994**, 10, 3279.
- (5) Fielden, M.L.; Hayes, R.A.; Ralston, J. *Langmuir* **1996**, 12, 3721.
- (6) Preuss, M.; Butt, H.-J. *Langmuir* **1998**, 14, 3164.
- (7) Carambassis, A.; Jonker, L.C.; Attard, P.; Rutland, M.W. *Phys. Rev. Lett.* **1998**, 80, 5357.
- (8) Ecke, S.; Preuss, M.; Butt, H.-J. *J. Adhes. Sci. Technol.* **1999**, 13, 1181.
- (9) Ralston, J.; Fornasiero, D.; Hayes, R., *Int. J. Mineral. Process.* **1999**, 56, 133.
- (10) Yakubov, G.E.; Vinogradova, O.I.; Butt, H.-J. *Colloid Journal* **2001**, 63, 518.
- (11) Nguyen, A.V.; Nalaskowski, J.; Miller, J.D. *Minerals Engineering* **2003**, 16, 1173.
- (12) Mulvaney, P.; Perera, J.M.; Biggs, S.; Grieser, F.; Stevens, G.W. *J. Colloid Interface Sci.* **1996**, 183, 614.
- (13) Basu, S.; Sharma, M.M. *J. Colloid Interface Sci.* **1996**, 181, 443.
- (14) Snyder, B.A.; Aston, D.E.; Berg, J.C. *Langmuir* **1997**, 13, 590.
- (15) Hartley, P.G.; Grieser, F.; Mulvaney, P.; Stevens, G.W. *Langmuir* **1999**, 15, 7282.
- (16) Aston, D.E.; Berg, J.C. *J. Colloid Interface Sci.* **2001**, 235, 162.
- (17) Aston, D.E.; Berg, J.C. *Ind. Eng. Chem. Res.* **2002**, 41, 389.
- (18) Nespolo, S.A.; Chan, D.Y.C.; Grieser, F.; Hartley, P.G.; Stevens, G.W. *Langmuir* **2003**, 19, 2124.
- (19) Attard, P.; Miklavcic, S. *Langmuir* **2001**, 17, 8217.
- (20) Attard, P.; Miklavcic, S. *J. Colloid Interface Sci.* **2002**, 247, 255.
- (21) Chan, D.Y.C.; Dagastine, R.R.; White, L.R. *J. Colloid Interface Sci.* **2002**, 236, 141.
- (22) Dagastine, R.R.; White, L.R. *J. Colloid Interface Sci.* **2002**, 247, 310.
- (23) Bhatt, D.; Newman, J.; Radke, C.J. *Langmuir* **2001**, 17, 116.
- (24) Bardos, D.C. *Surf. Sci.* **2002**, 517, 157.
- (25) Gillies, G.; Prestidge, C.A. *Adv. Coll. Interf. Sci.* **2004**, 108 –109, 197.
- (26) Uricanu, V.I.; Duits, M.H.G.; Filip, D.; Nelissen, R.M.F.; Agterof, W.G.M.; *J. Coll. Interf. Sci.* **2006**, YJCIS 11947 (in press, available online).
- (27) Werf, K.O., van der; Putman, C.A.J.; Grooth, B.G., de; Segerink, F.B.; Schipper, E.H.; Hulst, N.F., van; Greve, J. *Rev. Sci. Instrum.* **1993**, 64 2892.
- (28) Evans, G.M.; Habgood, M.G.; Boddy, G.; Galvin K.P.; Biggs, S.R. *Asian Pacific Conf. Chem. Eng.* 2002 Christchurch, New Zealand, conference proceeding.
- (29) Valenzuela, F.; Salinas, C.; Basualto, C.; Sapag-Hagar, J.; Tapia, C. *J. Chil. Chem. Soc.* **2003**, 48(1).

- (30) Opwale, F.O.; Burgess, D.J. *J. Colloid Interface Sci.* **1998**, 197, 142.
- (31) Peltonen, L.; Hirvonen, J.; Yliruusi, J. *J. Colloid Interface Sci.* **1998**, 240, 272.
- (32) Oliveira, R.C.G.; Gonzalez, G.; Oliveira, J.F. *Colloids Surf. A* **1999**, 154, 127.
- (33) Li, J.; Miller, R.; Wustneck, R.; Mohwald, H.; Neumann, A.W. *Colloids Surf. A* **1995**, 96, 295.
- (34) Lobo, L.; Svereika, A. *J. Colloid Interface Sci.* **2003**, 261, 498.
- (35) Campanelli, J.R.; Wang, X. *J. Colloid Interface Sci.* **1999**, 213, 340.
- (36) Preuss, M.; Butt, H-J. *Int. J. Miner. Process.* **1999**, 56, 99.
- (37) Wolf, F.A., de; “*Collagen and gelatin*” in “*Industrial Proteins in Perspective*”, Aalbersberg, W.Y. et al. (Eds.), Prog. Biotech. **2003**, 23, 133-218.
- (38) Uricanu, V.I.; Duits, M.H.G.; Nelissen, R.M.F.; Bennink, M.L.; Mellema, J., *Langmuir* **2003**, 19, 8182.
- (39) For a didactic presentation of the Hertz mechanical contact theory, the reader can consult: (a) Johnson, K.L. “*Contact Mechanics*”, Cambridge University Press, Cambridge, London, 1985, or (b) Wang, Y.C.; Lakes, R. *Internat. J. Solids & Structures* 2002, 39, 4825.
- (40) Bot, A.; Amerongen, I.A. van; Groot, R.D.; Hoekstra, N.L.; Agterof, W.G.M., *Polymer Gels & Networks* **1996**, 4, 189.

CHAPTER 4. Microrheology of Aggregated Emulsion Droplet Networks*

ABSTRACT

We studied the mechanical behavior of densely packed (up to ~30% v/v), sedimented layers of (1 μm) water-in-oil W/O emulsion droplets, upon indentation with a (10 μm) large spherical probe. In the presence of attractive forces, the droplets form solid like networks which can resist deformation. Adding a polymer to the oil phase was used to control droplet attraction. The droplet layers were assembled via normal gravity settling. Considering that both the network structure and the droplet interactions play a key role, we used a combination of atomic force microscopy (AFM) and confocal scanning laser microscopy (CSLM) to characterize the mechanical behavior. Here the AFM was used both as indentation tool and as force sensor. Indentation experiments were performed via a protocol consisting of approach, waiting and retract stages. CSLM was used to observe the network structure at micron resolution in real time. Use of refractive index matched fluorescent droplets allowed the visualization of the entire layer. Upon compression with the probe, a markedly non-homogeneous deformation occurred, evidenced by the formation of a dense corona (containing practically all the displaced droplets) in the direct vicinity of the probe, as well as more subtle deformations of force-chains at larger distances. Upon decompression, both the imprint of the indenter and the corona remained, even long after the load was released. The force-distance curves recorded with the AFM correspond well to these observations. For each deformation cycle performed on fresh material, the retract curve was much steeper than the approach curve, thus corroborating the occurrence of irreversible compaction. Contrary to classic linear viscoelastic materials, this hysteresis did not show any dependence on the deformation speed. Our force-indentation approach curves were seen to scale roughly as $F \sim \delta^{3/2}$. The pre-factor was found to increase with the polymer concentration and with the density of the network. These findings suggest that this new AFM-CSLM method could be used for rheological characterization of small volumes of “granular networks” in liquid. Our hypothesis that the mechanical resistance of the networks originates from interdroplet friction forces, which in turn are set by the interdroplet potential forces, is supported by the predictions from a new mechanical model in which the interdroplet bonds are represented by stick-slip elements.

* Published as: D. Filip, V. I. Uricanu, M. H. G. Duits, D. van den Ende, J. Mellema, W. G. M. Agterof and F. Mugele, in *Langmuir*; 2006; 22(2), p. 560 - 574

4.1. INTRODUCTION

Emulsions form the basis of a wide variety of natural and manufactured materials, including food products, pharmaceuticals, biological fluids, agro-chemicals, petro-chemicals, cosmetics, etc. [1]. The mechanical properties of emulsions are important in preparing products that can easily flow or that behave like solids (eg., margarine, mayonnaise). For low volume fractions (well below close packing) and purely repulsive interdroplet interactions, the surface tension ensures that the droplets are spherical in shape, the emulsion as a whole has no elasticity and flows easily under shear. However, in concentrated emulsions, packing constraints force the droplets to slide along each other (dissipating energy via friction), and to deform elastically (storing energy at their interface). This energy is the origin of emulsion elasticity and allows tuning emulsion behavior from fluidlike to elastic solidlike. A review on this subject can be found in ref. [2]. Another factor that can become more important at high concentrations is (if applicable) the presence of attractive forces between the droplets. Such forces influence both the structures that are formed and their resistance to deformation.

In the present chapter, we study the mechanical behavior of weakly aggregated emulsions at concentrations which are high enough to cause structural arrest, but still significantly lower than the maximum packing fraction in systems with just excluded volume repulsions. The droplets are gelled by adding a biopolymer in the water phase prior to emulsification. For this kind of material, different systems could serve as a reference case: highly concentrated stable emulsions, reversibly aggregated particle suspensions, or granular materials.

The macroscopic rheology of concentrated stable emulsions has been extensively documented in the literature. For (close to) monodisperse emulsions, some universal behaviors were reported. Above a critical volume fraction of ≈ 0.64 , associated with the random close packing of monodisperse spheres, a marked change in the rheological behavior occurs. The emulsion then becomes compressed, and starts to behave like a glassy material [3]. In this regime, a low-frequency plateau of the storage modulus G' was found, with a magnitude that scales quasi-linearly with the droplet volume fraction ϕ . Also the loss modulus G'' was found to be (almost) frequency-independent at low frequencies [4]. Comparing different emulsions, the magnitude of the G' plateau was found to show a universal dependence on ϕ when scaled by the Laplace pressure [5]. Nonlinear rheological properties such as the yield stress were also found to scale with the Laplace pressure [6]. Also theoretical approaches aimed at obtaining stress-strain relationships for highly concentrated emulsions have been undertaken [7].

For emulsions having a low volume fraction and weakly attractive interactions between the droplets, the dispersed phase may form tenuous solid aggregates or gels of droplets [8, 9]. A study into the elasticity of depletion-flocculation induced emulsion gels was done by Meller et al [10] using rheology and diffusing wave spectroscopy. The elasticity in this system was found to be controlled more by structural features (packing of the clusters) than by the osmotic pressure setting attraction between the droplets. Also networks of aggregated solid particles belong to this class of materials. To explain the elastic behavior of such networks, assumptions were made regarding the particle chains: either noncentral forces or multiply

connected chains were needed to render elastic properties [11, 12]. Due to the reversible nature of two-particle bonds, irreversible compaction of aggregates and networks was occasionally observed at low particle volume fractions. Macroscopically this was manifested via a dependence of the rheological properties on mechanical history [13].

Alternatively, our materials could also be compared to granular matter systems. One description of a granular system is that it concerns “packed, hard and rough objects”, “hard” meaning that elastic deformation is negligible, and “rough” meaning that all motion is confined to sliding and rolling after a friction threshold is overcome. Although there are still many problems in granular matter which are unresolved, it is clear that strains and stresses are highly non-uniform and that efforts are still being undertaken, to infer which structural elements are associated with mechanisms of supporting applied stresses. Motivated by the expected similarity between the micromechanics of packed emulsions and packing of ball bearings or glass beads, Brujic et al [14] used confocal microscopy to study the micromechanics of jammed emulsions. The similarity in behavior between jammed emulsions and granular matter was pointed out by Makse [15]. Chang et al studied macroscopic stress-strain relationships as a function of interparticle stiffness, particle size and packing density [16]. Goldenberg found that friction enhances elasticity of granular solids [17].

An extension of granular matter to systems with cohesion between the particles was addressed by Kadau et al [18]. They found that cohesion combined with rolling friction could explain compaction behavior, as seen for example in nanopowders. They state that only the combination of Coulomb friction, rolling friction, and cohesion can stabilize particle chains such that they can carry a load.

These reported findings make it clear that still a lot of research needs to be done to identify the possible mechanisms via which consolidated particle (e.g., emulsion droplet) networks can resist deformation, and how a control over these mechanisms can be exerted. Eventually, insight in these mechanisms should also allow making a connection between the microscopic mechanisms and the macroscopic rheological behavior of the material. With the present chapter, we want to make a contribution to this field, by reporting about experiments in which forces and displacements are measured with microscopy techniques.

Several complementary techniques have been developed in recent years to measure viscoelastic properties of soft materials on micrometer scales, to connect the micro- and macroscopic properties [19]. For instance, the use of colloidal particles as diffusive probes, in conjunction with high-resolution microscopy and modern image processing techniques, has permitted this [20]. Another technique used to study microscopic viscoelasticity of soft materials is atomic force microscopy (AFM). In the “force mapping method” the AFM tip or a spherical colloidal probe attached to the cantilever is brought slowly into contact to indent the material and then retracted. The force-distance response can vary from purely elastic for small loads, to plastic ones if the load exceeds the material’s yield stress. For soft (colloidal) materials, most of the existing knowledge concerns the (visco)elastic deformation of polymer gels, droplets or bubbles [21-26]. Interpretation of the measured force-distance curves has in many cases been done with the Hertz model for the contact of elastic bodies [27]. Elastic-to-plastic transitions have been used to describe the deformation of solid materials [28-31] or granular matter [32].

In this work, we used two complementary microscopy techniques. AFM was used to impose given loads to aggregated sediments. The dynamic and the static mechanical responses of the network under compression with a larger (than the droplets size) colloidal probe were measured. During compression, the changes of the network structure were observed in detail, using a confocal scanning laser microscope (CSLM). The AFM data collected by means of homemade software were specifically processed to provide information regarding (a) the mechanical stiffness and (b) stress relaxation under load. Both aspects were looked upon as function of polymer concentration, structure porosity and loading speed.

Our results will show the utility and potential of the AFM-CSLM combination to study mechanical properties of aggregated networks at the microscale and to identify the contributions of (i) bond strength and (ii) droplets' configurations. We will also show that such experiments, together with a new model proposed by us, provide an up-till-now missing link between emulsion rheology (elasticity, yielding) and mechanics of granular matter (elasto-plastic deformation, interparticle friction).

4.2. EXPERIMENTAL

4.2.1 Emulsion preparation

Gelatin powder (from alkali-treated source, isoelectric point at $\text{pH} = 5$ and Bloom strength of 180 g) was kindly provided by Delft Gelatin BV, The Netherlands. The fluorescent dye rhodamine B isothiocyanate (RITC, from Sigma-Aldrich), glycerol (Merck), analytical grade (99+% purity) dodecane (Aldrich) and silicon oil (PDMS, from Fluka – product 85415) were used as supplied. The surfactant: Span 80 (sorbitane monooleate, Fluka), had a hydrophile-lipophile balance (HLB) value of 4.3.

A batch of water-in-oil (W/O) emulsion was prepared at 60°C by slowly pouring a “water phase” into an “oil phase” while mixing for 5 minutes with a T18 Ultraturrax (IKA, Germany) operated at 17000 rpm. The water phase was prepared as follows: first, RITC was dissolved in Milli-Q water, afterwards gelatin powder was left to soak in the solution for 30 min, then kept for 1 h at 60°C to dissolve the gelatin granules, after which the hot liquid solution was homogenized by stirring. Warm glycerol was added to this mixture as to increase its refractive index n_D and the final solution was mixed again. If glycerol was added before gelatin, the granules would not solve well.

When the temperature of the gelatin-containing mixture drops below $30\text{-}35^\circ\text{C}$, the biopolymer starts to gel. To avoid this process during preparation of the W/O emulsion, the oil phase (dodecane with 1 wt% Span 80) was preheated to the same temperature as the gelatin solution. The amount of oil was chosen so as to obtain an emulsion containing 10 wt% of water phase.

After the droplet formation, the batch emulsion was cooled at room temperature under continuous stirring. The droplet size distribution, as observed with CSLM, was rather broad (diameter $D \sim 0.5 - 15 \mu\text{m}$). To obtain a model sample with monodisperse droplets, the batch emulsion was fractionated. 40 ml from the W/O emulsion was diluted to 3 times the original volume by adding more oil phase, and stored in a narrow cylinder where it occupied a height of 20 cm. Three “phases” were

formed: a concentrated sediment at the bottom, a large middle phase and a clear transparent layer on top which grew with approximately 1 cm per day. After 3 days, about 100 ml of middle phase was carefully extracted. It had a much narrower size distribution, with droplets of 0.5-2 μm diameter, at an average diameter of 1 μm . This fraction turned out to be stable against aggregation/coalescence for several months, and was used as a stock for all further preparations. All experiments with this emulsion were performed at room temperature.

To stimulate droplets' aggregation, fixed amounts of the stock emulsion were mixed with PDMS-containing oil phases. The selection of (medium molar mass) PDMS was made after exploratory experiments and literature search.

Scrutinizing the literature, we have found that Leal-Calderon and co-workers [33] studied "the behavior of water droplets (0.28 μm in diameter) dispersed in a mixture of poly(dimethylsiloxane) (PDMS) chains and dodecane (with 1 wt% Span 80)". Except the different content of the droplets (water instead of the gelatine gel), the system used by these authors is identical with ours. Hence, we have chosen to take their findings as guide lines with respect to the type and strength of the interaction potential induced by PDMS.

Since the molecular mass of our silicon oil sample was not provided by the manufacturer, we had to use the viscosity vs molar mass masterplot [34] to calculate it. For the measured 320 mPa.s viscosity, an average molar mass of 13 kg/mol is obtained. Knowing the chemical formula of PDMS chains, $(\text{CH}_3)_3\text{Si}[\text{OSi}(\text{CH}_3)_2]_n\text{CH}_3$, we estimated an index $n = 174$ and a gyration radius of 3.4 nm.

In reference [33], based on the values of the n -index, two regimes of aggregation were identified. Whereas for $n > 500$ a hard core depletion potential [35] operates, for $n < 100$, this potential must be subjected to corrections because small molecular weight PDMS molecules could (eventually) swell the surfactant layer. A value of $n = 174$ (as calculated for our polymer sample) is close to the intersection of the two aggregation regimes, but still on the pure depletion branch of the phase diagram (see insert of Figure 5 in ref.[33]). The observed increase in networks strength for higher silicone oil concentrations (see Results) (*i*), the (short term) reversibility of droplet aggregation (*ii*) and the small PDMS concentration (only 1.5 % w/w) for which droplet's pair attraction becomes noticeable (*iii*) can be taken as indications that PDMS does not adsorb on the droplet's surfaces. These observations are consistent with polymer depletion as the probable aggregation mechanism, which means that droplets attract each other weakly, via an equilibrium pair potential set by the PDMS concentration.

To ensure a good dispersion of the silicon oil with the surfactant/dodecane, the PDMS was premixed with the oil phase and well stirred/equilibrated before adding the stock emulsion. The surfactant concentration was always kept constant at 1 wt%. The viscosities of the continuous phases as measured with a Bohlin VOR rheometer are given in Table 4.1.

For the AFM-CLSM experiments, a given amount (1.3 mL) of the aggregating emulsion was poured into custom-made liquid cells (diameter 24 mm, height 4 mm) immediately after preparation and left to sediment. For droplets with 1 μm diameter, the calculated sedimentation speed is around 0.07 $\mu\text{m/s}$, which means that roughly 8 h are needed to collect all single droplets in a layer at the bottom. After preparation, the samples were left undisturbed for 4 days, a time interval long enough for the

droplets to stick to each other and for the network to consolidate under normal gravity. In cases where more PDMS was added in a second step (after the 4 days), 1 more day was given, to allow for equilibration. Inspecting (with CLSM) the samples before compression experiments, no freely floating droplets were seen in the clear liquid above the droplet layer.

Table 4.1. Viscosity (η) of the oil phases (dodecane/ 1wt% Span 80 / PDMS)^a

PDMS (%wt)	5%	10%	15%	20%	100%
η (mPas)	18	26	33.7	45	320

^a Adding PDMS ($n_D=1.40$) decreases the refractive index of the Span 80 / dodecane mixture ($n_D=1.43$). Hence, the ratio between the compounds in the initial water phase (i.e., 0.05% RITC, 10% gelatin and 55 wt.% glycerol) was chosen to have not only a good fluorescent labeling of the droplets but also refractive index matching between them and the oil phase with 10% PDMS ($n_D=1.415$).

4.2.2 Microscopy Techniques

An inverted microscope with a confocal scanning laser unit attached (CSLM) was combined with a homemade atomic force microscope (AFM). The CLSM equipment (Ultraview, from Perkin Elmer, UK) was used with a 100x, N.A. 1.30 oil immersion objective. The objective is mounted into a high speed, computer-controlled piezoscanner, thus allowing for reproducible vertical displacements of the objective, with submicron resolution. The fluorescent RITC dye inside the droplets is excited with a Kr laser ($\lambda=568$ nm). The confocal images (672×512 pixels, each pixel corresponding to $(130 \text{ nm})^2$) are recorded with Yokogawa double Nipkow disk system and a Hamamatsu CCD camera and stored into the computer. A typical exposure time per image was 100 ms. Both Z series (i.e., stacks of images taken at consecutive Z positions inside the samples) and time series (i.e., images recorded at a fixed Z-location, but at consecutive moments in time) are possible.

A home-built AFM was used to measure the forces associated with the compression, relaxation and decompression stages. A piezoscanner (from Physik Instrumente, Germany), with XYZ position feedback, is fixed to the CSLM table and the AFM head is mounted on top of it (see Figure 4.1a). The setup is arranged such as to enable a good visualization of both the sediment layer and the AFM cantilever. For compression experiments, we used cantilevers having a spring constant: $k = 0.01$ N/m, with attached borosilicate glass spheres ($10.9 \mu\text{m}$ diameter). The roughness of these beads was checked with SEM, and no sharp substructures were evidenced. The values of the cantilevers' spring constants, calculated using the thermal excitation spectrum, agreed within 10% with the ones given by the supplier (Novascan Technologies, Ames, USA). Although this was the smallest spring constant that could be chosen (in combination with the bead), k turned out to be relatively large compared to the stiffness of our samples. As a result, the cantilever deflection was always very small compared to the deformation within the droplet layer. Before each experiment, the cantilever was rinsed thoroughly with ethanol and left to dry at room temperature.

To allow thermal and adsorption equilibration, the cantilever was immersed in the oil phase and left for 30 minutes, far above the droplet layer (see Figure 4.1a).

Using the AFM-CLSM combination, we measured the characteristic mechanical and optical response of aggregated sediments under compression with the spherical indenter. In these experiments, the sample is kept immobile while the AFM piezoscanner makes controlled movements. The maximum up-down amplitude which can be applied is 20 μm . Each experiment represents a single cycle during which the piezoscanner is driven in the vertical direction by a truncated saw tooth (see Figure 4.1b). The AFM measuring cycle begins with a compression down to a preset amplitude value (i.e., depth). Once this value is attained, the piezoscanner remains immobile during a certain time-interval (waiting period). Afterwards, the retraction cycle brings back the cantilever to its initial position. The cantilever's deflection, generated by the sample's response to the applied load, is monitored during the entire AFM measurement. For each AFM cycle, 3 sets of CLSM Z-scans are recorded: (i) before compression, (ii) in the waiting period and (iii) after the cantilever is fully retracted. Of the waiting period (typically 7 minutes), we used the first half to monitor the cantilever deflection due to eventual stress relaxation under load, and the second half for acquisition of the CLSM Z-scan of the structure.

Typically 20 AFM cycles were measured for each investigated sample at different locations. The compression speed was varied between: 5×10^{-2} and 3.75 $\mu\text{m/s}$. Unless otherwise stated, all presented data sets were recorded for a compression speed equal to 0.1 $\mu\text{m/s}$.

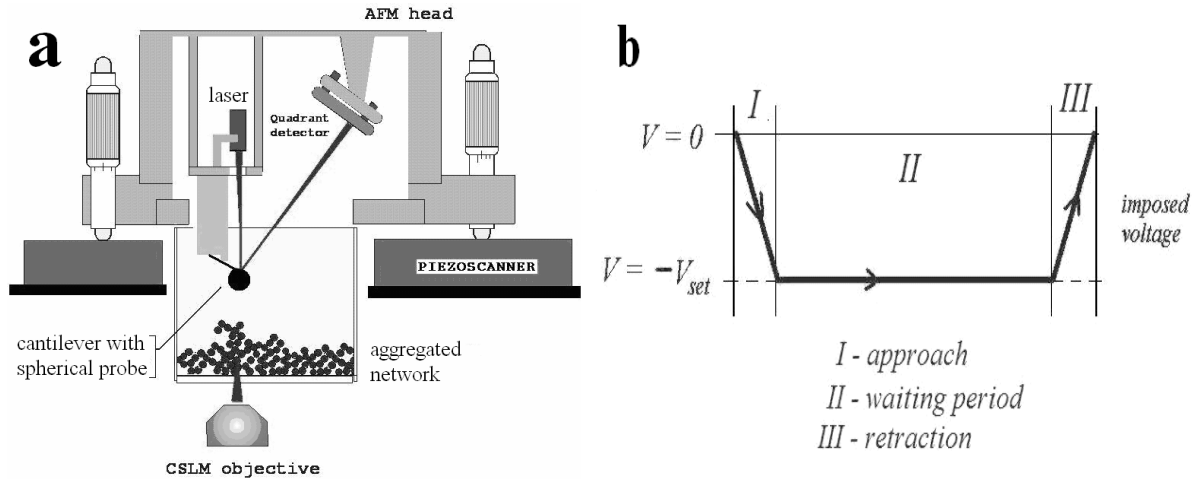


Figure 4.1. (a) Schematics of the AFM-CLSM experimental setup (not drawn to scale).
(b) Signal (voltage) imposed on the piezoscanner during a complete AFM cycle.

4.2.3 Data processing

4.2.3.1 AFM data processing

Prior to the AFM measurements on the droplets (sediments), the sensitivity of the laser – detection system for the used cantilever was determined via calibration scans on a hard glass substrate, under the respective oil phase. In all of these experiments, no interactions (between the glass probe and the flat hard substrate) could be sensed before entering the direct contact regime. Also the samples with the sedimented emulsion layers did not show any evidence for additional long-ranged interactions. Therefore, we assigned in all further calculations the (tip-sample) contact point to the first piezoscanner position (ZP_0) where the cantilever deflection (D) deviates from zero by more than twice the noise level. Subsequently, the D-ZP recordings were translated to force - ZP curves and, further, into force (F) - indentation (δ) graphs. This approach requires the calculation of δ values from the D-ZP curves, with the indentation depth defined as:

$$\delta = (ZP - ZP_0) - D \quad (4.1)$$

For homogeneous (or continuum-like) purely elastic samples, without any interaction prior to the direct contact between the indenter and the material, having a smooth tip-sample contact during loading and without adhesion at contact, the $F - \delta$ loading (i.e., compression) curve and the unloading (retraction) curve should superimpose. Any hysteresis between the two curves is an indication for dissipative processes during material deformation. For purely linear elastic materials, such dissipative processes do not occur and a so-called equivalent relative Young modulus: E^* , can be obtained from the slope of the AFM loading curve, using the Hertz model [27]. In this model, the local geometry during compression determines fully the functional F - δ dependence. For a spherical probe with radius R_p , compressing into a droplet with radius R_d , the F - δ loading curve is described by:

$$F = k D = \frac{4 E^*}{3} \left[\frac{1}{R_p} + \frac{1}{R_d} \right]^{-1/2} \delta^{3/2} \quad (4.2)$$

If the same spherical indenter deforms an initially flat material, equation 4.2 must be replaced by:

$$F = \frac{4E^*}{3} R_p^{1/2} \delta^{3/2} \quad (4.3)$$

At present, there is no simple equation associated with our case of a spherical indenter compressing into particulate networks. The results of our tentative modeling (see also the Appendix) to fit the experimental findings will be presented in section 4.3.5.

4.2.3.2. CSLM image analysis

Post-recording processing of the CSLM (Z scans and time series) was done using several software packages. Most (XY) images contained 672×512 pixels, corresponding to $87 \times 67 \mu\text{m}^2$. To characterize the structure from the images, three parameters were extracted: a correlation length, an “average aggregate size” and an “average area fraction”.

Correlation lengths (λ) were obtained by applying 2D self-correlation to a selected region of interest ($65 \times 65 \mu\text{m}^2$) and calculating pixel intensity correlation functions along eight lines, arranged in a star pattern (angle = 45°), with the intersection point in the center of the self-correlated image. Averaging over these functions resulted in profiles as shown in Figure 4.2. The location of the first peak next to the central peak (corresponding to self-correlations, i.e., within the same object) reflects the (characteristic) nearest neighbor distance between different objects, objects defined as “bright structures” separated by “dark regions”. The software used was WSxM v.2.1, developed for scanning probe microscopy (SPM) by Nanotech Electronica, Spain.

The “average aggregate size” was determined by “morphological sieving” [36]. This analysis was performed on the three most prominent structures. It involved noise reduction using a median filter (filter size 3 pixels) and smoothing using a Gaussian kernel with a sigma of 60 pixels. The image analysis toolbox was DIPlib (vers. 1.4.1), running under Matlab (version 7r14 from Math Works).

Another structure parameter of interest was the area fraction (ϕ) of the bright objects in the images. Image Pro Plus software was used to identify bright areas, using an object-finding algorithm, with an intensity threshold. ϕ was also computed as a function of Z . The found $\phi(Z)$ dependences (shown in Figure 4.3) revealed profiles with some scatter. From these Z -dependent ϕ -data, average values were calculated up to a height of $12 \mu\text{m}$ above the glass level (i.e., the point where the transition zone from concentrated sediment to clear liquid begins). In this $12 \mu\text{m}$ zone, variations around the average ϕ were at the most 10%. We would like to add here that the ϕ values appeared to depend (weakly) on the (Z and sample dependent) optical resolution. Hence, they should be taken as semiquantitative measures.

Image processing was also used to analyze the deformation (pattern(s)) inside the structure upon indentation and retraction. Movies (i.e., image time series) of indentation experiments as recorded at a given Z location in the material were transformed into so-called *difference movies*, by subtracting the first image from all consecutive frames. This was done with Image Pro Plus software.

The deformation profile (i.e., the displacement of droplet material) caused by the spherical probe in its lowest position was quantified by measuring radial intensity difference distributions as a function of Z location (shown in Figure 4.5, where the procedure is also further explained). This was done with IDL software.

4.3. RESULTS AND DISCUSSION

4.3.1. Layer structure before indentation

Aggregation and sedimentation were used to make cohesive multilayers of inter-connected W/O emulsion droplets on a substrate. In principle, different routes are possible to make such materials, which should allow creating different structures, even at the same composition. In method A, an aggregating mixture is freshly prepared and subsequently poured in the microscope cell. This procedure allows the droplets to aggregate while they settle to the bottom. In method B, one starts with a stable (i.e., non-aggregated) emulsion and allows all droplets to settle to the bottom before the flocculation agent is added.

Both methods have their own advantages and drawbacks when it comes to making droplet networks with constant properties (i.e., not dependent on the location in (X,Y) or Z). In method A, aggregation and sedimentation are coupled since bigger aggregates settle faster. As a consequence, the size (distribution) of the aggregates arriving at the bottom will be a function of time. This may or may not give rise to a Z -dependent layer structure, depending on how the arriving aggregates become incorporated in the already existing network and on the eventual compaction of this network.

Method B does not suffer from this potential drawback, since all entities arriving at the bottom are single droplets, which due to their high diffusivity ($D = kT/6\pi\eta a \approx 2 \cdot 10^{-13} \text{ m}^2/\text{s}$) and their repulsive (excluded volume) interactions, will form an equilibrium fluid with a density that is governed by the pair interactions and gravity only. The sedimentation length ($= 3 k_B T / 4\pi R_d^3 \Delta\rho g$) of $\approx 3 \text{ }\mu\text{m}$ is small enough to ensure that practically all droplets will eventually end up at the bottom. A bigger issue is that the structure of the network has to be kept intact when the flocculation agent, used to “switch on” the attractive droplet interactions, is added via liquid flow. In our case, droplet layers formed in the complete absence of flocculation agent were too fluid to withstand the liquid flow. Therefore we slightly modified the procedure, by starting with a “method A” preparation in the presence of a small amount of flocculation agent: high enough to obtain a “flow-resistant” network but small enough as to still have a dense droplet network (see below). More PDMS is then added in a second step. From now on we will refer to this preparation as method B. Using CSLM to monitor the network structure during the liquid replacement revealed that a PDMS content of 5 wt% was sufficient to create networks that remained intact. This was also the lowest concentration where a mechanical response could still be sensed with the AFM.

Table 4.2 summarizes the various formulations that were investigated. Essentially, three different types of structures were obtained (see Figure 4.2a-c). Layers prepared via method A1 and 5-15 wt % PDMS contents have similar, rather regular structures, in which the pore size of the network was comparable to the droplet diameter and the packing of the interconnected droplets was relatively open (i.e., small coordination number). For 20 wt% PDMS, method A1 resulted in larger pores and a denser packing (large coordination number) for the droplets in the network chains. Method A2 (the same as A1 but at twice the droplet fraction) resulted also in a rather open network, with large branched aggregates and large pores.

Table 4.2. Emulsion Layer Formulations ^a

Prep. Meth.	Bulk Droplet Fraction Φ_m (wt%)	PDMS Conc. c(wt%)	Average Area Fraction Φ (%)	Layer Height h(μ m)	Correlation Length λ (μ m)	Average Size D_a (μ m)	Pore Size D_p (μ m)	Apparent Young Modulus E^* (Pa)	Sample code
A1	0.006	5	25-26.6	15	4.6	2.6	1.9	5.7 ± 2	L05P05
A1	0.006	10	28.1	17	3.8			10.0 ± 2	L04P10
A1	0.006	15	25.0	17-18	5.3			12.0 ± 3	L05P15
A1	0.006	20	26.9	15-17	9.6	4.9	5.0	24.0 ± 10	L10P20
A2	0.012	20	14.3	~ 45	17.4	5.5	9.7	6.1 ± 1.3	L17P20
B	0.006	15	23.9	15	3.7			20.8 ± 3	L04P15
B	0.006	20	25.6	15	3.6			44.5 ± 16	L04P20

^a Samples have been coded according to the correlation length and the polymer content. The apparent Young moduli (E^*) were obtained through fits of the AFM compression curves with the Hertz model (eq. 4.3).

The remarkable structure difference between the A2 and A1 samples, prepared at the same PDMS content but different droplet fraction (and hence a different characteristic aggregation time [37]), suggests that, at 20 wt% PDMS, the kinetics of aggregation has a significant influence on the structure. It seems that, due to stronger attractions, the droplets are less able to rearrange once they have become bonded. We imagine that this applies both to the aggregates formed in bulk and to the freshly arriving aggregates that have to connect to the existing droplet network at the bottom.

To characterize the structure in a more quantitative manner, intensity-distance correlation functions were determined (see section 4.2.3.2), from which correlation lengths λ were obtained by determining the distance between the position of the central peak and the first peak. Figure 4.2d-f show the results corresponding to the structures from Figure 4.2a-c. Also a morphological sieving [36] was applied to determine the average size of bright (aggregates) D_a and dark (pores) D_p objects. Although we cannot point out which of the three measures is the best, we have made the choice to code the samples using the correlation length (see Table 4.2). Another parameter linked to the droplet density of the network is the area fraction (ϕ) (see section 4.2.3.2).

For A1 and B sediments, deviations from the average ϕ are encountered for Z positions higher than 12 μ m, when few branches of the network extend further into the liquid.

To inspect the Z dependence of the correlation length (i) and the droplet concentration (ii), the above-described analysis of the XY images was performed over the accessible Z range. The variation in height of the correlation length was determined for sample L04P20 and was found practically constant (variation below 5%). The droplet concentration was roughly estimated using the area fraction values. Figure 4.3 illustrates typical results for the L05P5 (equivalent with L04P20, method B), L10P20 (method A1), and L17P20 (method A2) samples presented in Figure 4.2a-c. For the L04P20 or L05P05 samples, the sediment concentration appears to be almost Z-independent, except in the “transition zone” at the top of the sediment, where localized network branches or aggregates stick out from the average top

“interface”. We note here that for Z positions $> 15 \mu\text{m}$, the longer optical path gave rise to a noticeable “blurring” of the images. For this reason, it was not possible to make a precise measurement for the L17P20 sample, where the layer thickness was $\approx 45 \mu\text{m}$. A remarkable finding is that the area fractions (and hence the average network densities) are practically the same for the “regular structure” A1 samples prepared at 5-15 wt% (e.g., L05P05) and the “open network” L10P20 sample prepared with 20 wt% (see open symbols in Figure 4.3). This corroborates that, although ϕ is a useful parameter to characterize the average density, it should be complemented with other structure parameters (like the correlation length) to distinguish between different materials.

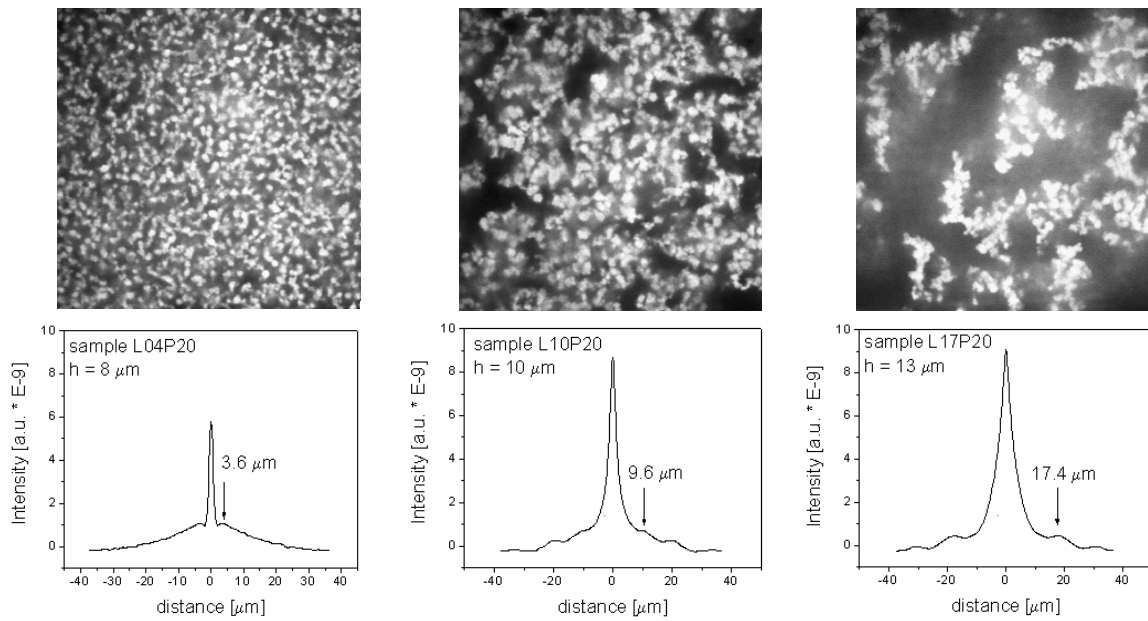


Figure 4.2. Representative CSLM images (a-c, scale $65 \times 65 \mu\text{m}^2$) and the corresponding average intensity – distance correlation spectra (d-f) for the three main types of structures obtained. The examples are: a) L04P20 (method B) – image typical for structures with $\lambda \sim 3 - 5 \mu\text{m}$, b) L10P20 (method A1) and c) L17P20 (method A2).

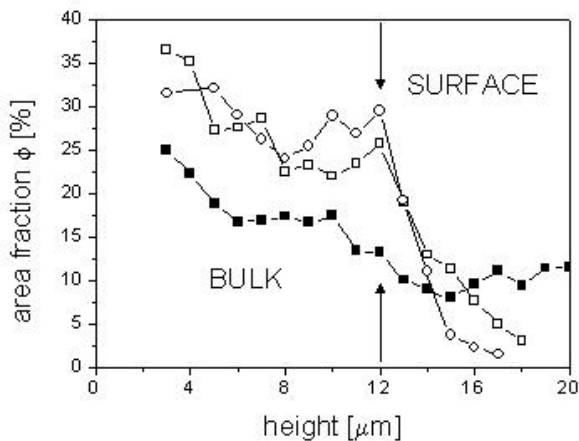


Figure 4.3. Area fraction (ϕ) as a function of Z-position for different samples. The symbols are solid squares for L17P20, open squares for L10P20, and circles for L05P05.

4.3.2 Structural changes during indentation

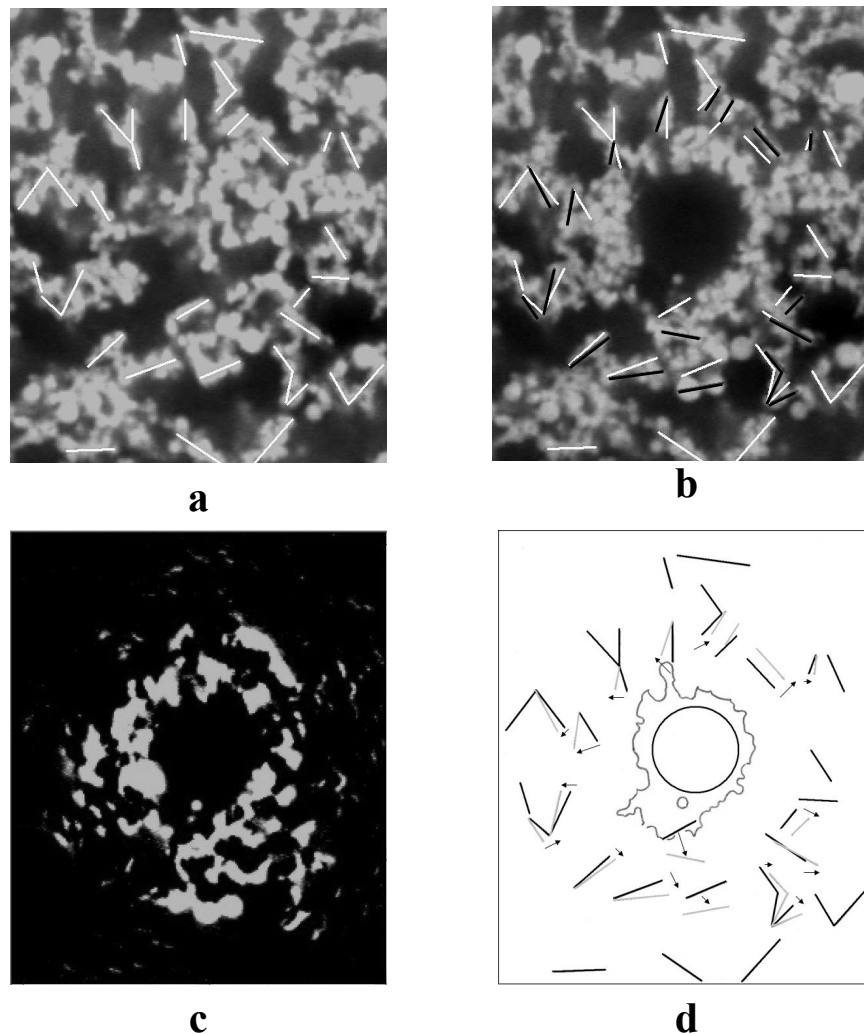


Figure 4.4. Typical CSLM images (scale: $25 \times 30 \mu\text{m}^2$) recorded for aggregated sample L04P20, before (a) and after (b) indentation. The white and dark bars present the orientation of chains before, respectively, after indentation. Short- and long-range deformations in the material are well evidenced by the intensity difference map (c). In panel (d) we show a sketch of the changes in direction for the activated chains. The black and grey bars are identical with the white, respective, black lines in panel (b). Displacements of the droplet chains, as induced by indentation, are indicated with arrows. Also the contours of the probe and the depletion zone are shown.

Under compression with an AFM probe, our aggregated droplets networks showed a remarkable behavior. The CSLM recordings revealed that the deformation of the droplet network occurs predominantly in the direct vicinity of the probe. Just looking at the direct camera images (Figure 4.4a,b), it becomes clear that a local densification of the droplet network takes place, within a corona of comparable size to the probe radius. This deformation turned out to be irreversible: upon retraction of the

probe, the “imprint” of the probe and the surrounding densified network remained (for weeks). We note here that, for non-aggregated sediments, the droplets were much more uniformly displaced and the dent was “repaired” quickly (10 min). The intensity difference map (Figure 4.4c) between the initial and the final state of the structure illustrates more precisely where the plastic deformation occurred.

A closer examination of the CSLM time-series showed that, simultaneously with the plastic deformation, also another type of deformation takes place. At large distances from the probe (i.e., well outside the compaction zone, reaching as far as 30 μm), small-amplitude deformations ($<1 \mu\text{m}$) carried by long (force) chains were observed. As could be observed in the retract stage, at the larger distances the deformation was reversible.

Analyzing these movies (by moving back and forth between consecutive images in the time series) allowed to recognize (though not with precision) which parts of the droplet network behaved like force chains. Figure 4.4d shows the initial and final orientation of these force chains. In some of the chains, not only compression but also bending occurred. After retraction, the chains that were close to the densified droplet ring could not relax completely and some preserved a bended shape. Others found a new orientation favored by the structural changes. The corresponding angular displacements ranged between 6° - 23° .

CSLM images in Z stacks were also analyzed quantitatively with IDL software. For each pair of images (before indentation and after retraction) recorded at the same Z position, an intensity difference map was calculated. Radial averaging over pixels at the same distance from the center of the probe then resulted in profiles as shown in Figure 4.5a. For Z positions below the probe (in its lowest position), positive excess intensities are observed (plot I in Figure 4.5a). Near the top of the layer the opposite is encountered: here only negative excess intensities occur (plot II). Between these Z regions, the profiles (not shown) show a negative excess up to a radial position R_1 , followed by a positive excess up to a radial position R_2 . The entire set of Z-dependent profiles, each with their assigned R_1 and R_2 values, can then be used to measure the three dimensional deformation profile. Figure 4.5b shows how the “depletion radius” R_1 (circles in Figure 4.5b) and the ‘excess radius’ R_2 (triangles) depend on Z. The depletion profile $R_1(Z)$ corresponds fairly well to the radius of the AFM probe. The $R_2(Z)$ profile clearly shows that a significant deformation takes place under the probe and that it reaches the hard substrate. Assuming proportionality between the excess intensity and the amount of displaced droplet material allows estimating the volume of displaced material for each Z position. This is displayed in the right-hand side of Figure 4.5b.

Although the roughly equal “positive” and “negative” areas appear to be in good agreement with the conservation of mass, we also like to point out some uncertainties in these results. One factor is that the correspondence between pixel intensity and the amount of material is not precisely proportional (even after background subtraction). This was demonstrated by the intensity map of the CSLM recording, which showed a non-uniform background at locations formally occupied by the (nonfluorescent) probe. Another factor is that our networks consist of discrete droplets and are also non-uniform on larger length scales. This is the cause of the oscillations as shown in Figure 4.5a, which give rise to ambiguity in choosing the locations of R_1 and R_2 in some of the profiles. For this reason, the trend that the ‘positive excess amount’ seems to approach zero at the bottom, should be interpreted

with some caution. If this were truly the case, then the AFM force-distance curves would correspond to the “bulk behavior” of the material, in the sense that the presence of a hard substrate would not play a role. The mechanical response of our finite layer would then be the same as that of a semi-infinite thick layer.

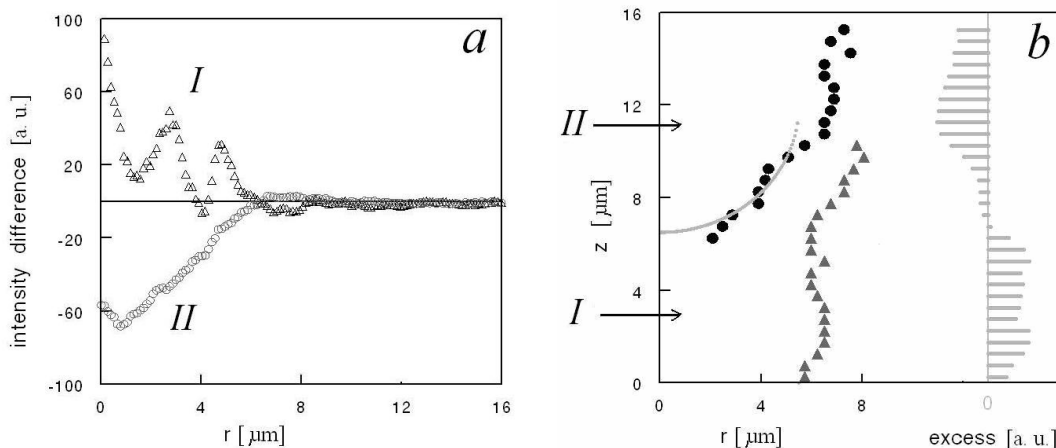


Figure 4.5. Image analysis for sample L04P15, based on intensity difference maps for a given height (after and before indentation). a) Radial averages around the center of the probe, taken at 3 μm (plot I) and 11 μm (plot II) above the hard substrate. Positive and negative excess regions can be localized from these profiles. b) Z dependent radial deformation profile, defined from the positive and negative excess regions in Figure 4.5a, along with a circular section representing the AFM probe. Radial integration over the profiles yields an estimate for the net amount of displaced material. This is displayed as function of Z in the right-hand side of panel b).

4.3.3 Force curves during indentation

The recorded AFM force curves correspond well to the CSLM observations. Figure 4.6a shows a typical force-distance curve obtained with one approach-wait-retract sequence. A clear hysteresis is observed. Whereas in the approach part the compressive force gradually increases (and occasionally small-amplitude jumps are superimposed), in the retract part, the force decays much more steeply with distance. This illustrates that the droplets that were squeezed into the “densification corona” were not able to store all the mechanical work as (recoverable) elastic energy. Considering that, in the approach stage, droplets were displaced over distances of the order of a whole droplet diameter (or more), this makes sense. In particulate networks such as ours, elasticity is practically entirely stored in the bonds between the droplets [Note that, we also performed AFM experiments on single droplets (similar to those in chapter 3 and ref. [38]) but now for the 1 μm -diameter droplets used in the present study. An E^* value of 2.5 kPa was found, corresponding to a droplet deformation of 0.7 μm per droplet for a droplet pair compressed with a force of 1 nN. Considering that O(100) droplets are in direct contact with the probe, the deformation per droplet should remain $< 0.01 \mu\text{m}$.]. For large displacements, these bonds have to be broken (a dissipative process), resulting in the formation of a new structure. Naturally, besides

bonds being broken, also new bonds are formed in this process. With this change in the structure, also the deformation is renewed and the mechanical properties are changed. This explains why the retract curve is more steep and short-ranged. Another general observation is that, in the retract curve, the force goes to zero without passing through a minimum. This confirms the absence of significant adhesion between the emulsion droplets and the glass probe. Although the use of such an “inert” AFM probe may cause “slip” to occur at its interface with the droplet network, even with such a slip, one principally still measures the mechanical properties of the droplet network. This is because both the deformation and the force loss in a thin slip layer are negligible, the former being obvious from the large indentations and the latter from a simple calculation on lubrication hydrodynamics and from the speed-independence of the force curves (see section 4.3.4).

In the following, we will focus on the approach curves.

4.3.3.1. Influence of bond strength

One of the main goals of this work was to investigate how the mechanical behavior of aggregated droplet networks is related to the properties of the bonds between the droplets. Since adding PDMS to the emulsions was found to be a reproducible way for controlling the strength of droplet adhesion, we first measured AFM force-distance curves as a function of PDMS concentration. As can be seen from Figure 4.6b, the resistance against deformation grows when the adhesion between the droplets is stronger.

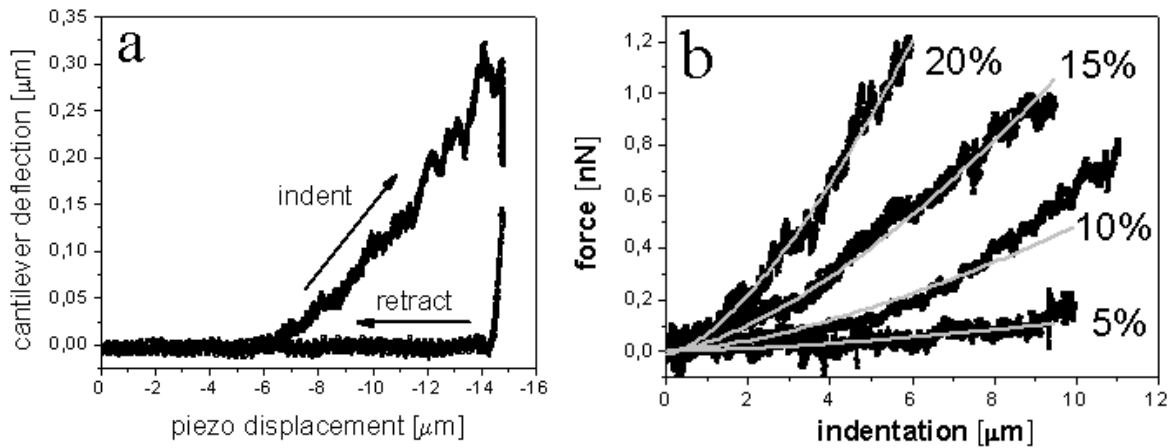


Figure 4.6. (a) AFM approach and retract curves for L10P20 sample. (b) Selected force-distance approach curves for A1-samples at different PDMS concentrations. Bright lines are fits with the Hertz model (eq. 4.3).

The general shape of the curve turned out to be reproducible, following a $F \sim \delta^{3/2}$ dependence, like in the Hertz model for continuum elastic materials. Although our samples clearly do not meet the assumptions of this model, we have fitted our curves with this model (eq. 4.3), to obtain the prefactor E^* (an apparent modulus) as a measure for the mechanical resistance. Average values of E^* , obtained by fitting several curves (taken at different locations), are shown in Table 4.2. Depending on the

XY location, the E^* values were found to vary. The relatively high variability for the L10P20 sample is in line with the large correlation length: $9.6\ \mu\text{m}$, which is about equal to the diameter of the AFM probe. This is a spatial variation which cannot be simply “averaged out” by the probe.

4.3.3.2. Influence of network structure

In the A1 preparations with 5-15% PDMS, the structure of the droplet networks was found to be (weakly) coupled to the PDMS concentration, presumably via the aggregation mechanism(s). Since both the structure and the bond strength could influence the mechanical response, we have attempted to study their separate influences. Careful replacement of the continuous phase liquid allowed us to increase the concentration of the flocculation agent without changing the structure of the droplet network. In this way, PDMS contents of 15 and 20 wt % were achieved, for a droplet network originally created at 5 wt% PDMS. An additional waiting time of 1 day was given, to allow the (small) PDMS molecules to diffuse through the droplet network and set the new concentration everywhere. Figure 4.7a shows how the added PDMS increases the strength of the network. This corroborates that the interdroplet bonds are responsible for the plastic resistance of the whole network as measured with the AFM.

Within the same framework, one can also study the influence of the network structure on the mechanical response by comparing force curves at the same PDMS concentration but for networks having different structures (i.e., structural parameters). Figure 4.7b clearly shows that the structure has an influence. Under the assumption that our structures are adequately characterized by their volume fraction and the correlation length (λ), it is obvious that the influence of λ is rather dominant. For samples with roughly the same volume fraction (like L04P20 and L10P20), a small correlation length corresponds to a stiffer network (see Figure 4.7b and Table 4.2, for the apparent moduli E^*).

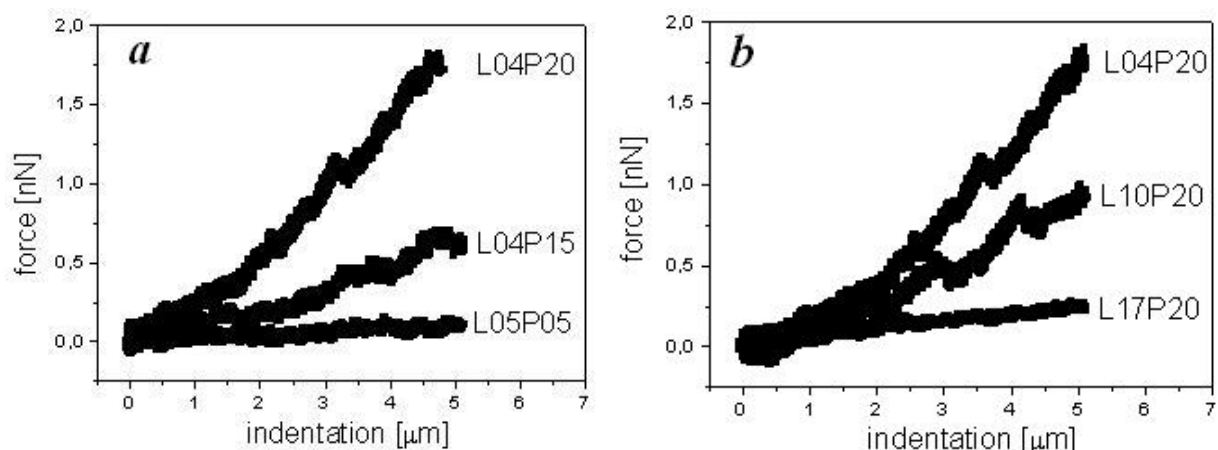


Figure 4.7. AFM compression curves for (a) networks having the same morphology but different PDMS concentrations and (b) networks with 20 wt % PDMS but with different morphologies. Sample codes are given in Table 4.2.

4.3.4. Influence of deformation timescale

Considering that our experiments are dynamic, carried out in a liquid environment, and that the probed droplet networks may contain viscoelastic elements, we also measured how the force curves depend on the speed of the indentation. Remarkably enough, on varying the approach speed between 5×10^{-2} and $3.75 \mu\text{m/s}$, no significant (i.e., larger than the spread between curves measured at the same speed) dependence of the force curves was found (see Figure 4.8). The same observation was also made for the retraction curves. This indicates that the hysteresis displayed in Figure 4.6a is not related to viscous dissipation in the droplet network (due to droplet fluid interactions) but to a speed-independent mechanism like the breaking of bonds between droplets that move with respect to each other. Hydrodynamic forces (proportional to flow rate), like viscous drag on the cantilever or a lubrication force near the probe, do not play a significant role either (during the approach and retract stages).

More insight into the (mechanisms behind the) dynamic response of the droplet networks can be obtained by monitoring the relaxation of the cantilever during the waiting period between the approach and retract scans. This resulted in relaxation curves as illustrated in Figure 4.9a, which show a more or less exponential decay down to an apparently constant force level. The constant force level indicates the presence of elastic elements (“springs”) in the (compressed) network.

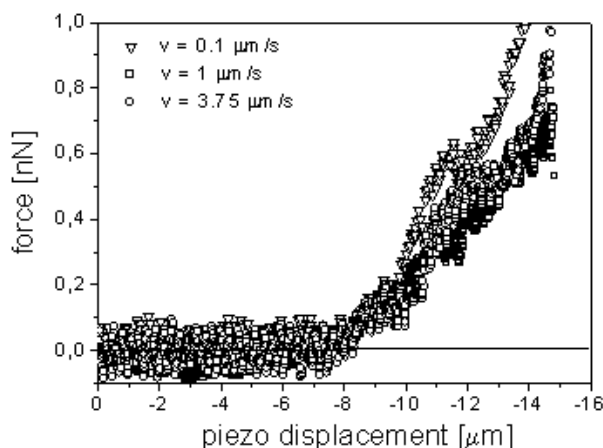


Figure 4.8. AFM approach curves for sample L10P20 recorded at different speeds.

It should be noted here that the compressive force on the AFM cantilever can only be diminished if the probe goes deeper into the material. This implies that any already compressed “springs” in the droplet network must undergo a further compression (instead of a decompression) in the relaxation stage. To explain this apparent contradiction, one has to assume the additional presence of a viscous resistance (i.e., proportional to a deformation speed) working in parallel to the elastic resistance. The decay of the viscous force during the waiting stage then allows the relaxation of the cantilever spring against the “droplet network” springs. The simplest viscoelastic element which could meet these requirements is the so-called Voigt-Kelvin element, which consists of a linear spring and a linear dashpot in parallel arrangement.

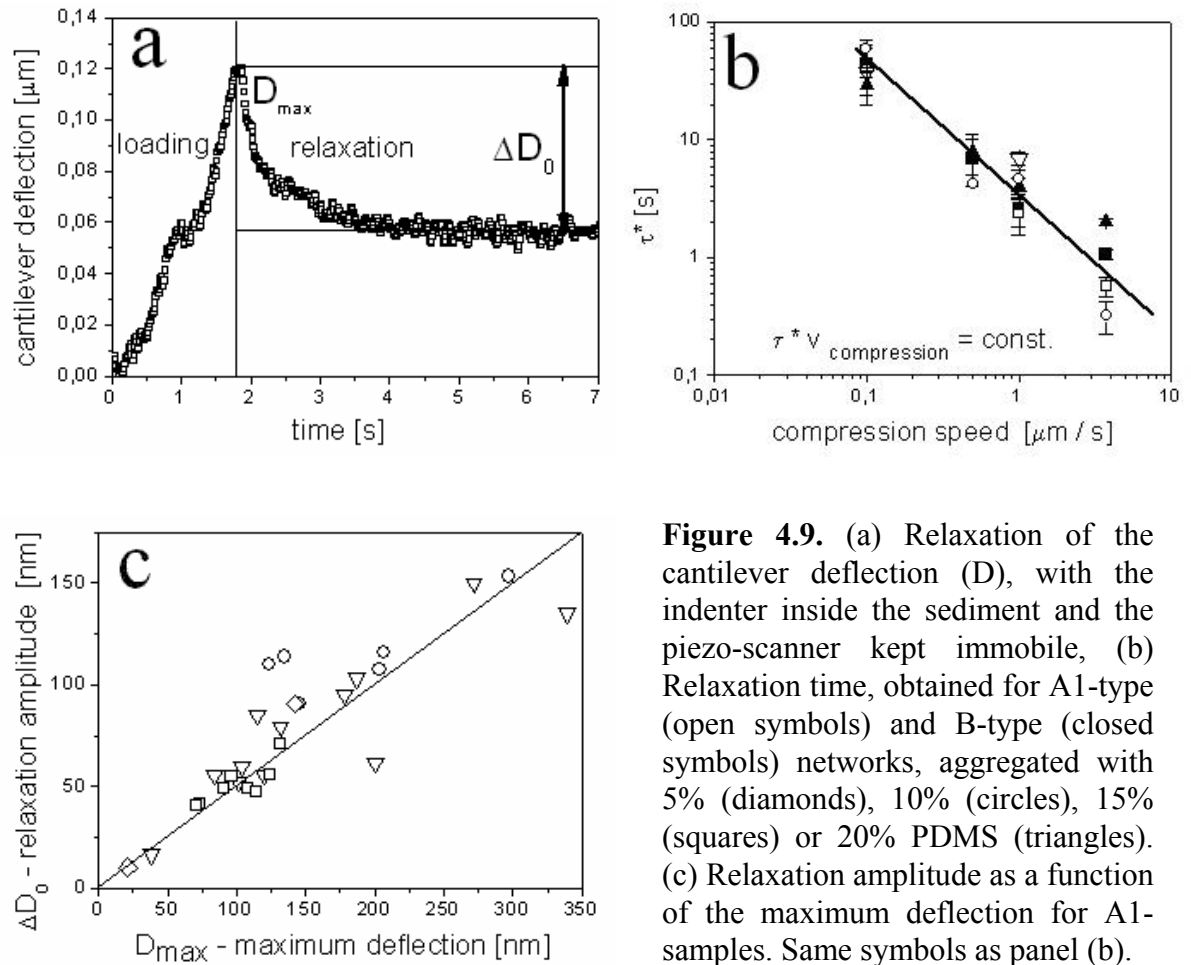


Figure 4.9. (a) Relaxation of the cantilever deflection (D), with the indenter inside the sediment and the piezo-scanner kept immobile, (b) Relaxation time, obtained for A1-type (open symbols) and B-type (closed symbols) networks, aggregated with 5% (diamonds), 10% (circles), 15% (squares) or 20% PDMS (triangles). (c) Relaxation amplitude as a function of the maximum deflection for A1-samples. Same symbols as panel (b).

To quantify the relaxation behavior, deflection vs time profiles were fitted with an exponential function:

$$\Delta D(t) = \Delta D_0 \exp\left(-\frac{t}{\tau_{exp}^*}\right) \quad (4.4)$$

for the entire range of deformation speeds and amplitudes. Remarkably, the characteristic relaxation time (τ_{exp}^*) was found to depend on the compression speed but not on the PDMS concentration (see Figure 4.9b). The relaxation amplitude (ΔD_0) turned out to be proportional to the maximum deflection (D_{max}) attained during compression (Figure 4.9c), but independent of the PDMS concentration or the ramping speed.

4.3.5. Rheological modeling

Three different stages were addressed in each AFM experiment: compression, relaxation and decompression. These stages were studied at different PDMS concentrations (i), as a function of maximum deformation amplitude (ii) and deformation speed (iii). It is interesting to see if the whole set of observed dependencies could be described by a single mechanical model, consisting of macroscopic elements (e.g. springs, dashpots, ...). We believe that a successful modeling could help to corroborate what kind of mechanical contributions play a role and to help to identify, to which microscopic mechanisms they could correspond. Eventually, we were able to construct a model which captures the dynamic mechanical behavior in a semi-quantitative way. Key aspects in the model are as follows:

1. Near the indenter there is a region where plastic deformation occurs; outside that region the sample deforms viscoelastically.
2. The collective of droplets is represented by a fixed set of mechanical elements whose properties (e.g., spring or damping constants) show a dependence on indentation depth (because the larger the indentation, the larger the contact area between sample and indenter).
3. Deformation outside the plastic region is transmitted in 3D via a stress field corresponding to and viscoelastic continuum. This imposes requirements on how the mechanical elements should behave as a function of indentation depth.
4. The droplet-droplet contacts near the indenter (where plastic deformation occurs) are modeled via a Coulomb friction force, equal to a friction coefficient times a normal force. This yields a so-called *stick-slip* element.
5. The friction coefficient, which originates from the strength of a droplet-droplet bond, (which depends on the local momentary arrangements of droplets in the plastic region) is not one value but distributed.
6. The viscoelastic deformation outside the plastic region is modeled via Voigt-Kelvin elements, i.e., parallel arrangements of a spring and a dashpot. The spring constant depends on the deformation, in agreement with aspect 3. The relaxation times are constant. These elements are arranged in a serial circuit with each other and with the stick-slip element.
7. There are two Kelvin elements to model the most simple relaxation spectrum.

Aspect 4 was formulated in terms of a Coulomb friction in analogy with granular matter modeling but one could also think of the breaking of bonds between the particles where it has been assumed that the yield force for breaking is proportional to the local stress in the emulsion, indicating that the exclude volume effects become important in the region of plastic deformation.

Aspect 5 was incorporated to capture the force-jumps observed in the compression stage. Aspect 6 was needed to capture the relaxation behavior. Aspect 7 is needed to achieve a quantitative description of the data, i.e., to understand (in macroscopic terms) the dependence of the relaxation curve on the approach velocity of the indenter.

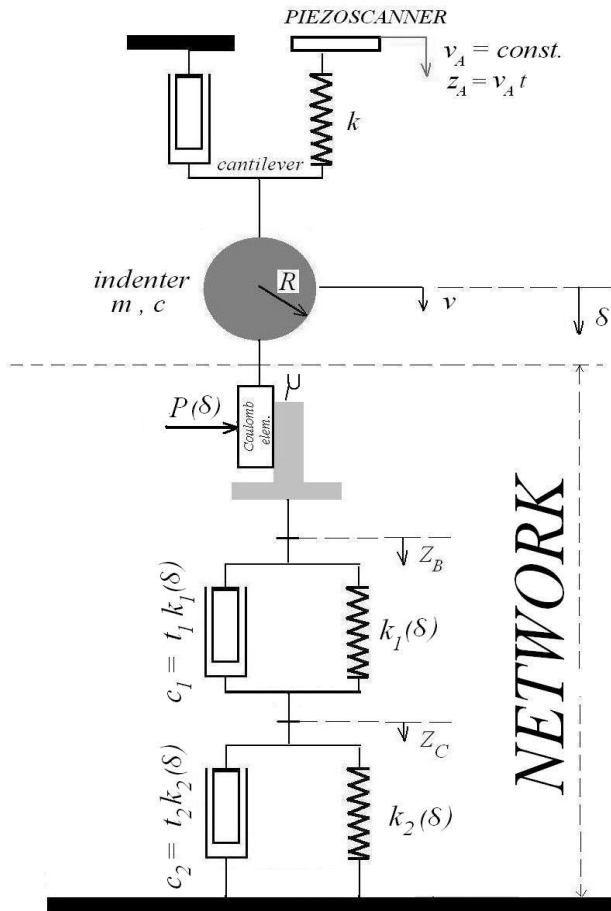


Figure 4.10. Equivalent mechanical circuit representing the combination of the AFM probe and our droplet network. In our model, δ , which has the meaning of an indentation depth, is the coordinate of the indenter, and v is its (local) speed. A more elaborate description of the model can be found in the Appendix.

Besides the elements representing the material (i.e., the droplet network), also the AFM parts which contribute to the equation of motion have to be accounted for. These are the cantilever and the spherical indenter (see Figure 4.10). Hence, the equations of motion (see eq. A6 in the Appendix) also incorporate the contribution of the cantilever's elastic spring and the damping due to motion in liquid.

Figures 4.11a,b show the capabilities of this model for a typical experiment. Both the compression and the relaxation stage of the AFM experiment are quantitatively described. If the friction coefficient μ is taken as a constant (Figure 4.11a), then the irregular jumps in the compression stage are not captured. However, allowing for μ to be described by a distribution around an average value $\langle \mu \rangle$, more or less pronounced force-peaks can be generated (see Figure 4.11b). In the retraction part, it is captured that the force decays more steeply than it rises in the approach part.

Figures 4.11c,d illustrate how the relaxation stage of the experiment is captured by the model, by comparing the average relaxation time and the relaxation amplitude, as extracted from the experimental curves, to simulated counterparts. In Figure 4.11c this is done for the relaxation time as a function of the compression speed. The connection between the model and the experiments is not entirely straightforward here. In the model, we had to incorporate two Kelvin elements, each with their own relaxation time (respectively t_1 and t_2) to represent the droplet network. This was the simplest way to obtain a dependence of a relaxation time on the speed of the compression: the faster the compression, the more prominent the contribution of the shortest relaxation time to the “average relaxation time”. Although the model does

reproduce the observed decrease of the apparent relaxation time with increasing approach speed as a trend, a quantitative agreement is clearly not achieved. In our opinion, this probably indicates that the model is too simplistic. At the same time, it is also not clear which extension of the model would be appropriate.

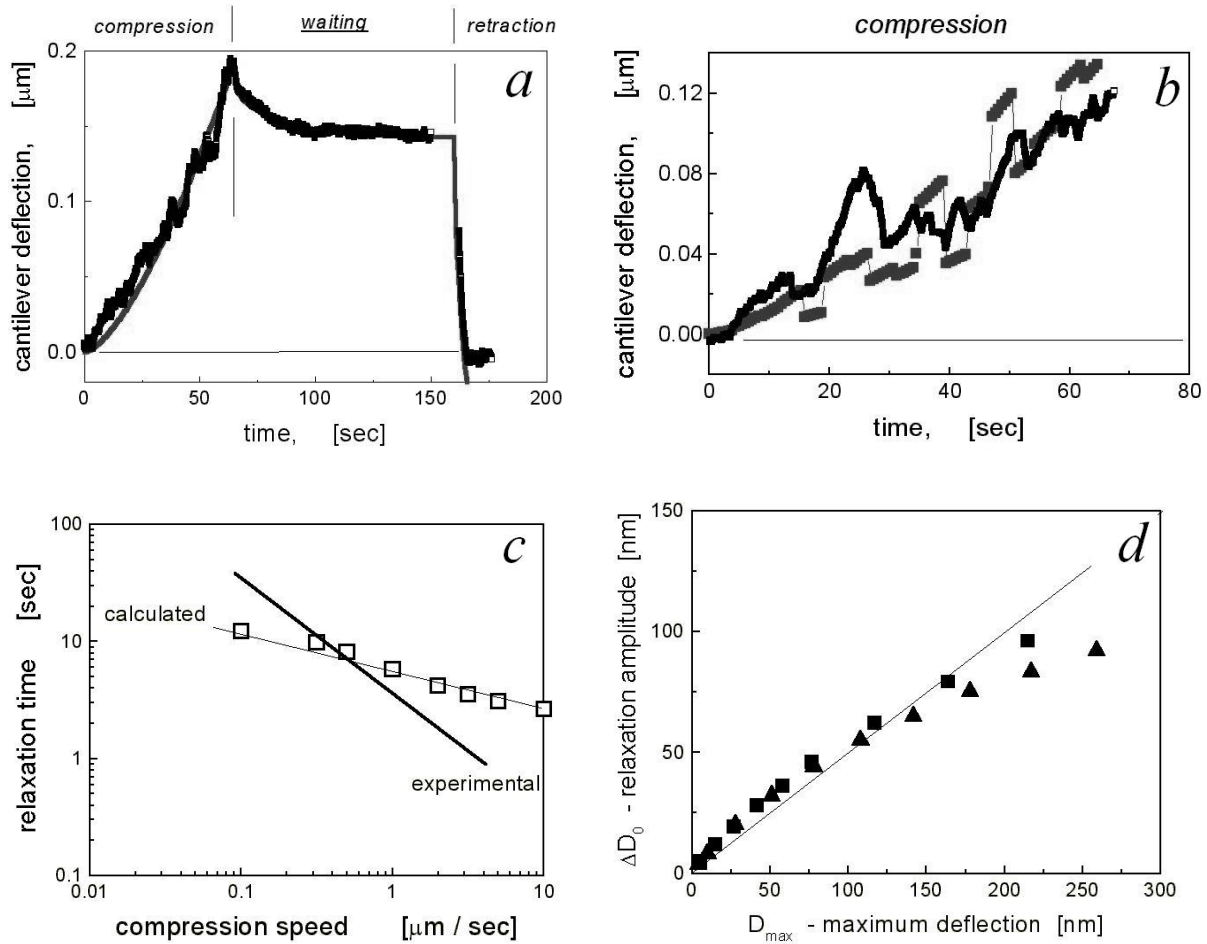


Figure 4.11. (a-b) Experimental (black) and calculated (gray) force-time curves for sample L10P20. (a) Example of a complete AFM force-distance cycle. The fitting parameters were adjusted for optimal superposition between the measured and model-generated results, and are: $k_{eff} = 4.5 \cdot 10^{-4}$ N/m, $k_{l0} = 8 \cdot 10^{-4}$ N/m, $t_1 = 36$ s, $t_2 = 5$ s, $B_0 = 1.22 \cdot 10^{-4}$ N/m, and $\Delta\mu = 0$. In the piezo-driven stages of the cycle, the speed was $0.1 \mu\text{m/s}$. (b) To simulate the fluctuations superimposed on the approach curve, a distribution for the friction coefficient μ is needed. Results are shown for $\Delta\mu = 0.5$. (c) Average relaxation time τ_{calc}^* (symbols) as predicted by the model for sample L10P20 with the parameters given under panel a). The experimental results for this sample are given by the thick line. (d) Simulated values for the relaxation amplitude ΔD_0 . As input values, we used the model-generated parameters for samples L04P15 (squares) and L04P20 (triangles). To guide the eye, a line with slope 0.5 was added to the plot.

In Figure 4.11d, the relation between the indentation depth and the amplitude of the subsequent cantilever relaxation is considered. Clearly the trend as observed with the experiments (Figure 4.9c) is well reproduced by the model. Also shown by the model calculations of Figure 4.11d is that essentially our mechanical model is essentially nonlinear. This is due to the presence of the stick-slip element.

Our equivalent mechanical model also allowed us to study in more detail what was the behavior of the separate elements during the approach-wait-retract cycles. Here it turned out that different mechanical elements dominate in different stages. In the approach part, the stick-slip element dominates the response, which is in good correspondence with the speed independence of the approach curves. In contrast, the force relaxation during the waiting stage and the rapid force decay in the retract stage are largely set by the Kelvin elements. This is also in line with the absence of irregular jumps in these curves.

A natural follow-up question is, how these separate mechanical behaviors correspond to the different types of structural changes described in section 4.3.2. Clearly, the suggestion from the foregoing analysis is that the compression regime corresponds to the formation of the densified corona (Figure 4.5), whereas the relaxation regime corresponds to a further compression of the force-chains (Figure 4.4a,b).

In this light, it is interesting to consider how the normal force (multiplier B_0) at the stick-slip element and the spring constant of the Voigt-Kelvin elements, depend on the PDMS concentration. These dependences, obtained by fitting AFM force curves for the A1-type samples, are shown in Figure 4.12a. The average friction coefficient (defined as $\langle \mu \rangle = B_0 / k_{eff}$) as derived from Figure 4.12a is shown in Figure 4.12b.

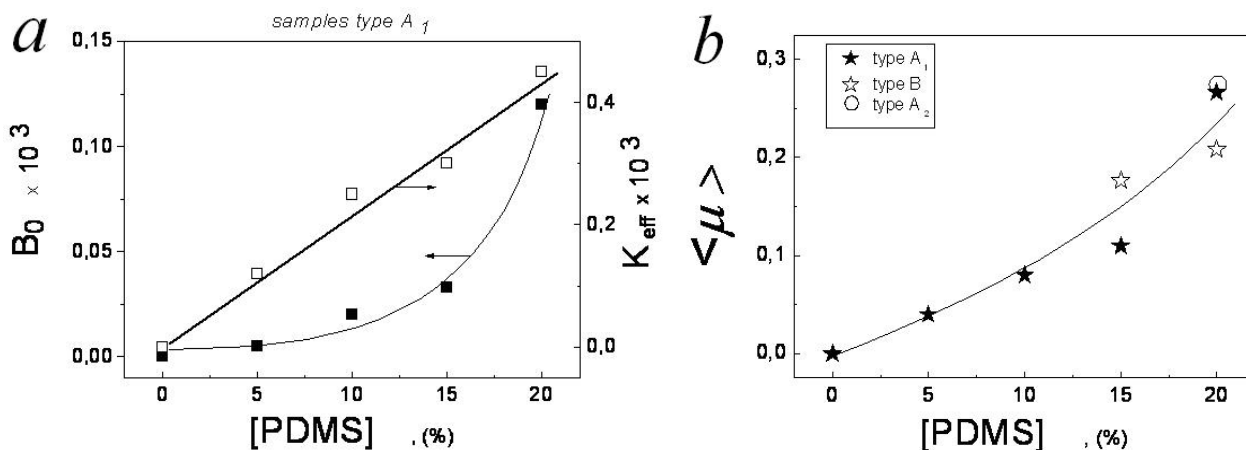


Figure 4.12. Overview of fitted model parameters as a function of PDMS concentration for the A1 samples. (a) Effective stiffness, k_{eff} (open symbols), and multiplier for the normal force, B_0 (both in N/m) and (b) average friction coefficient, $\langle \mu \rangle$. See text for further details.

Although the increase of B_0 with the PDMS concentration corroborates that the droplet network increases its resistance to plastic deformation via an increased normal force, and hence an increased friction force, it is also found that k_{eff} increases

with the PDMS concentration. This could suggest that also the force chains grow stronger when the PDMS concentration is raised. Although this would fit within our picture (a stronger attractive pair potential between droplets at higher [PDMS] could conceivably lead to stronger chains), we also feel that a more precise characterization of the (structure of the) force chains would be required to say more about their role. For the present emulsion, this was not possible, but for particles or droplets with a fluorescent core this should be possible.

4.4. DISCUSSION

With the present chapter, we aim to make a contribution to the research on the mechanical properties of particulate networks, by studying a model aggregating W/O emulsion with an experimental setup in which AFM and CSLM are combined for simultaneous use. This approach has yielded insights into the material behavior as well as into the utility of AFM-CSLM as a measurement technique.

4.4.1. Mechanical behavior of our aggregated emulsion network

Considering our aggregated emulsion networks formed via gravity settling, we found that all samples were soft (i.e., showing a weak mechanical resistance) and plastic (i.e., solidlike, but with irreversible structure changes upon deformation). Because of the latter, the mechanical properties of the samples as formed under normal gravity settling could only be measured during the first approach (i.e., stress loading) curve at the selected sampling area.

Force-indentation approach curves obtained with a large spherical probe as indenter were seen to scale approximately as $F \sim \delta^{3/2}$ (as was also found for non-particulate materials showing elasto-plastic deformation [36]). The prefactor (which is proportional to an elastic modulus E^* in the Hertz model for continuum elastic solids) was taken as a measure for the resistance of the material against deformation. Our E^* values showed a clear dependence on the strength of the interdroplet attractions, as set by the concentration of the PDMS flocculant. This was most convincingly demonstrated by experiments in which the flocculant concentration was increased while the structure of the droplet network was kept intact.

The deformation of the network as measured optically, in 3 dimensions and with micron resolution, clearly indicated an irreversible local compaction of the network in a shell around the probe, with a thickness of a few droplet diameters. A more precise inspection of the structure changes revealed that, in parallel, also a (more or less) reversible structure deformation takes place through force chains, originating at the periphery of the densified shell.

Analysis of the combined AFM and CSLM observations allowed us to relate the (mesoscopic) plastic behavior to (microscopic) stick-slip events, i.e., droplets sliding past each other after a yield threshold has been overcome. The speed independence of the AFM approach curves, as well as their superimposed force-jumps are clear indicators for this behavior. The dependence of the “plastic resistance” E^* on the PDMS concentration then indicates that the critical yield force grows with the

droplet-droplet attraction strength, which is at least in agreement with simple Coulomb friction.

The choice to include a waiting time between the loading and unloading in our experimental AFM protocols allowed us to identify an additional contribution to the mechanical behavior of the material, manifested as a stress relaxation. The finding that these relaxations always led to a residual stress clearly points at the presence of elastic elements which can only be attributed to the droplet network. We think that these correspond to the force chains as observed with the CSLM.

These proposed mechanisms are corroborated by an equivalent (macroscopic) mechanical model in which the aggregated emulsion network is represented as a serial arrangement of a stick-slip element and two Kelvin elements (i.e., parallel arrangements of springs and dashpots), each of them with a magnitude that follows a prescribed dependence on the indentation depth. With this model, it was possible to reproduce the most prominent AFM observations quantitatively.

Considering the approach-wait-retract protocol, it turned out that the approach stage is dominated by the stick-slip element. At the microscopic level this element represents the yield force between the droplets which have to rearrange their bonds with the environment to allow for the relatively large deformations in the plastic region. Both the number of droplet-droplet bonds and their strength are covered for, respectively via the prescribed dependence on indentation depth and via a linear dependence on the normal force. Even the force-jumps occasionally seen in the approach stage can be predicted, by assuming a distribution of friction coefficients (yield strengths) between droplet pairs.

In contrast, the waiting and retract stages are dominated by the Kelvin elements. Although we cannot assign a specific mechanism to the dashpots, their presence is essential for predicting the observed time-dependent behavior. We think that the spring elements represent the force chains.

4.4.2. AFM-CSLM as a microrheological method

In the here-described study, a new type of micromechanical experiment was performed: a local indentation, with simultaneous registration of the dynamic forces (using AFM) and structural rearrangements (using CSLM). To our knowledge, this was the first time that AFM and CSLM were simultaneously applied to investigate the mechanics of soft colloidal systems like our adhesive droplet network.

Compared to the more classical macroscopic rheological techniques, an evident advantage is that with AFM-CSLM the question: “via which mechanism(s) the material resists to deformation” can be addressed at the microscopic level. In the present study, this allowed us to identify two mechanisms: 1) an irreversible local network compaction and 2) a (partially) reversible elastic deformation via force chains. We note here that our (still somewhat) polydisperse emulsion was not the most optimal system for resolving the structure (changes). With monodisperse particles with fluorescence restricted to a small core (e.g., ref. [37] and [40]), structures can be resolved at the single particle level, allowing an even more detailed look on the structure (changes). This should also allow studying more concentrated particle gels or granular networks.

AFM-CSLM could have the potential to develop into a new method for studying the rheology of (small quantities of) particulate networks. Two questions which have to be considered before adopting their results as rheological quantities are (1) whether the proximity of a hard substrate (i.e., the cover slip of the CSLM) contributes to the measurement and (2) whether the microscopic measurement can be linked to a macroscopic rheological property.

The first question can be addressed with the AFM-CSLM measurement itself. In the present study, two indications were obtained that the contribution of the glass substrate to the measured force curves is small. The first one comes from our image analysis (as in Figure 4.5) and showed that, although the displacement of droplets did extend down to the substrate, the amount of excess material appeared to go to zero. The second clue is given by analysis of the $F - \delta$ approach curves; the same functional dependence was observed at the largest indentation and at half its value. Although this suggests that identical AFM-CSLM results would have been obtained with layers of the same material (structure and composition) but with a height much larger than the extent of the deformation, we could not rigorously check this for the emulsion system used in this study. Blurring of the images, as observed for the present emulsions at optical depths beyond 20 microns, could perhaps be diminished by an even better refractive index matching.

The second question is equally important but turned out to be difficult for the present emulsion system, since the mechanical response is not only very weak, but shows also a large history dependence due to the compaction. On the other hand one could say that this illustrates another advantage of the AFM-CSLM method: its ability to probe the mechanics of very soft materials, as formed by gravity settling. Given the abundance of such systems in practice, this makes the AFM-CSLM combination more attractive.

Finally, we would also like to point out that the AFM-CSLM method has a very interesting potential for networks in which the particle interactions develop over time. If this occurs with negligible rearrangements in the particle positions, then one could study the separate effect of changes in the particle interactions. Our aggregation emulsion turned out to fit this case, as was observed after long ageing times. This will be discussed in chapter 5. Also this application of AFM-CSLM could have relevance for practical systems which may alter during their shelf life.

APPENDIX

The *stick-slip* process can be described by a Coulomb friction force (F_{fr}), with a friction coefficient μ and a force P normal to the sliding surface. The normal force will be proportional to the local stress in the gel, thus will increase with the indentation, δ , according with the formula

$$F_{fr} \leq \mu P(\delta) = \mu B_0 \delta^{3/2} \quad (A1)$$

Moreover, the friction coefficient μ is supposed to vary for different droplet-droplet and droplet-indenter contacts; that is, μ is not fixed, but will assume variable (instantaneous) values, according with a random distribution $Q(\mu)$.

$$Q(\mu) = \begin{cases} \frac{1}{2 \Delta \mu} & \text{for } \mu \in [\langle \mu \rangle - \Delta \mu, \langle \mu \rangle + \Delta \mu] \\ 0 & \text{for } \mu \notin [\langle \mu \rangle - \Delta \mu, \langle \mu \rangle + \Delta \mu] \end{cases} \quad (\text{A2})$$

The Coulomb element will be in the *stick* condition as long as the local force loading the element remains smaller than a threshold value:

$$F_{fr} < \mu P(\delta) \quad (\text{A3})$$

As soon as the threshold is crossed, *slip* and hence local plastic deformation will occur.

Because μ depends on the instantaneous geometry, its value will ‘renew’, on the average, after the indenter has displaced over a distance comparable with a particle diameter. Therefore, also the time interval Δt after which μ is renewed, is mediated by a distribution function

$$Q^*(\Delta t) = \begin{cases} \frac{1}{2 \Delta T} & \text{for } \Delta t \in [\langle T \rangle - \Delta T, \langle T \rangle + \Delta T] \\ 0 & \text{for } \Delta t \notin [\langle T \rangle - \Delta T, \langle T \rangle + \Delta T] \end{cases} \quad (\text{A4})$$

where $\langle T \rangle \approx 2R_d / v$, with v the local velocity of the indenter.

In our mechanical model, the Coulomb element is serially linked with two spring-dashpot (Kelvin) elements (see Figure 4.10) [A simplified version of the model, with only one Kelvin element, was insufficient to generate force-distance curves similar to the experimental ones.]. These last two building blocks incorporate the viscoelastic properties of the network. The elastic contributions k_i are not taken as constants but depend on the indentation depth:

$$k_i = k_{i0} \delta^{1/2} \quad (\text{A5})$$

Neglecting the inertia of the cantilever-probe (as it was proven by calculations to be appropriate in our case), the equations of motion are given by

$$\left\{ \begin{array}{l} c \frac{d \delta}{d t} + k \delta = k z_A - F_{fr} \\ c_1 \frac{d z_B}{d t} + k_1 z_B = c_1 \frac{d z_C}{d t} + k_1 z_C + F_{fr} \\ c_2 \frac{d z_C}{d t} + k_2 z_C = F_{fr} \end{array} \right. \quad (\text{A6})$$

$$\text{and } F_{fr} = \mu B_0 \delta^{3/2} f_c, \text{ where: } f_c = \begin{cases} 1 & \text{if } \frac{d\delta}{dt} > \frac{dz_B}{dt} \\ -1 & \text{if } \frac{d\delta}{dt} < \frac{dz_B}{dt} \end{cases}$$

The system of equations (A6) can be rearranged into:

$$\begin{cases} \frac{d\delta}{dt} = \frac{k}{c}(z_A - \delta) - \frac{1}{c}F_{fr} \\ \frac{dz_B}{dt} = \frac{k_1}{c_1}(z_C - z_B) - \frac{k_2}{c_2}z_C + \left(\frac{1}{c_1} + \frac{1}{c_2}\right)F_{fr} \\ \frac{dz_C}{dt} = \frac{1}{c_2}F_{fr} - \frac{k_2}{c_2}z_C \end{cases} \quad (\text{A7})$$

The relative velocity over the stick-slip element is:

$$v = \frac{d\delta}{dt} - \frac{dz_B}{dt} = v_0 - \Lambda F_{fr} \quad (\text{A8})$$

where the coefficients are given by:

$$v_0 = \frac{k}{c}(z_A - \delta) - \frac{k_1}{c_1}(z_C - z_B) + \frac{k_2}{c_2}z_C \quad (\text{A9a})$$

$$\Lambda = \left(\frac{1}{c} + \frac{1}{c_1} + \frac{1}{c_2}\right) \quad (\text{A9b})$$

To solve the system of equations (A7), we define the “computational”

$$\text{time-scale: } t_0 = \frac{c}{k} \text{ and length-scale: } z_0 = v_A t_0 \quad (\text{A10a})$$

and the dimensionless parameters

$$\tau_i = \frac{t_i}{t_0} \text{ and } \xi = \frac{\delta}{z_0}, \quad \xi_X = \frac{z_X}{z_0} \quad (\text{A10b})$$

where : $i = 1$ or 2 (see Figure 4.10) and the index X is related to the “moving” elements: $X = A$ for the piezoscanner base, $X = B$ or C for displacements at the points B and C, respectively.

The working equations have now the following expressions:

$$\left\{ \begin{array}{l} \frac{d \xi}{d \tau} = (\xi_A - \delta) - \beta f_c \xi^{3/2} \\ \frac{d \xi_B}{d \tau} = \frac{1}{\tau_1} (\xi_C - \xi_B) - \frac{1}{\tau_2} \xi_C + \left(\frac{1}{\gamma_1} + \frac{1}{\gamma_2} \right) \beta f_c \xi \\ \frac{d \xi_C}{d \tau} = \frac{1}{\gamma_2} \beta f_c \xi - \frac{1}{\gamma_2} \xi_C \end{array} \right. \quad (\text{A11})$$

where β and γ_i are defined by

$$\frac{\mu B_0 z_0^{1/2}}{k} = \beta \quad (\text{A12a})$$

$$\frac{c_i}{c} = \frac{k_i t_i}{k t_0} = \frac{k_{i0} z_0^{1/2} \tau_i}{k} \xi^{1/2} = \gamma_i \xi^{1/2} \quad (\text{A12b})$$

The dimensionless relative velocity $u = \xi^* - \xi_B^*$ over the stick-slip element is

$$u = u_0 - \lambda f_c(u) \quad (\text{A13a})$$

with

$$u_0 = (\xi_A - \xi) - \frac{1}{\tau_1} (\xi_C - \xi_B) + \frac{1}{\tau_2} \xi_C \quad (\text{A13b})$$

$$\lambda = \left(\xi^{1/2} + \frac{1}{\gamma_1} + \frac{1}{\gamma_2} \right) \beta \xi \quad (\text{A13c})$$

The function $f_c(u)$ determines the (relative) velocity-dependence of the friction force, over the stick-slip element. The shape of $f_c(u)$ is a symmetric step-function (see Figure 4.13, thick curve), defined by the following restrictions:

When the Coulomb element is in the stick phase, $f_c(u)$ can take any value between -1 and +1;

$$(a) \text{ in the slip phase, } f_c(u) \text{ is constant and } f_c(u) = \begin{cases} 1 & \text{for } u > 0 \\ -1 & \text{for } u < 0 \end{cases}$$

We have to calculate $f_c(u^*)$, where u^* is the relative speed for which the equality (A19) is satisfied.

$$f_c(u^*) = \frac{1}{\lambda} (u_0 - u^*) \quad (\text{A19})$$

Graphically, finding u^* is equivalent with determining the intersection between two curves: $f_c(u)$ and a straight line, with slope $1/\lambda$ (see Figure 4.13)

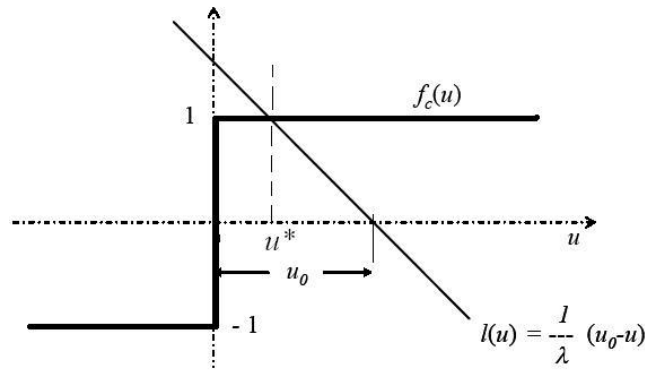


Figure 4.13. Equality A19 can be solved using the graphic representations for $f_c(u)$ (thick curve) and $l(u)$ (thin line).

The value of f_c is given by (A20)

$$f_c = \begin{cases} 1 & \text{if } u_0 > \lambda \\ \frac{u_0}{\lambda} & \text{if } -\lambda < u_0 < \lambda \\ -1 & \text{if } u_0 < -\lambda \end{cases} \quad (\text{A20})$$

The set of equations (A11) can be solved by integration, using a fourth order Runge-Kutta scheme.

The complete force-distance curves were fitted, using eq. (A11) and the fitting parameters: k_{10} , k_{20} , t_1 , t_2 , B_0 and $\Delta\mu$. The first two parameters can be combined into an effective stiffness of the network: k_{eff} , with

$$k_{eff} = \frac{k_{10} k_{20}}{k_{10} + k_{20}}.$$

The values of k_{eff} should be larger than B_0 , otherwise the stick-slip element does not slip in the approach phase. To calculate the friction coefficient, we have to use an intuitive argument. The pressure between the two components of the stick-slip element should be proportional to the normal stresses between adjacent particles and these stresses must be proportional with the indentation force. With this arguments, the average friction coefficient is: $\langle\mu\rangle = B_0 / k_{eff}$.

Table 4.3. In the mechanical model, the parameters were estimated based on the following values

<p><u>CANTILEVER</u></p> <p>stiffness: $k = 10 \text{ mN m}^{-1}$; resonance frequency in air: $4.4 \times 10^4 \text{ s}^{-1}$ resonance frequency in liquid: $8.8 \times 10^3 \text{ s}^{-1}$ mass: $M_0 = 5.17 \times 10^{-12} \text{ kg}$ drag coefficient ^a: $C_0 = 4.45 \times 10^{-7} \text{ Ns m}^{-1}$</p>	<p><u>INDENTER</u> (spherical bead)</p> <p>radius $R_p = 5.45 \times 10^{-6} \text{ m}$; density: $2.20 \times 10^3 \text{ kg m}^{-3}$ mass: $M = 1.50 \times 10^{-12} \text{ kg}$ drag coefficient: $C = 1.03 \times 10^{-7} \text{ Ns m}^{-1}$</p>
<p><u>CANTILEVER + INDENTER</u></p> <p>Total mass: $m = M_0 + M = 6.67 \times 10^{-12} \text{ kg}$ Total drag coefficient: $c = C_0 + C = 5.48 \times 10^{-7} \text{ Ns m}^{-1}$</p>	
<p><u>OTHER PARAMETERS</u></p> <p>$\lambda = \frac{c}{\sqrt{m k}} = 2.12$ $F_0 = v_A \sqrt{m k} = 2.58 \times 10^{-11} \text{ N}$ $t_0 = \sqrt{\frac{m}{k}} = 2.58 \times 10^{-5} \text{ s}$ liquid viscosity: $\eta = 10^{-3} \text{ Ns m}^{-2}$</p>	

^a The drag coefficient of the cantilever was estimated based on the theory of damped free-oscillations, using the measured resonance frequencies in air and in liquid [41].

REFERENCES

- (1) Dekker, M. "Encyclopedia of *emulsion* technology", vol.2, Becher, P. (Eds), New York **1985**.
- (2) Mason, T.G. *Current Op. Coll&Int. Sci.* **1999**, 4, 231.
- (3) Mason, T.; Lacasse, M-D; Grest, G.S.; Levine, D.; Bibette, J.; Weitz, D.A. *Phys Rev E* **1997**, 56, 3150.
- (4) Buzza, D.M.A.; Lu, C.-Y.D.; Cates, M.E. *J. Phys. II France* **1995**, 5, 37 .
- (5) Mason, T.G.; Bibette, J.; Weitz, D.A. *Phys Rev Lett* **1995**, 75, 2051.
- (6) Mason, T.G.; Bibette, J.; Weitz, D.A. *J. Coll. Interf. Sci.* **1996**, 179, 439.
- (7) Princen, H.M. *J. Coll. Interf. Sci.* **1983**, 91,160.
- (8) Bibette, J.; Mason, T.G., Gang, H.; Weitz, D.A. *Phys Rev Lett* **1992**, 69, 981.
- (9) Bibette, J.; Mason, T.G.; Gang, H.; Weitz, D.A.; Poulin, P. *Langmuir* **1993**, 9, 3352.
- (10) Meller, A.; Gisler, T.; Weitz, D.A.; Stavans, J. *Langmuir* **1999**, 15, 1918
- (11) Potanin, A.A.; de Rooij, R.; van den Ende, D.; Mellema, J. *J.Chem. Phys.* **1995**, 102, 5845.
- (12) De Rooij, R; van den Ende, D.; Duits, M.H.G.; Mellema, J. *Phys Rev E (Part A)* **1994**, 49, 3038.
- (13) Wolthers, W; Duits, M.H.G.; vandenEnde, D.; Mellema, J. *J. Rheology* **1996**, 40, 799.
- (14) Brujic, J; Edwards, S.F.; Hopkinson, I.; Makse, H.A. *Physica A* **2003**, 327, 201.
- (15) Makse, H. *Eur. Phys. J. E* **2002**, 9, 265.
- (16) Chang, C.S.; Shi, Q.; Liao, C.L. *Int. J. Solids & Struct.* **2003**, 40, 5565.
- (17) Goldenberg, C.; Goldhirsh, I. *Nature* **2005**, 435, 188.
- (18) Kadau, D.; Bartels, G.; Brendel, L.; Wolf, D.E. *Comp. Phys. Comm.* **2002**, 147,190.
- (19) MacKintosh, F.C.; Schmidt, C.F. *Curr. Op. Coll. Interf. Sci.* **1999**, 4, 300.
- (20) Breedveld V.; Pine D.J. *J. Mat. Sci.* **2003**, 38, 4461.
- (21) Domke, J.; Radmacher, M. *Langmuir* **1998**, 14, 3320.
- (22) Uricanu, V.I.; Duits, M.H.G.; Nelissen, R.M.F.; Bennink, M.L.; Mellema, J. *Langmuir* **2003**, 19, 8182.
- (23) Dimitriadis, E.K.; Horkay, F.; Maresca, J.; Kachar, B.; Chadwick, R.S. *Biophys. J.* **2002**, 82, 2798.
- (24) Attard, P.; Miklavcic, S.J. *Langmuir* **2001**, 17, 8217.
- (25) Gillies, G.; Prestidge, C. A. *Adv Coll & Int Sci.* **2004**, 108-109, 197.
- (26) Dagastine, R.R.; White, L.R. *J. Coll. Interf. Sci.* **2002**, 247, 310.
- (27) Hertz, H. J. *Reine Angew. Math.* **1882**, 92, 156.
- (28) Chen, C.; Lu, T.J. *Int. J. Solids & Structures* **2000**, 37, 7769.
- (29) Du, B.; Tsui, O.K.C.; Zhang, Q.; He, T. *Langmuir* **2001**, 17, 3286.
- (30) Park, Y.J.; Pharr, G.M. *Thin Solid Films* **2004**, 447-448, 246.

- (31) Cappella, B.; Kaliappan, S.K.; Sturm, H. *Macromolecules* **2005**, 38, 1874.
- (32) Chang, C.S.; Hicher, P.-Y. *Int. J. Solids & Structures* **2005**, 42, 4258.
- (33) Leal-Calderon, F.; Mondain-Monval, O.; Pays, K.; Royer, N.; Bibette, J. *Langmuir* **1997**, 13, 7008.
- (34) <http://www.dowcorning.com/content/sitech/sitechms/default.asp>
- (35) Poon, W.C.K. *Curr. Opinion Coll & Interf.Sci.* **1998**, 3, 593.
- (36) Bont, P.W. de; Luengo Hendriks, C.L.; Kempen, G.M.P. van; Vreeker, R. *Food Hydrocolloids* **2004**, 18, 1023.
- (37) Tolpekin, V.A; Duits, M.H.G.; van den Ende, D; Mellema, J. *Langmuir* **2003**, 19, 4127.
- (38) Filip, D; Uricanu, V.I; Duits, M.H.G.; Agterof, W.G.M.; Mellema, J. *Langmuir* **2005**, 21, 115.
- (39) Ferranti, L. Jr.; Armstrong, RW; Thadhani, NN. *Mat. Sci. & Eng A* **2004**, 371, 251.
- (40) Verhaegh N.A.M.; van Blaaderen, A. *Langmuir* **1994**, 10, 1427
- (41) "Engineering Mechanics: Dynamics", 4-th edition, J.L. Meriam, L.G. Kraige (Eds.), pg. 605 – 607, John Wiley, NY **1998**

CHAPTER 5. Plastic-to-Elastic Transition in Aggregated Emulsion Networks*

ABSTRACT

In this chapter we demonstrate how the simultaneous application of atomic force microscopy (AFM) and confocal scanning laser microscopy (CSLM) can be used to characterize the (local) rheological properties of soft condensed matter at micrometer length scales. Measurement of AFM force curves as a function of the indentation amplitude and speed (magnitude and direction) can produce a ‘mechanical fingerprint’ that contains information about material stiffness, hysteretic losses and timescales for stress relaxation and/or network recovery. The simultaneous CSLM visualization of changes in the material’s structure provides complementary information about how the material accommodates the indentation load. Since these experiments are done on areas of $O(100 \mu\text{m}^2)$ on materials having a surface of $O(1 \text{cm}^2)$, the measurements can be repeated on ‘fresh’ material many times, contrary to traditional rheometers where the whole sample is loaded at once. As a particular example we consider the case of a network of aggregated W/O emulsion droplets, in which the mechanical behavior changes drastically over time. Whereas the freshly prepared material shows a soft plastic behavior, after a time lapse of several weeks, the very same sample shows a much stiffer and elastic response. This drastic change in behavior is clearly reflected both in the signature of the AFM force curves and in (the reversibility of) the structural deformations observed with CSLM. The fact that these drastic mechanical changes take place without significant changes in the structure of the material (before loading) indicates that the stiffening of the droplet network is caused by an increase in the strength of the bonds between droplets. A remarkable finding for the elastic droplet network is that, while the structure recovers completely after the indenter is taken out, there is still an appreciable hysteresis in the force curves, indicating that also dissipation occurs. This hysteresis was not found to depend on the indentation speed.

* *Published as: D. Filip, M. H. G. Duits, V. I. Uricanu and J. Mellema, in Langmuir; 2006; 22(10), p. 4558 - 4566*

5.1. INTRODUCTION

Understanding the structure and dynamics of colloidal particle gels is of considerable interest for controlling the rheological properties of many complex materials in daily life, like food and personal (health)care products, ceramics or coatings. It also of interest from a more fundamental point of view (e.g. [1-3])

Different length scales are involved in the formation of a particulate network that can resist macroscopic stress. At the length scales comparable to, or bigger than the size of a single particle, one has to consider the mechanism that brings the particles together close enough to link up and form or extend a network. Brownian motion, as well as more collective transport mechanisms like flow or gravity can be responsible for this. The formation of the particle links (or bonds) itself is a process which takes place at a much smaller length scale. Here one has to consider the pair interaction, which can be an attractive potential [4,5] or a bonding via a less well-defined mechanism like the formation of polymer bridges [6,7] or capillary necks [8].

While a transport mechanism (to bring particles together) plus a mechanism for bond formation are sufficient to obtain an aggregated network, together they do not necessarily warrant that the network will be able to resist mechanical stress. A good example is given by gels that are unable to bear their own weight, giving rise to network collapse, and the formation of a soft sediment at the bottom of the container [9].

In gels that do resist macroscopic (gravitational, shear or compressional) stresses, there should be backbones which can transmit (and hence resist) stress via single particle bonds that can withstand non-central forces and/or via a multiple connectivity [10,11]. Usually, the forces supported by these backbones have an upper limit, above which rupture occurs, a behavior which manifests itself at the macroscopic level as a yield stress. At the level of a network backbone, the rupture force should depend on the strength of the attractive forces and the number of stress bearing contacts/bonds between particles [12].

Yet another element which can play a role in setting the mechanical properties of particulate gels is time. The structure of the gel network is in many cases the resultant of a thermodynamic driving force and a kinetics which slows down to the point of a structural arrest. Clearly, the result is an out-of-equilibrium system, which still has the potency to change its structure when given enough time or when given a stimulus. An example of the latter is the mechanical history dependence of rheological properties, found for a weakly aggregating particle network [13]. Another example is that of gravity in combination with time. Poon et. al. [14] studied colloid-polymer gels which exhibited “delayed sedimentation” with a well-defined lifetime (before rapid collapse). Gels with a definite lifetime were further sub-categorized [15], considering the dependence of the lifetime on the initial height of the sample and even on the shape of the container. Gels with very weak interparticle attractions were not observed to exhibit such geometrical dependence [14,15]. Also Verhaegh et al [16] studied transient gelation, and found that a growing number of fractures eventually leads to collapse of the gel. Besides such an ageing at length-scales comparable to or bigger than the particle or droplet, ageing can also take place at the level of the bonds, e.g. reference [17].

Given all these contributions to the mechanical behavior of aggregated particle networks, an important question is: how to study such systems. Characterization in a conventional rheometer may be difficult and *in situ* formation inside the rheometer may be required to avoid non-recoverable network disruption when transferring the sample from the container to the rheometer. Another limitation is often related to the small amounts of the sample available for the measurements. The aspects sketched in the foregoing make it interesting to study the added value and limitations of other (up to now not used) methods for mechanical characterization of small amounts of history dependent soft colloidal networks, whether they are formed by solid (suspensions) or liquid (emulsion) particles. Our approach was to go to the meso-/microscopic level and to study the local material rheology.

Several complementary techniques have been developed in recent years to measure viscoelastic properties of soft materials on micrometer scales, to connect the micro- and macroscopic properties [18]. One example is the use of colloidal particles as diffusive probes, in conjunction with high-resolution microscopy and modern image processing techniques [19]. Another is the combination of a rheometer with a confocal scanning laser microscope (CSLM) proposed by Nicolas *et al* [20]. In this manner, continuous shear, linear oscillations or compression can be imposed while following the sample deformation with the CSLM. Still, network sedimentation and a rather large amount of sample required can be a problem. Another technique used to study microscopic (visco)elasticity of soft materials is atomic force microscopy (AFM) [e.g. 21-24]. In the "force mapping method" the AFM tip or a spherical colloidal probe attached to the cantilever is indented into the material.

In the work presented in this chapter, we used two complementary microscopy techniques. AFM was used to impose given loads to aggregated sediments. The dynamic and the static mechanical responses of the network under compression with a larger (than the droplets size) colloidal probe were measured. During compression, the changes in the network structure were observed in detail, using the CSLM. The AFM data collected by means of home-made software were specifically processed and provided information regarding the mechanical stiffness (a) and its changes as induced by ageing (b).

Our results will show the utility and potential of the AFM-CSLM combination to study mechanical properties of aggregated networks at the microscale and to identify the contributions of (i) bond strength and (ii) ageing. We will also show that such experiments provide the means to differentiate between the typical fingerprints of a plastic or elastic colloidal network. The advantage in our case is that we can perform multiple experiments on different places of the same sample, which is particularly attractive for ageing systems.

The samples used were aggregated sediments of water-in-oil (W/O) emulsion droplets. To avoid coalescence over the ageing period, the water phase (interior) of the droplets was gelled by incorporating gelatin. These gelled droplets are also stabilized by adding surfactant (Span 80) in the continuous (dodecane oil) phase. Aggregation was induced by adding a polymer (PDMS) to the oil phase. In the aggregated state, the droplets are connected and form a rather dense network (droplet volume fraction higher than 10-15%, typical for fractal-like networks, but still well below *close packing fraction* of 66% for polydisperse droplets).

The CSLM was used to observe the structural features of the emulsion network before and after indentation with the AFM colloidal probe. The

reproducibility of the mechanical response (i), the dependence of the mechanical resistance on the sample local (in)homogeneity (ii-a) and on the cantilever ramping speed (ii-b), and the sample relaxation between the approach and retraction AFM stages, when the network is under constant load (iii) were followed by means of AFM recordings. The results and discussions focus on showing the change in the mechanical properties of the same sample from 4 days to 3 weeks of ageing.

5.2. EXPERIMENTAL

5.2.1 Sample preparation

The preparation of the emulsions has been extensively described in chapter 4 [25]. Immediately after preparation a given amount (1.3 ml) of the aggregating emulsion was poured into custom-made liquid cells (diameter 24 mm, height 4 mm) and left to sediment. Initially, the samples were left undisturbed for 4 days, a time-interval long enough for the droplets to stick to each other and for the network to consolidate under normal gravity. No freely floating droplets were seen in the clear liquid above the droplet layer when inspecting (with CLSM) the samples before the compression experiments. After the first series of measurements (done after 4 days), the samples were kept further for several weeks and the AFM-CSLM experiments were repeated.

5.2.2 Microscopy Techniques

The details of the AFM and CSLM microscopes have been described in chapter 2 and chapter 4. Using the AFM-CLSM combination (see Figure 5.1a), we measured the mechanical and optical response of aggregated droplet sediments under compression with the spherical indenter (a glass sphere with diameter 10 μm). Here the sample is kept immobile while the AFM piezoscanner makes controlled movements (maximum up-down amplitude: 20 μm). Each experiment represents a single cycle during which the piezoscanner is driven in the vertical direction by a truncated saw tooth (see Figure 5.1b). The AFM measuring cycle begins with a compression down to a preset amplitude value (i.e., depth). Once this value is attained, the piezoscanner remains immobile during a certain time interval (waiting period). Afterwards, the retraction cycle brings back the cantilever to its initial position. The cantilever's deflection is monitored during the entire AFM measurement. For each AFM cycle, 3 sets of CLSM Z-scans are recorded: (i) before compression, (ii) during the waiting period and (iii) after the cantilever is fully retracted. Of the waiting period (typically 7 minutes), we used the first half to monitor the cantilever deflection due to eventual stress relaxation under load and the second half for acquisition of the CLSM Z-scan of the structure. Typically 20 AFM cycles were measured for each investigated sample at different locations. The compression speed was varied between: 5×10^{-2} and 3.75 $\mu\text{m/s}$. Unless otherwise stated, all presented data sets were recorded for a compression speed equal to 0.1 $\mu\text{m/s}$.

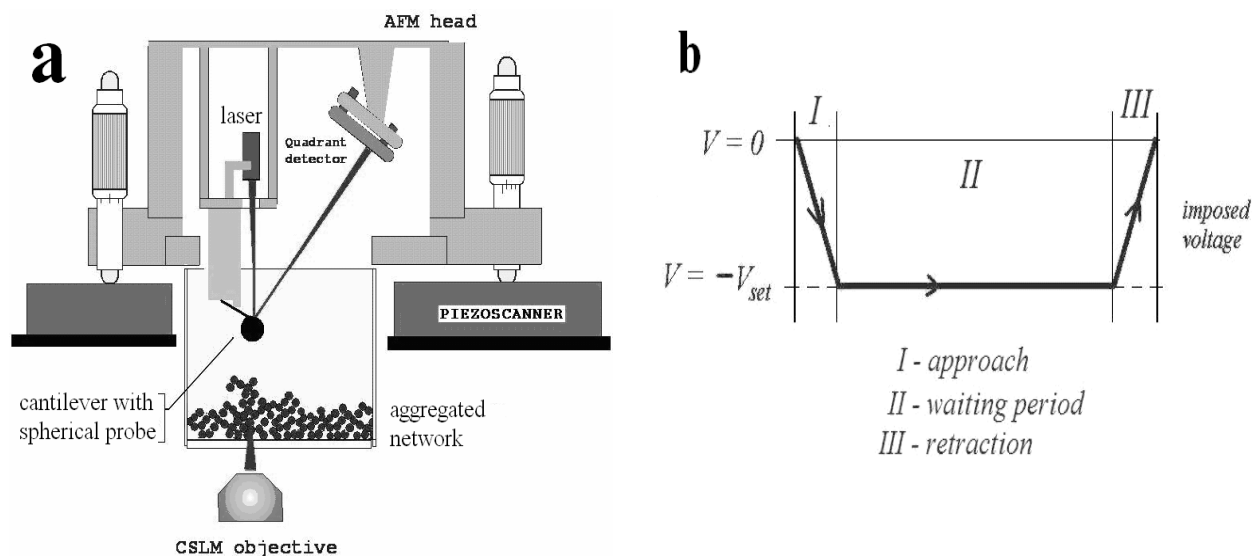


Figure 5.1. (a) Schematics of the AFM-CSLM experimental setup (not drawn to scale).
 (b) Signal (voltage) imposed on the piezoscanner during a complete AFM cycle.

5.3. RESULTS AND DISCUSSION

We focused our investigations on the particular case of a network of aggregated W/O emulsion droplets, in which the mechanical behavior changes drastically over time. Whereas the freshly prepared material shows after *4 days* a soft plastic behavior, after a time lapse of *3 weeks*, the very same sample shows a much stiffer and elastic response. This drastic change in behavior is reflected both in the signature of the AFM force curves and in the structural deformations observed with CSLM.

An increase in network stiffness may originate from different causes. One is that the structure of the droplet network can change over time; for example a (gravitationally or thermodynamically driven) densification of the network on a local or global scale. Another cause can be that the strength of the droplet-droplet attraction grows with time, due to processes at the droplet/oil interface (at molecular length scales).

We compare the two mechanical behaviors of the same sample (as changed by ageing), focusing on four elements: 1) the time evolution of the network structure, 2) the structural changes during and after indentation, 3) the force response curves of the network and 4) the influence of the deformation timescale. The observations along these lines will be shown to give a distinctive ‘mechanical fingerprint’ of the material. Also, they will be used in an attempt to find a mechanistic explanation in terms of the processes which could take place inside the network.

5.3.1. Evolution of the droplet network structure

5.3.1.1. Layer structure before indentation

Considering that weakly aggregating systems have the tendency to change their structure over time (via the breaking and reforming of bonds) towards a state where the free energy is minimized, one might expect densification of the material during ageing (since this would increase the total number of bonds). Also gravity may be a cause for densification, if the droplet network has a low yield stress (i.e., if small loads on the bonds in the force-chains are already enough to exceed the rupture force). To inspect for eventual structural changes, the same sample was observed with the CSLM microscope after 4 days and after 3 weeks, at various (X,Y) and Z locations. With eye resolution, the structures seemed more or less similar (see Figure 5.2). The fluorescently stained droplets (visible as bright objects in Figure 5.2) are aggregated in small units and these last ones form further the network.

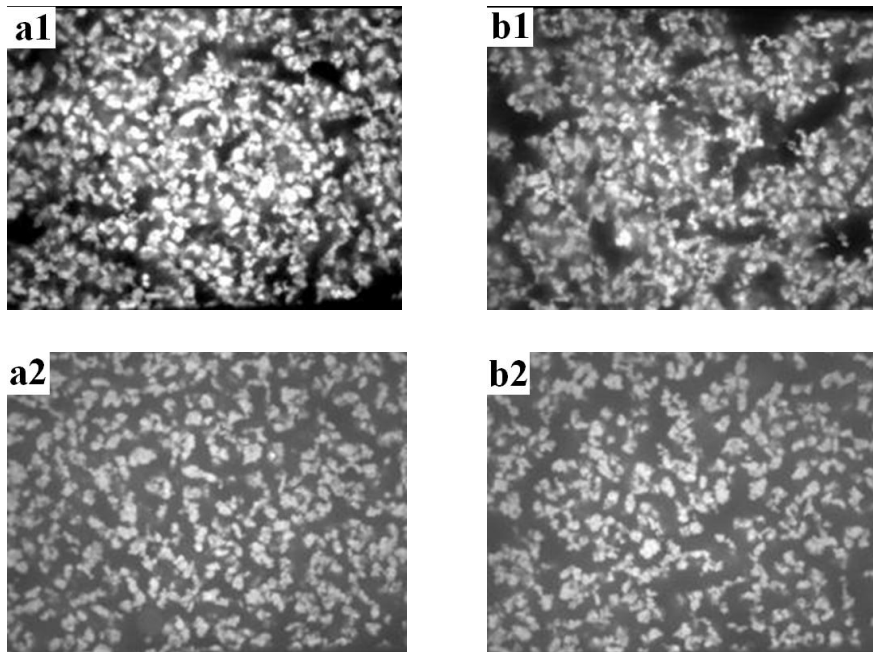


Figure 5.2. Representative images of the structure for the same sample after an ageing time of 4 days (a1,2) and 3 weeks (b1,2). These are (XY) images of $87 \times 66 \mu\text{m}^2$. The second index is related to the height of the snap-shots, i.e., index 1 for images taken at $Z=10 \mu\text{m}$ (which is near the top of the layer) and index 2: at $Z=2 \mu\text{m}$ above the bottom. The glass level is defined by $Z = 0$.

To characterize the structure in more quantitative terms, the whole stack of XY images at different Z positions was analyzed. Based on these images, we defined the layer height (calculated from the bottom towards the top of the droplet layer) and calculated apparent area fraction (ϕ) and correlation length (λ), versus the height. For a detailed definition of the last two parameters, the reader can consult chapter 4. We underline here that ϕ and λ are operationally defined quantities which, due to their dependence on settings in the image acquisition and analysis, give semi-quantitative

results. However, they are still suitable for characterizing the structure and prove to be very useful especially for making comparisons between samples imaged under comparable conditions [25].

Image Pro Plus software was used to calculate the area fraction (ϕ) of the bright objects in the Z-scans, using an object-finding algorithm with an intensity threshold. The so-calculated values as function of sample height are shown in Figure 5.3a and reveal a modest scatter. By averaging over (typically 10) XY slices, the uncertainty in the average value for ϕ could be reduced to 6% or lower. (for the first 13 μm from the bottom). Clearly these uncertainties are small enough to recognize the transition zones near the bottom (where depletion of material occurs due to confinement) and near the top (where the layer ends). At 14 μm or more above the bottom, hardly any objects were found by the algorithm. Although the gradual reduction of image quality with increasing optical depth (due to light scattering) may have contributed somewhat to this, the main cause is the scarceness of droplet material at these Z positions. The precise width of the transition zone from concentrated sediment to clear liquid was difficult to measure. As a (subjective) means of distinguishing the end of the sediment, we used the sharpness of the bright objects. (We take as end the slice in which all objects start to be blurred.) For a given sample, comparing the $\phi(Z)$ profiles (in Figure 5.3a) up to 12 μm from the bottom, at the two chosen time-marks, only marginal differences are found. The average area fraction in this Z-range amounts: $(29.7 \pm 2.5) \%$ for the 4 days-old sample and $(30.3 \pm 2.6) \%$ for the 3 weeks-old sample.

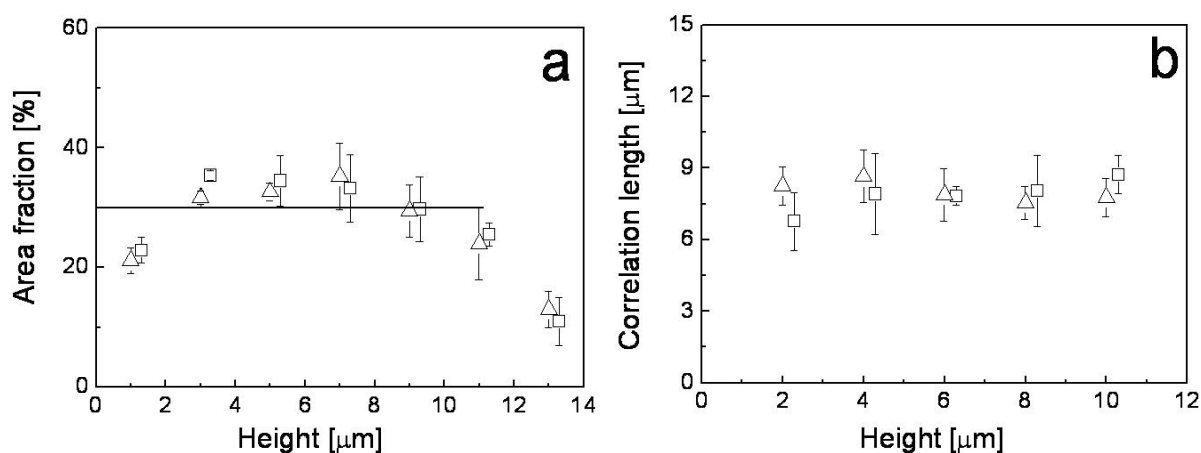


Figure 5.3. Structure parameters after 4 days (squares) or 3 weeks (triangles) of ageing.

(a) Estimated area fraction (ϕ) of droplets in XY slices. Error bars per height are $< 6\%$. (b) Average correlation length: λ , in the XY plane. Since most of the data for a given height superimpose, we have shifted (with 0.3 μm , along the height axis) the values obtained after 4 days of ageing.

Correlation lengths (λ) were obtained by calculating the 2D intensity self-correlation in a region of $65 \times 65 \mu\text{m}^2$, along 8 lines arranged in a star pattern (angle = 45°), with the intersection point in the center of the self-correlated image. The

location of the first peak next to the central peak reflects the (characteristic) nearest neighbor distance between different bright objects. As shown by Figure 5.3b, also the correlation length is unaffected by ageing (at least at the time-scale of observation: 3 weeks) and it does not depend on Z .

These findings indicate that ageing up to 3 weeks, did not bring about clear changes in the structure of the droplet network. Considering the semi-quantitative nature of our analysis, we cannot entirely exclude that a *slight* densification of the network may have taken place after all. However, based on our work presented previously in chapter 4, where non-aged systems were studied at several combinations of ϕ and λ (with $\phi= 20\text{-}35\%$ and $\lambda=6\text{-}9\ \mu\text{m}$), there is no reason to expect large changes in the mechanical behavior solely due to a small restructuring of the droplet network.

5.3.1.2. Structural changes during indentation

For the 4 days-old sample, the CSLM recordings revealed that the deformation of the droplet network occurs predominantly in the direct vicinity of the probe. Direct camera images (see Figure 4.4 in chapter 4) showed an (irreversible) local densification of the droplet network, within a corona of comparable size to the probe radius. CLSM time series showed that, simultaneously with the plastic deformation, also small-amplitude deformations ($<1\ \mu\text{m}$) carried by (droplet) chains were present (as far as $30\ \mu\text{m}$ from the center of the indenter). Only these latter deformations were recovered during or after retraction of the probe. This mechanical behavior for a relatively young sample could be used as a “label” and, from now on, *this sample will be termed “plastic”*.

For the 3 weeks-old sample, the network deformed in a rather different way; the structure seen before indentation recovered – as far as we could observe it with CLSM - completely after full retraction of the AFM probe out of the sediment. For this sample (which *will be termed “elastic”*) it was only possible to visualize the deformation while the probe was inside the material. We have recorded the whole indentation–retraction cycle, both as time series at a constant Z -position, and as Z -stacks during the time in which the probe was at its lowest position. Careful inspection of the time series allowed to identify which structural subunits deformed in organized patterns (like force transmitting) chains. Their spatial extent was again found to be $20\text{-}30\ \mu\text{m}$ from the center of the bead. Figure 5.4 shows a reconstruction in which the droplet-chains that were observed to deform (in the time series) are highlighted.

Analysis of the deformation pattern in the static situation, i.e., with the probe inside the material, turned out to be difficult when using the direct camera images. However, intensity difference maps turned out to be more revealing. These differential maps are constructed by pixel-wise intensity subtraction between the images of the material (i) under load and (ii) before loading, at a fixed Z location in the network. Representative examples are given in Figure 5.5, where such maps are shown both for the “plastic” and for the “elastic” case.

We note here that it was generally not possible to track individual droplets and that the deformation occurs in principle in 3D. Both vertical displacements of droplets

(i.e., from one focal plane to another) and horizontal (i.e., lateral) displacements can be responsible for features in a difference map. Inspection of the entire Z stack of difference maps indicated that some of the droplets were pushed *downwards* into another focal plane. If droplets are pushed outside the visualized Z location (by the AFM probe), black areas will show up in the intensity difference map. If only small lateral displacements occur, a “shadow effect” (i.e., the occurrence of a pair of dark and white areas with a similar shape and size) will be obtained.

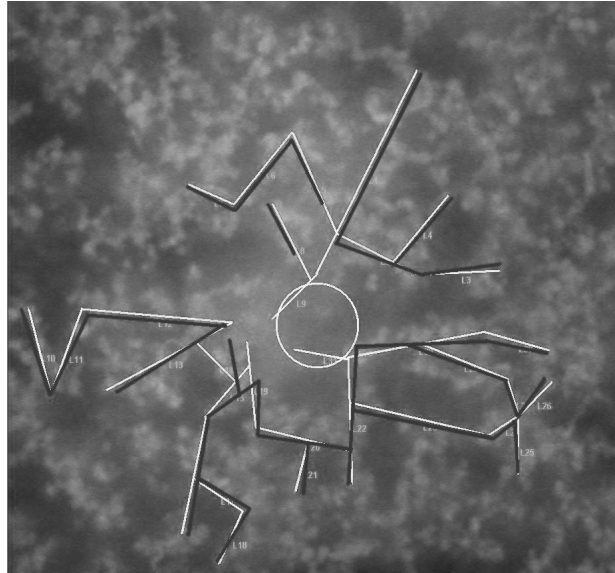


Figure 5.4. Visualization of network deformation via chains, during the compression of an ‘elastic’ sample. XY scale: $70 \times 65 \mu\text{m}^2$. The $10 \mu\text{m}$ diameter spherical indenter is marked by the circle. Additional lines highlight the network backbones which change their configuration (and hence also transmit stress). White lines: before indentation, black lines: at maximum indentation. This CLSM snap-shot was taken at $3 \mu\text{m}$ below the sediment interface (or $14 \mu\text{m}$ above the glass substrate).

As Figure 5.5 shows, the deformation patterns are qualitatively different for the two materials. This is most clearly visible in XY-planes which intersect the probe; here one can see that, for the “plastically” behaving material, there is a clear (radial) distinction between areas of depletion (black) and areas of excess (white) material. Droplets that are displaced by the indenter accumulate in the direct vicinity of the dent (without clear evidence for the displacement of droplets that were originally present in that area). Meanwhile, from the difference map for the “elastic” sample, it is clear that even droplets that were far enough away, as to never be touched by the probe, were displaced over several droplet diameters (see area indicated by the arrow). In addition, the “radial symmetry”, as observed for the plastic sample, is broken for the elastic sample: at the same radial distance from the center of the probe, one can find positive as well as negative intensity differences.

The marked area (ellipse) in the right image of Figure 5.5 is exemplary of droplets near the top of the layer which are missing in the image when the probe is

inside the material. The correlations over longer distances are indicative of structures in the network which respond as one unit to the imposed deformation.

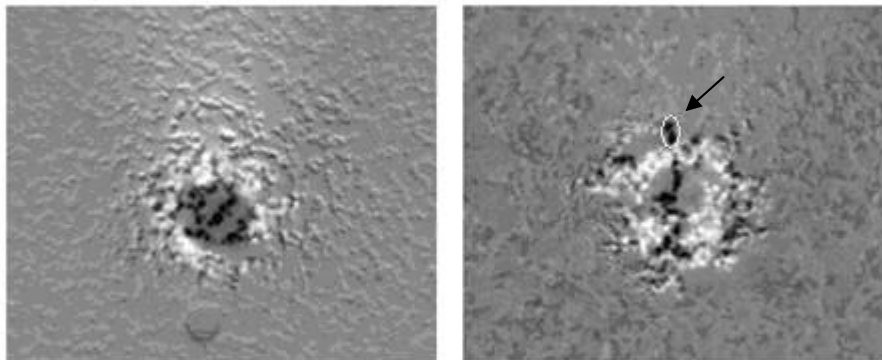


Figure 5.5. Typical deformation patterns for “plastic” (left) and “elastic” (right) droplet networks. The images shown are “intensity difference” maps, taken at the same height in the specimen, before and during indentation with a large spherical probe (observation scale $67 \times 57 \mu\text{m}^2$). Dark areas indicate depletion of material, while white areas indicate accumulation of excess material. The images correspond to heights where the indenter is encountered.

To inspect the extent of the structure recovery for the “elastic” material after the AFM probe was pulled out again, we also computed intensity difference maps comparing the structure “after” with the one before the indentation. When plotted on the same intensity scale as Figure 5.5, the difference maps (not shown) at the Z-positions where the deformations had been most prominent, turned out to be flat-grey, i.e., with intensity differences very close to zero. No evidence for droplet displacements could be obtained. These facts are consistent with the “elastic” label chosen for such samples.

5.3.2 Indentation force curves

Figure 5.6a shows a typical force-distance curve obtained for the first AFM cycle (on a previously untouched location) of the droplet network aged for 4 days. A clear hysteresis is observed. While in the approach part a soft response is found, with superposed small-amplitude force jumps, in the retract part the force decays smoothly and steeply. This behavior corresponds well to our CSLM observations that droplets, originally present in the volume to be occupied by the dent, were squeezed into the “densification corona” and that no recovery of the original structure occurred during removal of the indenter. The force-jumps in the approach curve are suggestive of discontinuous rearrangements, like droplets sliding past each other. This behavior has been extensively explained in our previous study presented in chapter 4 [25].

The response at loading of the same sample, but after 3 weeks of ageing, looks different in several respects (see Figure 5.6b). The cantilever deflection associated with a certain indentation is clearly larger than for the plastically deforming sample. (Note that the indentation is defined here as the piezo displacement from the first point of contact, minus the cantilever deflection.) No superposed jumps are observed

anymore in the approach curve and the retract curve is, relatively speaking (i.e., compared to the approach slope), not much steeper.

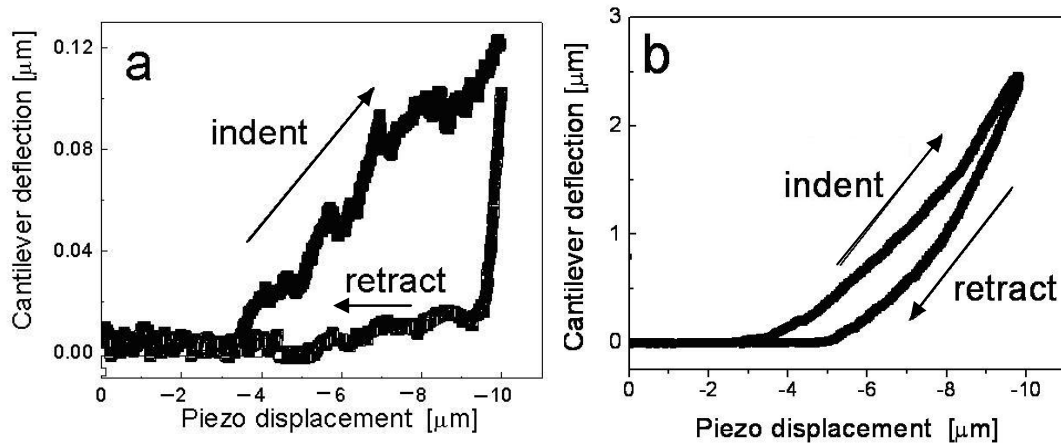


Figure 5.6. Typical AFM curves for plastic (a) and elastic (b) droplet networks.

These changes in the AFM fingerprint appear to be in line with a transition: from a soft droplet network, in which the droplet-droplet bonds are forced to break already at low stress, to an elastic network, in which the bonds are stronger and force chains can accommodate larger stresses without discontinuous rearrangements like the breaking of bonds. The fact that an approach-retract hysteresis is still observed for the 3 weeks-old material indicates that, either in the droplet network itself (i) or in the interaction between the cantilever and the droplet network plus the surrounding liquid (ii), a dissipative mechanism must be operative. Judged by Figure 5.6b alone, the hysteresis might suggest a partially plastic behavior for the material: the point where the retract curve reaches zero again, corresponds with a probe position still 2 μm inside the material. Considering that for the 2.5 weeks younger material a permanent dent with a depth of about 7 microns was formed (Figure 5.6a), it would not have been unexpected to still see some remnants of this behavior in Figure 5.6b. However, we recall here that the CSLM observations indicated a recovery of the structure after the AFM probe was pulled out. While this recovery could not be monitored in real-time, the result of this process could be visualized within minutes after the AFM experiment. Apparently, the 3 weeks aged sample was in no stage of the indentation brought so far out of equilibrium, that it could not restore its original structure anymore. This is rather in contrast with the 4 days old sample, where (according to our explanation) interdroplet bonds are broken, followed by a sliding of the droplets over distances so large that recovery of the structure is not possible.

5.3.2.1 Repeated indentations

How different the hysteretic behavior of the two materials is, becomes also evident when considering experiments in which repeated indentations are carried out at the very same XY location in the sample (see Figure 5.7). Experiments on the “plastic” sample, first of all confirmed our CSLM observation that once a dent is formed, it remains. In a repeated AFM experiment this is manifested via an approach

curve which retraces the previous retract curve, up to the point where the maximum indentation of the preceding cycle is reached. From that point on, the cantilever's deflection starts to follow a new curve, which behaves like a continuation of the original indentation experiment (as if it was not interrupted). This behavior confirms once more the yield behavior of the material.

In contrast, for the “elastic” sample, a perfect superposition between the first and second (and any subsequent) approach-retract cycles was obtained. This indicates a recovery of the structure after removal of the indenter, during the waiting time between the two scans. This waiting time was typically 3 minutes, which was longer than the time available for structural recovery *during* the AFM retract curve: at the (standard) speed of $0.1 \mu\text{m/s}$ and the largest attainable indentation, the retract curve still takes only 1 minute. In the simplest picture, in which the recovery of the structure is governed only by a time scale, these findings would indicate a recovery time somewhere in between 1 and 3 minutes.

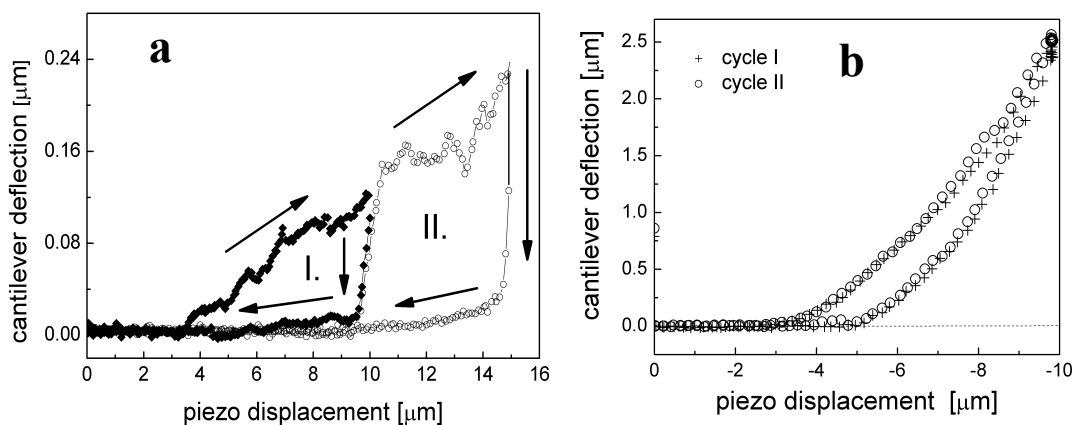


Figure 5.7. Repeated force-distance curves on the same XY spot for (a) plastic and (b) elastic droplet networks. In the plastic case the initial indentation cycle was done with a piezo displacement amplitude $A=10 \mu\text{m}$ and the second with $A=15 \mu\text{m}$. The arrows show the approach and retraction parts. Note the overlapping parts of the first retraction and the second approach. In the elastic case both cycles were made with an amplitude $A=10 \mu\text{m}$.

5.3.2.2 Influence of indentation amplitude

For the “elastic” material, we also studied how the force-displacement cycle depends on the indentation amplitude (at a constant XY location). The results are shown in Figure 5.8. Considering that the time interval in between successive approach-retract cycles was 15 minutes, one should expect the approach curves to superimpose in case of a full recovery of the initial structure (as was also observed in Figure 5.7b). Within the accuracy of the measurement, the data show that this is indeed the case.

The differences between the retract curves for the different deformation amplitudes clearly indicate that the structural deformation (or strain), which cannot be

recovered entirely during retraction, grows with the total deformation. This behavior is not unexpected, if one assumes that the principal effect of a larger indentation is that more volume elements of the same material are deformed (presumably in a similar way, with a similar time-dependent recovery per unit volume) and a larger total deformation is attained.

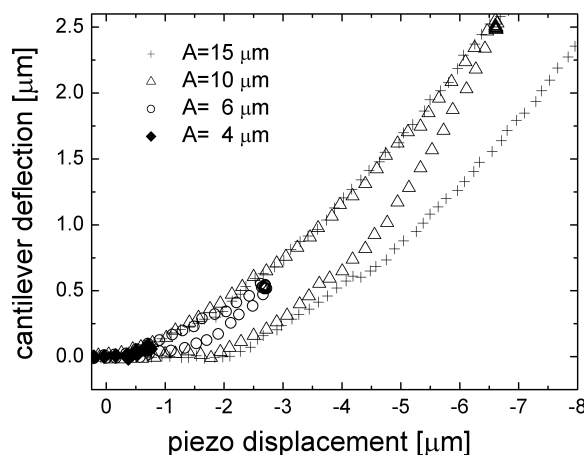


Figure 5.8. Hysteresis of the force-distance curves for increasing indentation amplitude. For deflection values higher than $2.7 \mu\text{m}$, the detection limit of the quadrant detector was reached.

5.3.2.3 Influence of indentation speed

Considering the potentially viscoelastic nature of the aggregated droplet networks (in liquid), we also investigated if / how the force curves depend on the speed of the indentation. For the “plastic” network, on changing the approach speed between 5×10^{-2} and $3.75 \mu\text{m/s}$, no significant variation of the force curves was found (see Figure 4.8 in chapter 4). This behavior is in line with our interpretation that it is the breaking of bonds between droplets (due to their relative movement), which is responsible for the force hysteresis: in this process, the force and deformation are the key parameters, but not the speed.

Remarkably, also for the “elastic” sample the force curves were found to be speed independent (Figure 5.9). In fact, two timescales are of importance here: the duration of one approach-retract cycle (which varied from 5 to 100 s) and the waiting time in between two cycles (which was taken as low as 1 minute). Neither of these times had a significant influence on the force curve (hysteresis) in the range of variation. This suggests that the hysteresis does not originate from viscous forces associated with large-scale liquid flow, like the pumping of the oil phase through the pores of the droplet network; for a given porous structure, the forces required: 1) to push the continuous phase liquid through the pores in the approach stage, and 2) to “suck in” liquid, in the retract stage, should be proportional to the speed of the indenter (Darcy’s law). If this would have applied, then the approach force should have shown an increase in magnitude (and the retract force a decrease) for higher deformation speeds.

The experiments in Figure 5.9 also indicate that the structure was able to recover within 1 min., whereas it was not able to recover during the retract scan (amongst which there is also one that lasts 1 minute). This suggests that the recovery of the structure can only take place below a certain stress or strain.

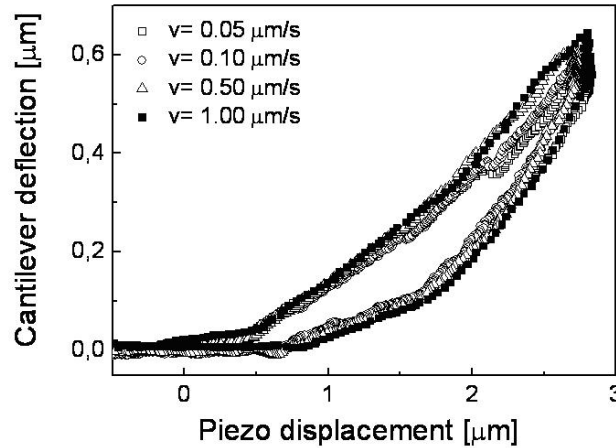


Figure 5.9. Speed (in)dependence for the “elastic” network. The deflection-vs-piezo displacement curves superpose well within the experimental errors.

5.3.2.4 Relaxation in between approach and retract scans

We also monitored the dynamic response of the AFM cantilever in the waiting period between the approach and retract scans, during which the cantilever base was held immobile, while the probe was inside the droplet network. For both “plastic” and “elastic” samples, the cantilever deflected downwards with an amount of 50 – 150 nm (depending on the indentation amplitude). For the “plastic” sample (see chapter 4), fitting the time curves with single exponentials gave a decay time $\tau^*_{plastic} = 30$ s at an

approach speed $v = 0.1 \mu\text{m/s}$ and an inverse proportionality: $\tau^*_{plastic} \propto \frac{1}{v}$.

Meanwhile, for the “elastic” samples, a $\tau^*_{elastic} = 7$ s was found for all indentation speeds. These “constrained relaxation” processes (in which the cantilever can only reduce its bending stress by increasing the indentation) suggest the presence of Kelvin-Voigt like elements (an elastic spring and a viscous damper arranged in parallel). The percentage by which the stress is reduced (“by switching off the dampers”) is rather small, typically 100 nm per 2 μm (= 5%). This corresponds well to the observation that there are no clearly visible manifestations of viscoelasticity in the approach/retract cycles for the “elastic” network.

5.4. DISCUSSION

With this chapter we aimed to make a contribution to the research on the mechanical properties of particulate networks, by studying an aggregating W/O

emulsion with an experimental setup combining an AFM and a CSLM for simultaneous use. This approach has given first-time ‘mechanical fingerprints’ for soft plastic networks and for elastic (but still partially dissipative) networks. In section 5.4.1 we will reflect on the utility of AFM-CSLM as a new microrheological measurement technique. In section 5.4.2 we discuss some possible mechanisms that could determine the change in the mechanical behavior between 4 days and 3 weeks of ageing.

5.4.1. AFM-CSLM as a microrheological method

In the here described study, a new type of micromechanical experiment was performed: a local indentation, with simultaneous recording of the dynamic forces (using AFM) and structural rearrangements (using CSLM). This technique allowed to register force curves as function of the amplitude and speed of the deformation and also to repeat measurements. Imaging in 3 dimensions was not possible on short timescales, but could be used to study the 3D deformation for static indentations. Also, the time dependent deformation in one focal plane could be studied.

The utility of the AFM-CSLM method was illustrated in the present chapter for an emulsion droplet network, whose mechanical properties changed drastically over time. Many aspects hereof could be captured, the most evident one being the change from a (predominantly) plastic to an (predominantly) elastic body. While this change was indicated both by the AFM and the CSLM, there were also unique observations from the separate techniques. The AFM results gave the stiffness of the material and clearly indicated a force hysteresis, which was for the “elastic” material not expected based solely on the CSLM observations. The CSLM, on the other hand, was used as a materials’ characterization technique prior to the indentation experiments, and also indicated what kind of deformations occurred due to compression. While very detailed information could not be obtained, the spatial range of the deformation could be quantified semi-quantitatively and indications were obtained for force-chains. These observations, which include effects that could be shown only by such a combination of microscopy techniques, prove the ability of the AFM-CSLM method to probe the mechanics of thin layers of soft condensed matter.

Another merit of AFM-CSLM is that many experiments are possible on the same sample. Especially for materials which show mechanical history dependence this is an attractive option. This applies for example to a material which shows yield behavior, without recovery on timescales suitable for experiments. Our “plastic network” is a good example thereof. In a macroscopic rheometer, exceeding the yield stress would lead to the destruction of the whole volume of the “starting material” at once.

Comparison with macroscopic rheological experiments also reveals a potential drawback of the AFM-CSLM method: in macroscopic terms, the deformation caused by indentation with a large sphere is not just a simple compression or shear. This makes it difficult to translate the results from the one technique to the other. Here it should also be remarked that even in a macrorheometer, the deformation of a droplet network at microscopic length scales is no longer organized in patterns like a shear flow.

A limitation of AFM-CSLM as a microrheological method is that structures which are heterogeneous at length scales larger than the AFM probe will give different mechanical responses, depending on the (XY) location selected for indentation. Averaging over force curves (or over quantities obtained from these curves) at different locations can reduce the problem, depending on the similarity of the curves. In our case, the compression curves could be fitted fairly well with the “Hertz model” [26] ($F \sim E^* \delta^{3/2}$ with F the force, δ the indentation, and E^* the apparent Young modulus), for both the “plastic” and “elastic” samples. This allowed to average over E^* . As can be seen from Table 5.1 and Figure 5.10, the scatter in between measurements is still appreciable, for both samples. This is in line with the relatively large correlation length ($\lambda \approx 8 \mu\text{m}$, see Figure 5.3b) of the material compared to the diameter ($10 \mu\text{m}$) of the AFM probe. Using bigger spherical probes is possible in principle, but only as long as the cantilever stiffness can still carry their gravitational load without deflecting too much. In this respect, our emulsion networks were not the ‘ideal samples’, since their softness necessitated the use of cantilevers with a low spring constant.

Table 5.1. Average and standard deviation for “apparent Young modulus” E^*

Sample	$\langle E^* \rangle$
Aged 4 days (plastic)	$24 \pm 8 \text{ Pa}$
Aged 3 weeks (elastic)	$370 \pm 105 \text{ Pa}$

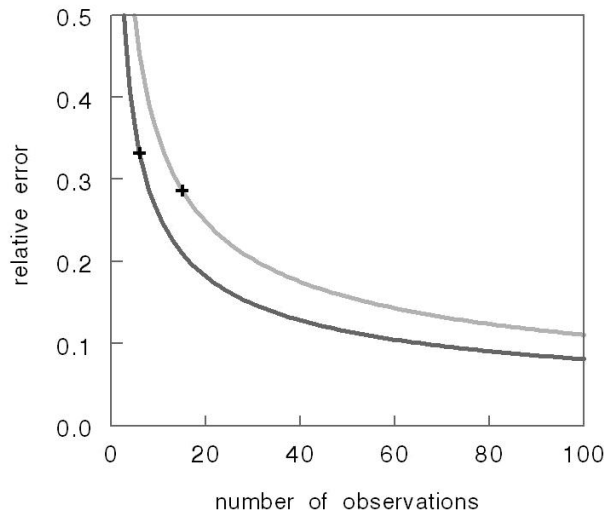


Figure 5.10. The plot indicates how the relative error in the average measurement for the apparent Young modulus E^* is expected to decrease with the number of observations. Performing a measurement (with random error σ) N times, the statistical error in the average is σ/\sqrt{N} . The light grey line corresponds to the elastic case, the dark one to the plastic case.

To check also the number of measurements needed to be done to achieve a certain relative error in the calculation of the average material stiffness (E^*), we

represented in Figure 5.10 the $1 / \sqrt{N}$ variation of the relative error as a function of N (= the number of measurements). Clearly, a relatively good average value is obtained after at least 20 -30 measurements.

5.4.2. Possible mechanisms for ageing

Ageing in colloidal systems and, particularly, in colloidal particle networks is known for its potential to change the mechanical properties of these materials [11, 28 and references therein]. Different mechanisms can be responsible. In many cases, the initial particle configurations do not correspond to a thermodynamic equilibrium, which means that there are driving forces which tend to change the network structure. Yet also the forces which “arrest” the particles in their local environment can be large. The droplet network studied in this paper was prepared in the presence of 20 wt% PDMS, i.e., well above the threshold of 1.5 wt% for interdroplet aggregation (see chapter 4 or ref [25]). No Brownian motion whatsoever (of droplets / bigger entities) was observed under these conditions, from the moment that the composition was made. This indicates that the attractive pair potential is large compared to $k_B T$ and hence there is a small probability per unit time for a droplet-droplet bond breakage. Even so, droplets could still increase the number of connections by rolling over neighbor droplets without breaking any bond. Whether this occurs or not, should depend on the presence or absence of counteracting forces, like torsional stiffness for a single bond or the confining effect of a “cage” surrounding the droplet.

While these issues could not be resolved, our CSLM observations of the 3D structure were of sufficient quality to reveal that rearrangements of the droplet configuration were at the most modest. The layer height, area fraction and correlation length were all found to be rather similar for the same sample aged for 4 days and 3 weeks. This suggests that the drastic change in the mechanical behavior of the network as a whole, must have originated predominantly from changes in the interdroplet bonds.

A clear indication for the occurrence of the latter process was obtained from an experiment in which the oil phase (with 20 wt % PDMS) of the 3 weeks old sample was replaced by a solution in dodecane of 1 wt% PDMS (below the aggregation threshold). Such an experiment had also been done with a freshly formulated emulsion at 20 wt% PDMS, giving as result a disaggregation into individual droplets and Brownian motion. In contrast, for the 3 weeks aged sample, the droplet network remained intact and immobile. In AFM force-distance measurements done after an additional day of equilibration (data not shown), essentially the same ‘elastic’ response as before the liquid replacement was recorded. In our opinion, this proves that the initial aggregation mechanism must have facilitated another mechanism for interdroplet bonding, which becomes dominant as the time passes.

In this context it is worthwhile to consider what is known about the aggregation of W/O emulsion droplets in dodecane/Span80 medium. Leal-Calderon et al [29] studied the phase behavior of (water + salt) droplets in dodecane/Span80 in the presence of PDMS. Their system is rather similar to ours, except for the presence of glycerol and gelatin in our aqueous phase and the choice of the PDMS type (i.e., molecular weight). Their hypothesis was that the PDMS acts as a depleting agent (depletion flocculation). Increasing the concentration of the silicone oil, they found a

transition from a non-aggregated fluid to an emulsion gel. For the same system, Poulin and Bibette [30] argued that Span80 surfactant can also precipitate at the surfaces of the droplets due to the presence of PDMS in the oil phase. Also this could create stronger bonds between droplets.

Considering that precipitation generally involves a lag time, this proposed mechanism could explain why in our system strong interdroplet bonds are formed over time (we still think that a different mechanism should be responsible for the initial aggregation). In an attempt to confirm the hypothesis of Span80 precipitation, we prepared a 20% PDMS solution in dodecane/ Span80 and studied it over time. In the same time, we also followed a 20% PDMS-dodecane solution (no surfactant) and an 1% Span 80-dodecane solution (no PDMS). While the latter two solutions stayed clear, an appreciable increase in turbidity was observed after 2 months for the Span 80-PDMS-dodecane solution, accompanied by the appearance of macroscopic droplets at the inner surface of the glass container. Analysis using confocal Raman microscopy (with detection of the Raman spectra), indicated that the precipitates are (dodecane-) solvated combinations between the surfactant and the silicone oil. While this confirms the potential role of Span80 precipitation also for our system, it cannot provide a definitive corroboration or falsification.

Another mechanism which could also be responsible for a strengthening of the bonds, is partial coalescence. In the stock emulsion from which all aggregated emulsions were prepared, we observed negligible coalescence, even months after it was prepared. However, on further ageing of the 3 weeks aged aggregated sample, for 2 more weeks, we did observe partial coalescence between droplet pairs on a large scale (no image shown). Considering that the droplets were prepared with an internal gelatin network to prevent coalescence, we think that the partial coalescence could be due to small amounts of aqueous liquid expelled from the gel network. The occurrence of such a liquid expulsion, which is well-known for macroscopic gelatin gels, was recently found to happen for gelatin-containing aqueous droplets [31]. Such a process could conceivably also take place with our micron-sized droplets, and hence lead to the formation of capillary bridges between droplets, which would make the bonds stronger.

Finally, we would like to remark that the strengthening of the interdroplet bonds alone, is not enough to fully explain the mechanical behavior of the 3 weeks-old “elastic” network. In this respect, one remarkable finding was the ability of the “elastic” material to restore its initial structure, in spite of energy dissipation in the approach-retract cycle. In principle, such behavior could correspond to that of a viscoelastic solid. However, for our sample, the approach-retract cycles turned out to be speed independent, contrary to linear viscoelastic materials. While this does suggest that the force curve hysteresis is not related to macroscopic flow of the oil phase, the precise nature of the dissipative process remains unknown. Its independence of timescale and the differences in deformation between approach and retract curves at a given indentation, suggest that somehow (part of) the droplets’ configurations can only be restored when given enough time and/or when the AFM probe is no longer exerting force on the material. To further address this issue, we would recommend to perform real-time CSLM in 3D (not possible with our setup), to resolve the restructuring process in more detail.

5.5. CONCLUSIONS

In summary, we have studied the deformability of aggregated water-in-oil emulsion networks, and characterized the mechanical behavior in two extreme cases. Following one sample over time, a transition from a plastic to an elastic-like behavior was found, without significant changes in the 3D network structure. This implies that the changes occurred at the interdroplet bond level. We could not prove whether these changes originated from an increase in the strength of the attractive pair-potential or from a change in the aggregation mechanism (e.g. from depletion- to bridging flocculation). The imposed deformations were for the elastic sample accommodated by droplet chains (“force-chains”), which (depending on the local configurations) could displace as entire units, rotate around a fixed point, bend if (the ends are fixed), or stretch longitudinally along the backbones.

We also showed that AFM-CSLM combination is a powerful new tool to characterize microrheological properties of thin, ageing particulate networks. The two techniques complement each other (e.g. we could not prove the force hysteresis only with CSLM as we could not prove without doubt the full recovery of the network by using only the AFM). By indenting two times in the same spot, it was possible to identify whether the sample deforms elastically or plastically, and by indenting with different amplitudes and speeds, more information could be obtained. A remarkable and yet not fully understood hysteresis was observed for the ‘elastic’ material, which was found to depend on indentation but not on indentation speed.

Finally, we have demonstrated another advantage of using the AFM-CSLM combination: the very small amount of sample probed and the possibility to re-use of the same sample for studying the effects of ageing. The network can be formed and studied in situ and the displacement of the material can be followed particle by particle. Thus, the AFM-CLSM combination provides an attractive complementary method in rheology.

REFERENCES

- (1) Ramakrishnan, S.; Chen, Y.L.; Schweizer, K.S.; Zukoski, C.F.; *Phys.Rev.E* **2004**, 70, art. no. 040401.
- (2) Sefcik J, Grass R, Sandkuhler P, Morbidelli M , *Chemical Engineering Research & Design* **2005**, 83, 926.
- (3) Solomon, M.J.; Varadan, P; *Phys. Rev. E* **2001**, 63, art no 051402.
- (4) Lyklema, J.; *Fundamentals of Interface and Colloid Science, part IV: Particulate Colloids*, Elsevier, Amsterdam, 2005.
- (5) Tolpekin, V.A.; Duits, M.H.G.; van den Ende, D; Mellema, J.; *Langmuir* **2003**, 19, 4127.
- (6) Swenson J, Smalley MV, Hatharasinghe HLM *Phys. Rev. Let.* **1998**, 81, 5840
- (7) Dickinson E; *J. Coll. Interf. Sci.* **1989**, 132, 274.

- (8) D. Geromichalos, M. Kohonen, F. Mugele and S. Herminghaus, *Contact Angle Wettability and Adhesion* **2003**, 3, 385.
- (9) Manley, S.; Skotheim, J.M.; Mahadevan, L.; Weitz, D.A.; *Phys. Rev. Let.* **2005**, 94, art. no. 218302.
- (10) Pantina, J.P. Furst, E.M.; *Langmuir* **2004**, 20, 3940.
- (11) Potanin A A, De Rooij R, Van den Ende D and Mellema J; *J. Chem. Phys.* **1995**, 102, 5845.
- (12) Dickinson; E.; *J. Coll. Interf. Sci.* **2000**, 225, 2.
- (13) Wolthers, W; Duits, M.H.G.; van den Ende, D.; Mellema, J.; *J. Rheology* **1996**, 40, 799.
- (14) Poon W.C.K, Starrs L, Meeker S.P., Moussaid A, Evans R.M.L., Pusey P.N., Robins M.M., *Faraday Discussions* **1999**, 112, 143.
- (15) Meeker S. P., **1997** thesis, Edinburgh University .
- (16) Verhaegh, N.A.M. ;Asnaghi, D.; Lekkerkerker, H.N.W.; *Physica A* **1999**, 264, 64.
- (17) Manley, S.; Davidovitch, B.; Davies, N.R.; Cipelletti, L.; Bailey, A.E.; Christianson, R.J.; Gasser, U.; Prasad, V.; Segre, P.N.; Doherty, M.P.; Sankaran, S.; Jankovski, A.L.; Shiley, B.; Bowen, J.; Eggers, J.; Kurta, C.; Lorik, T.; Weitz, D.A.; *Phys.Rev.Let.* **2005**, 95, 048302
- (18) MacKintosh, F.C.; Schmidt, C.F.; *Curr. Op. Coll. Interf. Sci.* **1999**, 4, 300.
- (19) Breedveld, V.; Pine, D.J.; *J. Mat. Sci.* **2003**, 38, 4461.
- (20) Nicolas, Y. ; Paques, M.; van den Ende, D.; Dhont, J.K.G.; van Polanen, R.C.; Knaebel, A.; Steyer, A. ; Munch, J.-P.; Blijdenstein, T.B.J.; van Aken, G.A.; *Food Hydrocolloids* 2003, 17, 907.
- (21) Aime, J.P.; Elkaakour, Z.; Odin, C.; Bouhacina, T.; Michel, D.; Curely, J.; Dautant, A.; *J. Appl. Phys.* **1994**, 76, 754.
- (22) Uricanu, V.I.; Duits, M.H.G.; Nelissen, R.M.F.; Bennink, M.L; Mellema, J.; *Langmuir* **2003**, 19, 8182.
- (23) Uricanu V.I.; Duits M.H.G.; Mellema J; *Langmuir* **2004**, 20, 5079.
- (24) Sun Y.J.; Akhremitchev B; Walker G.C.; *Langmuir* **2004**, 20, 5837.
- (25) Filip, D.; Uricanu, V.I.; Duits, M.H.G.; van den Ende, D.; Mellema, J.; Agterof, W.G.M.; Mugele, F.; *Langmuir* **2006**, 22, 560.
- (26) Hertz, H. J. *Reine Angew. Math.* **1882**, 92, 156.
- (27) Scheidegger, A.E.; *The Physics of Flow Through Porous Media*, University of Toronto Press, Toronto, 1947.
- (28) Evans, R.M.L.; Starrs, L.; *J. Phys. Condes. Matter* **2002**, 14, 2507.
- (29) Leal-Calderon, F.; Mondrain-Monval, O.; Pays, K.; Royer, N.; Bibette, J.; *Langmuir* **1997**, 13, 7008.
- (30) Poulin, P; Bibette, J, *Langmuir* **1998**, 14, 6341.
- (31) Uricanu, V.I; Duits, M.H.G.; Filip, D; Nelissen, R.M.F.; Agterof, W.G.M; *J. Coll. Interf. Sci.* **2006**, YJCIS 11947 (in press, available online).

SUMMARY

The work in this thesis describes the structural and mechanical properties of weakly aggregated emulsion networks at a meso- and microscopic level, achieved by using a simultaneous combination of two experimental techniques: atomic force microscopy and confocal scanning laser microscopy.

In the first chapter of the thesis we introduce the main aspects related to the physics of aggregated water-in-oil (W/O) emulsions: colloidal interactions between the micron sized emulsion droplets and techniques used to determine them, stability issues in emulsions (sedimentation, aggregation, coalescence), and the relevant literature about aggregated water-in-oil emulsions and emulsion gels.

Chapter 2 describes our approach to prepare a "model" system, *i.e.* an emulsion which was optimized for opto-mechanical experiments as described in this thesis. In this system the droplet deformability is controlled by gelation of the droplet interior, and the strength of the droplet-droplet attractions is tuned via the concentration of a non-adsorbing polymer in the continuous phase. Also described in this chapter are the home-made atomic force microscope (AFM) that was used to impose and measure (static or dynamic) loading forces as function of the probe-sample distance, such that the data could be translated into the mechanical properties of the studied sample, as well as the confocal scanning laser microscope (CSLM) that was used to follow the network structure and its deformation in 3D as result of indenting with the colloidal probe attached to the AFM cantilever. Using the combination of these two techniques, we aimed to get a deeper understanding of the mechanism(s) responsible for the elasticity, deformation and yielding of the aggregates composing the emulsion network.

In Chapter 3 we discuss the influence of bulk elasticity and interfacial tension on the deformability of gelled W/O emulsion droplets. We used AFM to study the deformation and wetting behavior of large (50-250 μm) emulsion droplets upon mechanical loading with a (much smaller) spherical glass probe. Adding gelatin to the water prior to emulsification, allowed studying droplets with bulk elasticity. Systematic variations of surfactant and gelatin concentrations were made, to investigate their effect on the deformation and wetting behavior of the droplets, and to identify the contributions of interfacial tension, bulk elasticity and expelled water.

We have studied first the deformability of pure water (in oil) emulsion droplets as a function of surfactant concentration. The equivalent spring method was applied to determine the average droplets spring constants, which were subsequently compared to literature values for the W/O interfacial tension. A good linear correlation was found, and the probe-droplet repulsion that prevented wetting (and as such, also droplet coalescence) was short-ranged (1-3 nm). Using the "equivalent spring" model it was possible to determine semi quantitatively the surface tension of W/O droplets with AFM.

The mechanical resistance of water droplets against deformation was determined by the interfacial tension, but only if the surfactant layer at the droplet interface provided sufficient colloidal stability. At surfactant concentrations below the CMC the steric barrier was weak, and wetting of the probe occurred, manifested via

jump-in events. While a frequent occurrence of the latter made it difficult to measure droplet spring-constants at low surfactant concentrations, the method could still be used to obtain a rough value for the interfacial tension. The CMC of Span 80 in dodecane was found to be ≈ 0.17 mM.

We also studied the influence of the gelatin concentration inside the droplet, on droplet stability and deformability. More gelatin made the system more stable against wetting as evidenced by a less frequent occurrence of snap-in events. Also the dependence on surfactant concentration diminished for higher gelatin concentrations. Hence both gelatin and surfactant contributed positively to the stability against interface breakup. The elastic response was strongly enhanced by gelatin. Below 15 wt% gelatin, the interface and bulk contributions to the elasticity were of a comparable magnitude (for small enough indentations). Above 15 wt% gelatin, a dominant Hertzian contribution was found for all indentations, irrespective of the surfactant concentration. The Young modulus values obtained by using the Hertz model to fit the force-indentation curves were of the same order of magnitude as the values obtained from macroscopic rheology experiments, but with different concentration dependence.

In Chapter 4 we describe a microrheological study on aggregated emulsion droplet networks. Considering that both the network structure and the droplet interactions should play a key role, we now used the combination of AFM and CSLM to characterize the mechanical behavior. Like before the AFM was used both as indentation tool and as force sensor. Indentation experiments were performed via a protocol consisting of approach, waiting and retract stages of the cantilever. CSLM was used to observe the network structure at micron resolution in real time. Use of refractive index matched fluorescent droplets allowed the visualization deep (*i.e.* many layers) inside the droplet network. Our networks consisted of densely packed (up to $\sim 30\%$ v/v), sedimented layers of (1 μm size) water-in-oil W/O emulsion droplets. Indentations in the (typically 15 μm thick) layers were performed with a 10 μm diameter glass probe. Adding PDMS to the oil phase was used to control droplet attraction. In the presence of > 5 wt% of the polymer, the droplets formed solid like networks which could resist deformation.

CSLM recordings showed that on compression with the probe, a markedly non-homogeneous deformation occurred, evidenced by the formation of a dense corona in the direct vicinity of the probe, as well as more subtle deformations of the network (due to force-chains) at larger distances. Upon decompression, both the imprint of the indenter and the corona were preserved, even long after the load was released. The force-distance curves recorded with the AFM corresponded well to these observations. For each deformation cycle performed on fresh material, the retract curve was much steeper than the approach curve, the hysteresis corroborating the occurrence of irreversible compaction. Contrary to classic linear viscoelastic materials, this hysteresis did not show any dependence on the deformation speed. Our force-indentation approach curves (on fresh spots) were seen to scale roughly as $F \sim \delta^{3/2}$. The prefactor (which is proportional to an elastic modulus E^* in the Hertz model for continuum elastic solids) was found to increase with the polymer concentration and with the density of the network.

Analysis of the combined AFM and CSLM observations suggested that this plastic behavior is related on a micro scale to stick-slip events, *i.e.*, droplets sliding past each other after a yield threshold has been overcome. The speed independence of

the AFM approach curves, as well as their superimposed force-jumps were clear indicators for this behavior. The dependence of the “plastic resistance” E^* on the PDMS concentration indicated that the critical yield force grows with the droplet-droplet attraction strength, which is in agreement with simple Coulomb friction. The choice to include a waiting time between the loading and unloading in our experimental AFM protocols, allowed measuring also the relaxation of the cantilever against the droplet network. The finding that these relaxations always led to a residual stress points at the presence of elastic elements which can only be attributed to the droplet network.

The proposed deformation mechanisms were corroborated by an equivalent (macroscopic) mechanical model in which the aggregated emulsion network was represented as a serial arrangement of a stick-slip element and two Kelvin elements (*i.e.*, parallel arrangements of springs and dashpots), each of them with a magnitude that followed a prescribed dependence on the indentation depth. With this model, it was possible to reproduce the most prominent AFM observations quantitatively. It was found out that the AFM approach stage was dominated by the stick-slip element. At the microscopic level this element represents the yield force between the droplets which have to rearrange their bonds. Both the number of droplet-droplet bonds and their strength were covered for, respectively via the prescribed dependence on indentation depth and via a linear dependence on the normal force. Even the occasionally observed force-jumps could be predicted, by assuming a distribution for the friction coefficient between droplet pairs. In contrast, the waiting and retract stages were dominated by the Kelvin elements. Although we cannot assign a specific mechanism to the dashpots, their presence was essential for predicting the observed time-dependent behavior. We think that the spring elements represent the force chains.

Chapter 5 describes a plastic-to-elastic transition in aggregated emulsion networks. In this chapter we demonstrated again how the simultaneous application of AFM and CSLM can be used to characterize the (local) rheological properties of soft condensed matter at micrometer length scales. Measurements of AFM force curves as a function of the indentation amplitude and speed produced a “mechanical fingerprint” that contained information about material stiffness, hysteretic losses and timescales for stress relaxation and/or network recovery. The simultaneous CSLM visualization of changes in the material’s structure provided complementary information about how the material accommodated the indentation load. Since these experiments were done on areas of $O(100 \mu\text{m}^2)$ on materials having a surface of $O(1 \text{cm}^2)$, the measurements could be repeated on “fresh” material many times, contrary to traditional rheometers where the whole sample is loaded at once.

As a particular example, we considered the case of a network of aggregated (and internally gelled) water-in-oil emulsion droplets described also in chapter 4, in which the mechanical behavior changed drastically over time. Whereas the freshly prepared material showed a soft plastic behavior, after a time lapse of several weeks, the very same sample showed a much stiffer and elastic response. This drastic change in behavior was clearly reflected both in the signature of the AFM force curves and in the reversibility of the structural deformations observed with CSLM. The fact that these drastic mechanical changes took place without significant changes in the structure of the material (before loading) indicated that the stiffening of the droplet network was caused by an increase in the strength of the bonds between droplets. A

remarkable finding for the elastic droplet network was that, while the structure recovered completely after the indenter was taken out, there was still an appreciable hysteresis in the force curves, indicating that also dissipation occurred. This hysteresis was not found to depend on the indentation speed. The underlying process is not yet fully understood and deserves to be studied further. The transmission of the stress happened in both cases via force-chains determined by the local configuration of the network, which can be displaced as entire units, can rotate around a fixed point, can bend if the ends are fixed, and can stretch longitudinally along the backbones.

To our knowledge, this was the first study in which AFM and CSLM were simultaneously applied to investigate the mechanics of soft colloidal systems like our adhesive droplet network. This makes it interesting to study its merits as a new (micro) rheological method. Compared to macroscopic rheological techniques, an evident advantage was that with AFM-CSLM we could address deformation mechanisms at the microscopic level. Such mechanisms are in some cases the primary reason for doing macroscopic rheological experiments! Another advantage of AFM-CSLM is the very small amount of sample probed and the possibility to re-use of the same sample for studying spatial variations, or the effects of ageing. An aspect still to consider when comparing AFM-CSLM to macroscopic rheology, concerns the precise meaning of the mechanical properties as measured with AFM-CSLM. All in all, this study showed that the AFM-CLSM combination provides an attractive complementary method in (micro) rheology. While the presented work was restricted to a particular aggregated water-in-oil emulsion, its potential, it could provide a starting point for further studies of aggregated particulate networks, or applied also to other types of materials/samples of general or particular interest, for example in areas as cell deformation and elasticity. The possibilities of using the combination of AFM-CSLM combination in this sense look very promising.

SAMENVATTING

Het onderzoek beschreven in dit proefschrift gaat over de relatie tussen de structuur en mechanische eigenschappen in zwak geaggregeerde netwerken bestaande uit emulsie druppels. Deze relatie werd op microscopisch niveau bestudeerd door gelijktijdig gebruik te maken van twee moderne technieken: Atomaire Kracht Microscopie (in het Engels afgekort als AFM) en Confocal Scanning Laser Microscopie (CSLM).

In het eerste hoofdstuk worden de meest essentiële natuurkundige kenmerken van de onderzochte materialen belicht: geaggregeerde water-in-olie (W/O) emulsies. Hierbij spelen de colloïdale interacties tussen de (micron grootte) druppels een belangrijke rol, alsmede de daaraan gerelateerde stabiliteit (tegen aggregatie en coalescentie). Ook het uitzakken van druppels door de zwaartekracht is hierbij van belang. Verder worden ook technieken om de colloïdale interacties te bestuderen, en de relevante literatuur over reeds verricht onderzoek aan geaggregeerde of gegeleerde W/O emulsies in dit hoofdstuk behandeld.

Hoofdstuk 2 gaat over de preparatie van een ‘model systeem’, dat wil zeggen een emulsie met eigenschappen welke geoptimaliseerd zijn voor de mechanische en optische experimenten met AFM en CSLM. De vervormbaarheid van de druppels wordt ingesteld door een gecontroleerde hoeveelheid gelatine toe te voegen aan de waterfase voordat deze wordt geëmulgeerd. De sterkte van de aantrekkende krachten tussen de druppels wordt ingesteld via de concentratie van (niet-adsorberend) poly-dimethyl-siloxane (PDMS) polymeer, dat aan de oliefase wordt toegevoegd. Ook de gebruikte apparatuur wordt beschreven in dit hoofdstuk: de (niet-commerciële) AFM, welke gebruikt is om kracht-afstand relaties te meten welke optreden bij het indeuken (‘indenteren’) van grote emulsiedruppels en netwerken van kleinere emulsiedruppels. Ook de CSLM wordt beschreven; deze is gebruikt om de netwerkstructuur vóór, tijdens en na het indeuken kwantitatief te karakteriseren.

In hoofdstuk 3 worden de invloeden van de bulk elasticiteit en van de grensvlak-spanning op de deformeerbaarheid van gegeleerde ‘emulsie’ druppels beschreven. Dit is onderzocht gebruikmakend van een AFM waarbij de cantilever tip is voorzien van een bolvormig glasdeeltje van 10 micron. De druppels zelf waren nog groter: 50-250 micron. Met AFM werd het verband tussen de indeuking (indentatie) en de kracht gemeten voor verschillende soorten druppels. Zowel de gelatine concentratie binnen de druppels als de surfactant (Span80, oppervlakte actieve stof) concentratie in de olie (dodecaan) werden gevarieerd om hun invloed op de druppels te onderzoeken.

In afwezigheid van gelatine bleken de druppels zich als eenvoudige (lineair elastische) veren te gedragen. Het zogenaamde ‘Equivalent Spring Model’ bleek van toepassing te zijn. In dit model wordt een kwantitatieve uitdrukking voor de grensvlakspanning van het water/olie oppervlak gegeven, hetgeen toelaat om de grensvlakspanning (semikwantitatief te ‘meten’ en met literatuurwaarden te vergelijken. Een goede overeenstemming werd gevonden, hetgeen bevestigt dat de grensvlakspanning de mechanische weerstand bepaalt. Niet altijd was het zo dat de druppels alleen werden ingedeukt: het kwam ook voor dat de glazen *probe* door de druppel werd bevochtigd. Dit laatste gebeurde vooral bij lage surfactant concentraties. In een emulsie gebeurt iets dergelijks tussen twee druppels, indien deze door te weinig

surfactant bedekt zijn, en derhalve onvoldoende colloïdale stabiliteit hebben. Bevochtiging van de glazen probe manifesteerde zich in de AFM metingen als een plotselinge verandering van de cantilever (de bladveer waaraan de tip is bevestigd) doorbuiging. Door metingen veelvuldig te herhalen was het toch mogelijk om ook krachten (en daarmee de grensvlakspanning) te meten van de druppel zonder dat bevochtiging optrad. Dit liet toe om de kritische micel concentratie (CMC) te bepalen op 0.17 mM.

De gelatine concentratie in de druppels bleek van invloed te zijn zowel op de stabiliteit (tegen bevochtigen) als op de vervormbaarheid. Meer gelatine leidde tot een verminderde kans op bevochtigen, en tot een grotere elastische stijfheid. Naarmate de concentratie verder verhoogd werd, werd de elastische stijfheid steeds meer verantwoordelijk voor de mechanische weestand tegen vervorming. Het omslagpunt lag bij (ongeveer) 15% gelatine (gewichtsbasis t.o.v. water). Bij hogere concentraties gedroegen de druppels zich elastisch, en kon door vergelijking van de gemeten krachtcurves met het Hertz model, een (effectieve) Youngs modulus bepaald worden.

Hoofdstuk 4 gaat over een microrheologische studie naar geaggregeerde emulsies welke qua samenstelling sterk lijken op de in hoofdstuk 3 onderzochte systemen, maar waarbij de druppels beduidend kleiner zijn (1 micron). Aansluitend bij de gedachte dat zowel de structuur van het druppelnetwerk (de rangschikking van de druppels) als de attractieve interacties tussen de druppels bepalend zijn voor het mechanische gedrag van het netwerk, zijn gelijktijdig AFM en CSLM metingen verricht. Het netwerk werd gemaakt in de vorm van een (10-20 micron) dunne laag op de bodem van de meetcel. Indentatie werd wederom uitgevoerd met een (10 micron) glazen bol. Omdat dit vanaf de bovenkant gedaan werd, terwijl de CSLM waarnemingen vanaf de onderkant gedaan werden, moest het netwerk optisch (bijna) transparant zijn. Hiertoe werd aan de druppel-fase niet alleen gelatine maar ook glycerol toegevoegd, om zodoende de brekingsindex (beter) gelijk te maken met die van de oliefase. De druppels werden gecontroleerd ‘plakkerig’ gemaakt door PDMS toe te voegen aan de oliefase. Bij meer dan 5 gewichts % PDMS bleken de gevormde netwerken sterk genoeg te zijn om een meetbare tegen-kracht te leveren bij indentatie.

CSLM opnamen lieten zien dat bij indentatie, een opmerkelijk inhomogene deformatie optrad, blijkens de vorming van een ‘kraag’ met hoge druppel dichtheid in de onmiddellijke nabijheid van de bolvormige indenter. Op grotere afstanden waren meer subtiele veranderingen van de druppel netwerkstructuur zichtbaar, via de vervorming van druppelketens. Bij terugtrekking van de indenter uit het materiaal bleek dat de gemaakte bolvormige krater intact bleef: een duidelijke indicatie voor ‘plastisch’ gedrag. De met AFM gemeten krachtcurves stemden goed overeen met deze observaties. Bij een compressie (indentatie) + decompressie cyclus in ‘vers materiaal’ bleek de kracht in het decompressie stadium veel steiler af te hangen van de afstand. Deze hysteresis bevestigt dat het druppelnetwerk een onomkeerbare structuur verandering heeft ondergaan. Deze hysteresis bleek niet afhankelijk te zijn van de snelheid waarmee de compressie -decompressie cyclus werd uitgevoerd. De compressie curve bleek qua mathematische gedaante (bijna) kwantitatief overeen te komen met het gedrag volgens het ‘Hertz model’ (ontwikkeld voor continuüm elastische materialen). De voorfactor bleek groter te worden voor hogere PDMS concentraties en voor netwerken met een hogere druppeldichtheid.

Analyse van de gecombineerde AFM en CSLM observaties leverde op dat het beschreven ‘plastische gedrag’ op microscopische lengteschalen waarschijnlijk

gerelateerd is aan zogenaamd ‘stick-slip’ gedrag, waarbij druppels langs elkaar schuiven nadat een zekere mechanische barrière overwonnen is. Zowel de onafhankelijkheid van de krachtkrommes van indentatiesnelheid als de op de krommes gesuperponeerde kracht-sprongjes wezen hier al op. De toenemende stijfheid van het netwerk bij toenemende PDMS concentratie suggereert in dit beeld dat een sterkere adhesie tussen druppels ook een grotere wrijvings-weerstand veroorzaakt. Observaties gedurende de wachttijd tussen compressie en decompressie leverden op dat de cantilever in enige mate relaxeert (doorbuiging verliest). Dit is in overeenstemming met de aanwezigheid van elastische elementen (bijvoorbeeld de genoemde druppelketens) in het netwerk.

Deze voorgestelde deformatie mechanismen werden bevestigd door een ‘equivalent macroscopisch model’ waarin het druppelnetwerk vertegenwoordigd werd door een serieschakeling van een ‘stick-slip’ element en twee zogenaamde Kelvin elementen (een Kelvin element is een parallelle schakeling van een lineaire veer en een lineaire demper), elk met een stijfheid welke afhankelijk was van de indringdiepte (indentatie) van de AFM probe. Met dit model konden de meest prominente AFM observaties kwantitatief beschreven worden. De compressie curve bleek vooral bepaald te worden door het stick-slip element. De kracht-sprongjes konden gemodelleerd worden door een verdeling aan te nemen voor de wrijvingscoëfficiënt. Het relaxatie stadium en de decompressie curve bleken vooral door de Kelvin elementen bepaald te worden.

Hoofdstuk 5 beschrijft hoe netwerken van geaggregeerde emulsiedruppels in verloop van tijd drastisch van mechanische eigenschappen kunnen veranderen. Deze bevinding werd gedaan voor het zelfde materiaal als beschreven in hoofdstuk 4. Echter, nu werden de geaggregeerde emulsiernetwerken niet kort na bereiding bestudeerd, maar na een verouderings periode van 3 weken. In de tussenliggende tijd bleek het druppelnetwerk elastisch te zijn geworden. Daarbij was ook de stijfheid aanmerkelijk toegenomen. Dit sterk veranderde gedrag manifesteerde zich zowel bij de AFM- als bij de CSLM-metingen. De AFM krachtkrommes bleken een andere karakteristiek te hebben; er trad nog steeds hysteresis op, maar de decompressie curve had nu een duidelijk andere vorm. Bij herhaling van de compressie-decompressie cyclus op dezelfde locatie vielen alle compressiecurves nu over elkaar heen, en hetzelfde voor de decompressie curves. De CSLM observaties lieten zien dat de netwerkstructuur na terugtrekken van de indenter zich (zo goed als) volledig herstelde. Een belangrijke waarneming bij dit onderzoek was dat de structuur van het druppelnetwerk (nog vóór de indentatie) gedurende de verouderings periode niet significant veranderd was. Dit suggereert dat de drastische veranderingen in de mechanische eigenschappen toegeschreven dienen te worden aan versteviging van de bindingen tussen de druppels.

Voor zover bekend was dit de eerste studie waarbij AFM en CSLM gelijktijdig zijn gebruikt om de mechanische eigenschappen van zachte colloïdale systemen zoals de hier beschreven geaggregeerde druppelnetwerken, te onderzoeken. Dit maakt het interessant om de ook merites van AFM-CSLM als rheologische meetmethode te beschouwen. Wanneer de hier beschreven AFM-CSLM methode vergeleken wordt met de gangbare macroscopische rheologische technieken, komt als duidelijk voordeel van AFM-CSLM naar voren dat het mechanisme van deformatie op microscopisch niveau bekeken wordt. In termen van dit proefschrift: krachten tussen de druppels worden op een directe manier gemeten, en ook de wijze waarop de

druppelstructuur zich aanpast onder mechanische belasting wordt gevisualiseerd. Het opsporen van dergelijke mechanismen is (zeker in het verleden) nog wel eens de reden (geweest) waarom macroscopische rheologische experimenten werden gedaan! Andere voordelen van AFM-CSLM microrheologie zijn dat er relatief weinig materiaal voor nodig is, dat eventuele ruimtelijke variaties in mechanische eigenschappen kunnen worden onderzocht, en dat op vele plaatsen in hetzelfde monster, nieuwe metingen (aan niet eerder mechanisch belast materiaal) kunnen worden gedaan. Het laatste is ook gedemonstreerd in hoofdstuk 5. Als tekort-koming van AFM-CSLM kan worden aangemerkt dat de precieze betekenis van de gemeten mechanische eigenschappen niet eenvoudig is aan te geven, in de zin dat een eenvoudige kwantitatieve vergelijking met begrippen behorende bij klassieke rheologische experimenten, nog niet in zicht is.

Al met al maakt dit de AFM-CSLM microrheologische methode een aantrekkelijke aanvulling op de bestaande rheologische methoden voor zacht gecondenseerde materie. Hoewel in het hierbeschreven proefschrift de methode alleen is toegepast op een specifieke geaggregeerde water-in-olie emulsie, zou deze ook toegepast kunnen worden op een reeks van andere systemen. Gedacht kan daarbij worden aan bijvoorbeeld andere geaggregeerde deeltjes netwerken, granulaire systemen of levende biologische cellen. In dit opzicht is de AFM-CSLM methode veelbelovend te noemen.

Acknowledgements

Writing this part of the thesis makes me really feel that the long waited moment is here: my Ph.D. research which benefited from the support and collaboration of so many people is about to be rounded. I will use this opportunity to express my appreciation to all the persons that, in one way or another, contributed to my work and well-being all these years.

First of all to Jorrit, my promotor, thank you for your help in my scientific work, for seeing the potential in me and for the constant belief that I am capable to develop into that “me” that would deserve a Ph.D. title. By accepting me as your student, you gave me the opportunity to explore many new things that opened my eyes about the world we live in and myself. For all these and more, I am truly grateful!

Wim, maybe you still remember the days when, as fresh Socrates student, I was coming and asking you questions about emulsions every time I could catch you... At that time I didn't know yet that our collaboration would continue for quite a number of years, and, now, I can only say I am happy that it did. Your advice, whether scientific or personal, was a big support for this little girl... Thank you for being my copromotor!

During the four years of my Ph.D. I had you, Michel, as my daily supervisor. There are so many things which I should mention; I don't know where to begin. Maybe the most important for me was the feeling that you were always there for me, taking so seriously your task. In your special way of managing me, you gave me a lot of freedom to finding my way as a scientist and, when needed, you helped me to not getting lost and to improving. I always appreciated our open discussions about various subjects. As I said, there are many things to say, but I will stop at these with a big: Thank you!

Another big piece of “Thanks” goes to Violeta, who was for me a little bit of everything: friend, office and lab mate, mother or sister and non-official “supervisor”. We shared so many things, the good and the bad moments, and even though we did not always agree with each other, I think we did a great job together. I could probably say that without your help and sometimes a “push” in the right moment to the right direction, maybe I wouldn't have reached the same. I sincerely admire your driving force in following what you set in your mind to achieve. It's good to have you as a friend!

To Dirk, who was my Socrates project supervisor and an important contributor to my Ph.D. work both on its theoretical and technical sides, I am indebted for always helping me whenever asked. I don't know how to thank you for your sincere kindness, I just can hope that you enjoyed helping me as much as I am grateful to you for doing it! And beside the work part, let me mention that it was nice to know you better as a person during our group lunches and going out trips.

Frieder, you came as new leader of the group towards the end of my Ph.D., but we had still enough time to work together. I'm not sure that I always managed good enough to show or tell you how much I appreciated your scientific input and interest

in my work. For your openness and help, I am thanking you now again with all my gratitude.

I was lucky enough to have the valuable help of our technicians: Jacob, Gerrit, Mariska and Klaas, and the warm and continuous commitment of our secretary, Annelies. Jacob, you taught me all the things I needed for working in the lab and did such a great job in helping me in the process of preparing all the systems I studied until finding the one(s) described in this thesis; you were a great moral support for me during all these years. Not only as a colleague, but also as a friend and almost like a father figure. I wish I would have your easy, and in the same time deep manner to reach people! Thanks for everything you did for me! Gerrit, your quiet and kind way of being, always there to help with solving the various “bugs” in our computers and all the things you did for helping me to have the experimental setup with the features I needed, I thank you for your unconditioned support. Mariska, we laughed and we worked together and shared thoughts about “life”, and all was fun. You helped me very much with building the new AFM head that I used in the latest stage of my work, thanks a lot for your commitment to finishing it in time. Klaas, always with a good word and a smile for everybody, but most important, with an excellent expertise for the mechanical work, you made my life easier by making the missing parts for my setup. Annelies, I can’t thank you enough for your constant kindness and warmth in helping me with everything you could, like arranging the official steps so I could have my Ph.D. defence in time.

Besides all the help I had from the people from our group or related to it, I had also valuable help coming from “outside” the group. My Ph.D. project was a collaboration between Unilever, FOM (via the Softlink programme) and the University of Twente. I would like to thank Rob Vreeker, my contact person from Unilever, for the constant support you gave me during all these years, for guiding me when needed towards what was relevant in my work both from fundamental point of view as well as for its applicability in (food) industry, and for being always open if some changes had to be made to the initial plan. Rob, I really enjoyed all our discussions! I would also like to thank the personnel of FOM for their support, whether on administrative, financial or educational issues. I specially enjoyed following all the courses were offered by FOM and I found them very useful for my development.

Let me continue by mentioning the two friends I must thank for (and not only) supporting my coming in The Netherlands: Diana and Mircea. Diana, you gave me the most beautiful present you could the very first Christmas I spent with you in this country. Mircea, you took me with my good and bad things and helped me be positive when I was going down. Thank you both for your true friendship!

Speaking about friends, maybe it is a good moment now to speak about all the special people I met at the University of Twente, during the 5 years I spent there. I will start with mentioning my colleagues that were part of the ex-Rheology, later the Physics of Complex Fluids group: Roland, Martijn, Yuri, Valentin, Emilio and Aracelli, Ana, Juan, Alexei, Jasper, Ryan, Renske, Eco, Benjamin, Zaosheng, Rina, Jane, Fahong, Menno ... you all were there around on daily basis, for shorter or longer time, making me see the variety and the common ground in people from all kinds of countries and different background and giving me constantly the feeling of being “in good hands”. The list continues with those whom, with their friendship and special way of being, made my days shine: Niki and Joris, Boris, Arup, Ileana,

Roman, Manu, Tamara, Helmut, Adi... I miss you “guys” constantly! Niki, you were all this time my true friend, sharing with me all the happenings, the happy and the bad moments. I can’t say about many persons that knew and accepted me as you did, and not many so close to my heart either ... Together with Joris, we had such a good time all these years, at parties, in holidays, lunches and evenings and you brought me so much joy! Thank you both for being such good friends. Boris and Arup, the “snakes”, such a perfect match for making us laughing with tears out of the blue, remember the “Brotherhood party”? Ileana, another piece of “something”, with your sharp humor cutting into the depth of the things, always so down on the Earth! I hope you enjoy your new job! Roman, Oksana, you had always such nice stories about Jeanette, I’m glad that we can still meet rather easily! In the last half year, for too short time, I had Manu, Tamara, Helmut and Adi (and their friends) as company for lunches and fun and we became good friends. Manu, the blond and curly fairy that is melting your heart with her laugh or her tears... Never give up hoping and dreaming! Tamara, so open in heart, such a survival spirit! I have no doubt that you will always find your way to see beauty in life and get out the best of it. Helmut, you make Don Quijote to look like a baby! You always try to bring quality in everything you do, whether fighting bureaucracy, helping a colleague or doing a nice party for your friends. Adi, I enjoy so much discussing with you about anything and I really love your jokes! I am confident that you will achieve whatever you will want, you have an incredible power of will and self-control.

It seems I also managed somehow to make friends outside work, and they helped me to maintain the balance and to have a rich “social” life. Stefan and Ileana, we had so much fun, sometimes together with Raluca and Mihai or the colleagues from your group, at parties, movies or sport activities. Geo, looking so fragile and still moving the mountains, it’s so good to have you and Michiel around. Adi, Raluca and Liviu, I enjoy a lot our “meetings”, like the unforgettable party from Belgium! Cazimir and Diana, I hope you are happy being home. Maria, Dela and Loredana, please come soon to Eindhoven, I have big plans! Victor, our Eindhoven-Enschede trips with your car were very pleasant. I wish you good luck in your new job.

Outside Twente, I also made many friends: Szili and Marinda, Misu and Magda, Gabita and “Francezu” Gwillerme, Catalin “Primaru” and Mihaela, Valica “Taxi” and Lacramioara, Oana and Odi, Mirko and Nicoleta, Dana, Bogdan, Mihai, all the Romanian gang from Groningen... I had so much joy at all the parties and in your homes, I really felt welcome! In Delft, Veronica and Adrian, a perfect example of how contrasting people can make a great couple, Eva and Gerrard, friends from older times, and Flavius, my dear ex-master colleague. In Eindhoven, I shared home in weekends with Csaba and we always had a good time speaking our mother tongue and spending time together. Veronica and Ruud, our friends and ex-neighbors, always there with excellent dinners and constant help whenever needed. Cristina, Robert and Tudor, Mihaela and Gabi (to whom I have to thank for doing my cover design), it is so good to have you here! In Haarlem, Catalin and Mihaela, we see each other not as much as we would like it, but whenever it happens it is as if we have never been apart.

Outside the Netherlands, I am lucky to have as friends Gabi and Pierre, Gilia and Sanyi, Iza, Moni and Virgil, Niki and Mandi, Carmencita and Kay, Hajnal, Nane, Catalin (Zorro), Simona, Petrica (who helped me doing a rigorous statistics on my AFM data with the program he wrote for me). Thank you all for being there for me whenever I need it!

However, I would probably not be at this point without my family. I was blessed to have the most supporting parents and brother. I don't have words to say how much they mean to me. I just hope, with all the physical distance, I am still capable to be the daughter and the sister they need. Mami, tati, Cristi, va multumesc din suflet pentru dragostea si grija pe care mi-o purtati!

More than that, I also have my close relatives that enlarge my family, whether in Romania, in Hungary or Canada... By alliance, Dana, my brother's partner, and Andrei's family accepted me with open heart. I am very happy to have all of them.

Not at last, for Andrei, my husband: I couldn't ask for a better partner and friend! I hope that we will always find in our hearts the way to stay happy together. Thank you for your understanding, for the constant support to grow as a person and in being free to be myself and most of all, for your love!

I kept the last words for my future child (or children): maybe sometime you will have a look at this book, at this paragraph, and though you will find that it doesn't contain the answer for all your questions, nor a toolkit for survival, I hope it will say something about your mother, this foolish person that loves life so much, and most of what comes with it! It should probably say that she's nothing of perfect and she's making lots of mistakes, but is always trying to be open in mind and soul. And if I will happen to be sometimes boring in my attempt to be the mother I would think you need, remember this: you were made with a heart filled with love and you will always have it! In every day that we'll share, I will be very happy for all the things I will learn from you and through you. So, challenge me!



Curriculum Vitae

Diana Filip – Boar

- jan '06 – patent attorney (in education) at DSM, Intellectual Property Department, Geleen, The Netherlands
- sept '01 – dec '05 Ph.D. candidate – Univ. of Twente, Faculty of Physics, “Physics of Complex Fluids” group of prof. dr. J. Mellema and prof. dr. F. Mugele.
Thesis: “AFM-CSLM Microrheology of Aggregated Emulsions”
- nov '00 – june '01 Socrates E.U. mobility scholarship, Univ. of Twente, Department of Applied Physics, “Rheology” group of prof. dr. J. Mellema
Research project: “Scaling viscosity of emulsions”
- sept '98 – jul '00 M.Sc. in Physics, West University of Timisoara, Romania; Department of Physics, section “Physics of Magnetic Materials”. Research thesis with prof. dr. L. Vekas at the “Institute of Complex Fluids”, Timisoara.
Thesis: “Magnetic Properties and Magneto-Granulometric Analysis of Ferrofluids”
- sept '95 – oct '00 teacher in various technical high-schools in Timisoara, at Recas Orphanage and at Izvin Secondary School, Romania;
- sept '90 – jul '95 B.Sc. in Physics, West University of Timisoara, Romania; Department of Physics, specialization “Materials Science”. Research thesis with prof. dr. N. Farbas at the “National R&D Institute for Welding and Material Testing (ISIM)”, Timisoara.
Thesis: “TEM-EDX: Basic Principles and Applications”
- sept '86 – jul '90 Baccalaureate, “Dragos Voda” High School, Sighetu-Marmatiei, Romania; Specialization Mathematics – Physics.

July 2, 1972 born in Timisoara, Romania

List of publications

Influence of Bulk Elasticity and Interfacial Tension on the Deformation of Gelled Water-in-Oil Emulsion Droplets: An AFM Study

D. Filip, V.I. Uricanu, M.H.G. Duits, W.G.M. Agterof and J. Mellema, Langmuir 2005, 21(1), p. 115-126

Microrheology of Aggregated Emulsion Droplet Networks, studied with AFM-CSLM

D. Filip, V.I. Uricanu, M.H.G. Duits, D. van den Ende, J. Mellema, W.G.M. Agterof and F. Mugele, Langmuir 2006, 22(2), p. 560-574

Plastic-to-Elastic Transition in Aggregated Emulsion Networks, Studied with Atomic Force Microscopy – Confocal Scanning Laser Microscopy Microrheology

D. Filip, V.I. Uricanu, M.H.G. Duits and J. Mellema, Langmuir 2006, 22(10), p. 4558-4566

Surfactant-Mediated Water Transport at Gelatin Gel / Oil Interfaces

V.I. Uricanu, M.H.G. Duits, D. Filip, R.M.F. Nelissen and W.G.M. Agterof, Journal of Colloid and Interface Science, accepted January 2006 (available on-line)